UNIVERSITÀ DEGLI STUDI DI NAPOLI FEDERICO II

DEPARTMENT OF CIVIL, BUILDING AND ENVIRONMENTAL ENGINEERING

Ph.D. Course in CIVIL SYSTEMS ENGINEERING

XXXVI cycle

Modeling and experimental investigations in a single-stage biofilm reactor for the simultaneous nitrogen and carbon removal from urban wastewater

SSD: ICAR/03

Course Coordinator:

Prof. Andrea Papola

Ph.D. Student:

Anna Lanzetta

Supervisors:

Prof. Stefano Papirio

Prof. Giovanni Esposito

Prof. Francesco Di Capua

ABSTRACT

Industrial, economic, urban, and social growth in recent decades has inevitably led to an increase in the production of nutrient-rich wastewater, particularly nitrogen (N) and phosphorus (P), which are responsible for environmental pollution phenomena such as eutrophication. This leads to serious cases of deterioration in the quality of rivers, lakes, and seas. The removal of N and P in wastewater treatment plants is, therefore, a key issue on which research efforts have been based in recent years to identify new technologies that can improve purification processes while optimizing energy efficiency. In this context, simultaneous nitrification and denitrification (SND), which involves the simultaneous implementation of aerobic nitrification and anoxic denitrification processes within a single treatment unit operating under identical conditions, offers several advantages including a reduced plant footprint, reduced capital and operating costs, minimized carbon and sludge generation, and reduced energy requirements for aeration.

From this perspective, this doctoral thesis aims to demonstrates the importance of mathematical modeling as a tool to improve the comprehension of treatment processes. Specifically, using the BioWin software it was possible to predict the experimental results collected during two different experimental campaigns aimed at investigating SND and shortcut SND in moving bed biofilm reactors (MBBRs). The calibrated and validated models satisfactorily reproduced the experimental data for all experimental campaigns and within specific acceptance criteria, resulting in a suitable tool for predicting the process efficiency. Moreover, calibrated and validated data were used to test different dissolved oxygen (DO) ranges (0.6–0.8 mg $O_2 \cdot L^{-1}$), pH (6.5–9.0), and

hydraulic retention times (HRTs) (0.5–1.0 d) to improve shortcut SND. Based on the different simulated scenarios, the intermittent DO conditions can induce and maintain the inhibition of the nitrite-oxidizing bacteria with an average $N\text{-}NO_3^-$ concentration of 0.05 mg $N \cdot L^{-1}$, while an HRT of 0.9 d resulted in average effluent $N\text{-}NH_4^+$, $N\text{-}NO_3^-$ and $N\text{-}NO_2^-$ concentrations of 4.0, 0.02 and 0.07 $mg \cdot L^{-1}$, respectively, indicating an efficient shortcut SND process.

Subsequently, (micro)aerobic carbon (C) and N removal from synthetic urban wastewater was experimentally investigated in a continuous double-column upflow aerobic granular sludge blanket (UAGSB) system under different DO ranges (0.01–6.00 $mg \cdot L^{-1}$), feed C/N ratios (4.7–13.6), and HRTs (6–24 h). At a DO range of 0.01–0.30 $mg \cdot L^{-1}$, feed C/N ratio of 13.6, and HRT of 24 h, the UAGSB achieved the highest chemical oxygen demand (COD), $N\text{-}NH_4^+$, and total inorganic nitrogen (TIN) removal efficiencies of 86, 99, and 84 %, respectively. A preliminary assessment of the energy and economic savings associated with the biological process was also carried out. The impact of capital and operating costs mainly related to the energy consumption of the aeration was taken into account. The assessment reveals that the capital and energy expenses of the UAGSB reactor would result in cost savings of around 14 and 7 %, respectively, compared with a modified-Ludzack–Ettinger (MLE) system. On the other hand, increased levels of $N\text{-}NO_3^-$ and $N\text{-}NH_4^+$ were detected in the effluent when the C/N ratio was reduced to 4.7-8.0 and the HRT was reduced to 6 hours.

This observation implies the need for post-treatment measures to reduce the residual concentrations under specific influent conditions. For this purpose, a duplicated two-chamber flow-through bioelectrochemical system (BES) was implemented for the

removal of residual N. The results indicated that a complete removal of $N\text{-}NO_3^-$ and $N\text{-}NO_2^-$ was achieved by the BES at an HRT of 2 h after 6 days of biomass acclimatization. Furthermore, the study showed that, although heterotrophic denitrification was predominant, the use of electron donors deriving from the electrodes kept the concentrations of $N\text{-}NO_3^-$ and $N\text{-}NO_2^-$ consistently below the Italian standard (D. Lgs. 152/2006, Annex V, Part III) for the discharge of industrial effluents into the sewer system. Therefore, integrating autotrophic and heterotrophic denitrification within the same system could ensure consistently high removal efficiencies, considering the significant variability in feed organic concentrations. Furthermore, in terms of energy consumption, a specific energy consumption rate of $2.3 \cdot 10^{-2}$ and $9.6 \cdot 10^{-5}$ kWh·g $NOx_{removed}^{-1}$ underpins the effectiveness of the BESs.

This study demonstrates how the integration of biofilm reactors with mathematical modeling can have a significant impact on scientific investigations into the removal of C, N, and P from wastewater promoting the advancement of sustainable treatment technologies.

TABLE OF CONTENTS

LIST OF FIGURES

Figure 4.1. Schematic diagram of the BES reactor configuration, consisting of anodic and cathodic chambers containing graphite granules (EC-100, Graphite Sales, USA), which acted as electrodes and supports for the biofilm. Anode loading (i.e., feeding from anode to cathode, in light blue) and cathode loading (i.e., feeding from cathode to anode, in dark blue) were implemented separately.

Figure. 4.2. Daily evolution of pH and CH_3COOH concentration ($mg \cdot L^{-1}$) in the anodic enrichment medium as well as at the anode and cathode during the anode enrichment.

Figure. 4.3. Daily evolution of pH and $N\text{-}NO_3^-$ concentration ($mg \cdot L^{-1}$) in the cathodic enrichment medium as well as at the anode and cathode during the cathode enrichment.

Figure 4.4. Temporal trends of $N\text{-}NO_3^-$(a,d), $N\text{-}NO_2^-$(b,e), and acetate concentrations (c,f) ($mg \cdot L^{-1}$) in the influent and effluent of the anode and cathode during the 7 experimental periods of R1 and R2 operation (**Table 1**). The red line indicates the Italian standard for industrial effluent discharge to sewers

Figure 5.1. Hypothetic schematics of the symbiotic microalgae reactor-UAGSB process.

LIST OF TABLES

total phosphorus (TP), total sulfur (TS), N-NO_3^-, pH, alkalinity, total inorganic suspended solid (tISS), calcium (Ca^{2+}) and magnesium ions (Mg^{2+}).

Table 2.6. Oxygen time variation (mg $O_2 \cdot L^{-1}$) of the dynamic simulation for each period of the modeled second experimental campaign.

Table 2.7. Calibration of the parameters of the dynamic models of the two experimental campaigns.

Table 2.8. Absolute variance S_{ai}, Thiel's inequality coefficient (*TIC*), and the normal objective function (*NOF*) used as acceptance criteria in the calibration and validation processes of the first experimental campaign.

Table 2.9. Absolute variance S_{ai}, Thiel's inequality coefficient (*TIC*), and the normal objective function (*NOF*) used as acceptance criteria in the calibration and validation processes of the second experimental campaign. The measured COD values could not be compared with the simulated data due to the COD value being lower than the detection value.

Table 2.10. Modeled scenarios for the shortcut SND process with different aeration patterns, pH, and HRT.

Table 3.1. COD, TIN, and N-NH_4^+ removal efficiencies (REs) for synthetic and real urban wastewater in continuous-flow aerobic and anaerobic granular sludge reactors.

Table 3.2. Operating conditions and duration of each experimental period during the continuous-flow operation of the UAGSB reactor.

Table 3.3. COD, TIN, and N-NH_4^+ removal efficiencies (REs) obtained in the UAGSB reactor at different DO concentrations (periods I-IV), C/N ratios (periods V-VIII) and HRT (periods IX-X). The percentages of total influent and removed nitrogen used for

biomass growth ($TIN_{inf, G}$ and $TIN_{rem, G}$, respectively), and of total influent inorganic nitrogen being denitrified (TIN_{den}) were calculated considering a COD:N ratio of 100:5 for aerobic cell synthesis.

Table 3.4. Main results of the preliminary economic evaluation aimed at evaluating the capital (CAPEX) and operating expenses (OPEX) of a UAGSB reactor and a MLE system both serving a population equivalent (PE) of 10,000 inhabitants.

Table 4.1. Operating conditions and duration of each experimental phase during the anodic and cathodic enrichment and continuous operation of the two-chamber flow-through bioelectrochemical system (Reactor 1 (R1) and Reactor 2 (R2)). NLR= nitrogen loading rate.

Table 4.2. NOx_{RE}, $NOx_{Rem,het}$, and $NOx_{Rem,aut}$ in R1 and R2 during the study.

Table 4.3. Performances of R1 and R2 in terms of intensity (I) and energy (E) calculated as reported in Eq. 6.

Table 4.4. Performances of R1 and R2 in terms of specific energy consumption (SEC) calculated as reported in Eq. 7. The value is not present in phase 7, as this phase was characterized by the absence of an applied potential.

Introduction

The expected growth of the urban population in the coming years will lead to an increase in the demand for water supply in urban areas and, consequently, to an increase in the volume of wastewater produced. The global wastewater production is projected to increase by 24% by 2030, followed by a more significant 51% increase by 2050 [1]. Municipal wastewater, which is rich in nitrogen (N) and phosphorus (P) compounds, may significantly contribute to intensifying the eutrophication process in surface waters if not adequately treated [2].

Eutrophication consists of an overgrowth of algae and aquatic plants, disrupting the natural balance of aquatic ecosystems. Specifically, several environmental factors have been identified as the main drivers of algal growth. These include water temperature, pH, dissolved oxygen (DO), N, P, and light intensity [3,4]. High nutrient levels create favorable conditions for rapid plant growth, which gradually results in a) reduction in light penetration into the water column, b) oxygen depletion in the aquatic environment, c) reduction in species diversity and harvestable fish biomass, d) reduction in the aesthetic perception of the water body and e) toxic emissions [5,6]. Urban and industrial wastewater discharges and climate change are significantly increasing N deposition and thereby altering the fluxes of reactive N to aquatic ecosystems [7]. In fact, the global rate of increase of reactive N from human activities has increased from 140 Tg $N \cdot year^{-1}$ in 1990 to 240 Tg $N \cdot year^{-1}$ in 2020, almost doubling the annual amount of N fixed in terrestrial ecosystems [8]. In addition, in the 20th century, the worldwide discharge of urban wastewater into surface waters surged by approximately 3.5-fold, reaching 7.7 $Tg \cdot year^{-1}$ for N and about 4.5-fold, reaching 1.0 $Tg \cdot year^{-1}$ for P [9]. However, anthropogenic activities also include the prolonged

use of N- and P-based chemical fertilizers, leading to nutrient leaching, surface and groundwater contamination, and aquatic biodiversity depletion [10].

Biological processes in wastewater treatment plants (WWTPs) are commonly conducted using conventional activated sludge (CAS) systems for organic matter removal and the modified Ludzack-Ettinger (MLE) process for combined carbon (C) and N removal through the nitrification and denitrification stages. Nitrification involves two sequential biological oxidation steps to convert ammonia (NH_4^+) into nitrate (NO_3^-). In the initial step, ammonia-oxidizing bacteria (AOB) oxidize NH_4^+ to nitrite (NO_2^-), catalyzed by ammonia monooxygenase (AMO) and hydroxylamine oxidoreductase (HAO), with the formation of hydroxylamine (NH_2OH) as an intermediate product [11]. During the subsequent stage, the oxidation of NO_2^- to NO_3^- occurs through the activity of nitrite-oxidizing bacteria (NOB) [12]. AOB and NOB use NH_4^+ and NO_2^- as energy sources, respectively, carbon dioxide (CO_2) as a carbon source and molecular oxygen (O_2) as an electron donor [13]. Denitrification is characterized by the stepwise reduction of NO_3^- to gaseous dinitrogen (N_2) under strictly anoxic conditions, with the intermediate formation of gaseous compounds such as nitric oxide (NO) and nitrous oxide (N_2O) [14]. Nevertheless, this method leads to energy-intensive aeration [15], elevated construction and operational expenses, a considerable footprint, and increased sludge generation [16].

P is mainly removed using techniques such as adsorption, chemical precipitation, or biological methods [17,18]. Adsorption is a physical-chemical process to retain phosphorus from wastewater using effective adsorptive media, such as natural, industrial waste, or man-made products [19,20]. This method is rarely used in WWTPs

due to the limited absorption capacity and high costs [20,21]. Chemical precipitation can be applied at several stages of wastewater treatment and is a very flexible approach to P removal [22], although requiring a higher chemical consumption and leading to increased sludge production [23]. Enhanced biological P removal (EPBR) with CAS is a cost-effective and environmentally sustainable alternative to chemical treatment [20,24]. EBPR achieves P removal by cycling anaerobic-aerobic metabolisms of polyphosphate-accumulating organisms (PAOs) [25]. During the anaerobic phase, PAOs hydrolyze polyphosphate (poly-P) and release P, as orthophosphate, into the wastewater [26]. The energy generated from the process is used to absorb the easily degradable low molecular weight volatile fatty acids (VFAs) into the cell to synthesize polyhydroxyalkanoic acids (PHAs) [26]. In the subsequent aerobic phase, PAOs uptake orthophosphates to recover the intracellular poly-P level by oxidizing the stored PHA, resulting in P removal [27].

Notwithstanding, conventional treatment methods for the removal of N and P from wastewater have several limitations. Specifically, the removal process becomes economically impractical for small WWPTs, and separate unit operations or improved designs are required to facilitate the N and P removal. Additionally, pathogens, heavy metals, and organic pollutants in wastewater tend to accumulate in the sludge, requiring safe disposal [28,29]. Furthermore, although WWTPs are designed to meet specific removal requirements, optimizing energy efficiency is undoubtedly a critical issue for management companies [30]. Total electricity consumption in municipal WWTPs is about 1% of a country's total annual electricity consumption [31]. In particular, the main contributors to energy consumption in a conventional WWTP are

mixed liquor aeration (55-70%), primary and secondary settling with sludge pumping (15.6%), and sludge dewatering (7%) [30].

In recent years, therefore, a lot of emphasis has been placed on introducing new technologies to improve the energy efficiency and effluent quality of WWTPs. These technologies include partial nitritation-anammox (PN/A) [32–35], microalgal-bacterial wastewater treatment systems [36–40], simultaneous nitrification denitrification and P removal (SNDPR) [41,42] and shortcut SNDPR [43,44]. The aim is not only to minimize nutrient discharge into the environment but also to explore treatment technologies that are both energy-efficient and cost-effective.

Therefore, the main objectives of this doctoral thesis were as follows:

a) to enhance understanding of the simultaneous C, N, and P removal via (shortcut) simultaneous nitrification-denitrification (SND) in a moving bed biofilm reactor (MBBRs) through a modeling approach;
b) study of a compact and cost-effective treatment solution for the simultaneous removal of C, N, and P in a continuous aerobic granular sludge (AGS) reactor;
c) investigating a post-treatment solution to improve NO_3^- removal from AGS reactor using a bioelectrochemical system (BES).

This Ph.D. thesis is composed of five chapters, including a preliminary bibliographical study, three research chapters, and a final section with a summary of observations and perspectives for the future. The structure of this thesis is given below:

Chapter 1 provides a comprehensive overview of recent literature studies concerning the simultaneous C, N, and P in biofilm systems employing both experimental and modeling approaches.

Chapter 2 presents the modeling and optimization of SND and shortcut (partial) SND process coupled to P removal in MBBRs based on data collected during two different experimental campaigns.

Chapter 3 investigates the simultaneous C and N removal in a continuous-double-column-upflow aerobic granular sludge blanket (UAGSB) system operated under different DO ranges (0.01–6.00 $mg \cdot L^{-1}$), feed C/N ratios (4.7–13.6), and hydraulic retention times (HRTs) (6–24 h).

Chapter 4 explores the possibility of using a bioelectrochemical system (BES) as a potential integrated treatment to the continuous UAGSB to improve NO_3^- removal.

Chapter 5 discusses the main findings of this doctoral study and provides recommendations for future research.

CHAPTER 1

Recent advances in the simultaneous nitrification and denitrification (SND) process and shortcut SND in biofilm reactors

1.1 Biological nitrogen removal: from conventional nitrification-denitrification to more recent technologies

The N removal pathway from wastewater consists of the nitrification and denitrification processes (**Fig. 1**). The nitrification process involves the complete oxidation of ammonia (NH_4^+) to nitrate (NO_3^-) under aerobic conditions carried out by chemolithoautotrophic microorganisms. This oxidation occurs in two consecutive steps involving two different classes of autotrophic bacteria that use NH_4^+ and NO_3^- as a source of energy, oxygen as an electron acceptor, and a carbon source for synthesis. In the first step of biological nitritation, ammonia-oxidizing bacteria (AOB) oxidize NH_4^+ to nitrite (NO_2^-) by consuming 1.5 mol of O_2. NH_4^+ is first oxidized to hydroxylamine (NH_2OH) by the enzyme ammonia monooxygenase (AMO). Next, NH_2OH is oxidized to NO_2^- by hydroxylamine oxidoreductase (HAO) [45]. In the nitratation step carried out by nitrite-oxidizing bacteria (NOB), the NO_2^- produced during nitritation is rapidly converted to NO_3^- through the catalysis of the enzyme nitrite oxidoreductase (NXR) with the consumption of 0.5 mol of O_2 [46,47]. Ammonium oxidation is mainly performed by *Nitrosomonas* and other genera such as *Nitrosococcus, Nitrospira,* and *Nitrosovibrio*. In contrast, the oxidation of NO_2^- involves bacterial genera such as *Nitrobacter*, *Nitrospira*, *Nitrospina*, *Nitrococcus*, and *Nitrocystis* [12].

Biological denitrification is performed by denitrifying bacteria (DNB) using NO_3^- as a terminal electron acceptor and organic, inorganic, or both substances as electron donors in heterotrophic, autotrophic, and mixotrophic denitrification, respectively, and as energy to maintain microbial growth [48]. Specifically, DNB catalyze the sequential

reduction of NO_3^- to NO_2^-, nitric oxide (NO), nitrous oxide (N_2O), and dinitrogen (N_2) using enzymes such as nitrate reductase (Nar), nitrite reductase (Nir), nitric oxide reductase (Nor), and nitrous oxide reductase (Nos) [46,49]. Heterotrophic DNBs require an organic carbon source as an electron donor for their rapid growth, using NO_3^- as an electron acceptor. In contrast, autotrophic DNBs use inorganic carbon (carbon dioxide (CO_2) and bicarbonate (HCO_3^-)) as carbon sources and inorganic materials such as H_2, reduced sulfur, and Fe^{2+} as electron donors [50,51]. In wastewater treatment, the majority of autotrophic denitrifiers belong to *Thiobacillus* sp. while heterotrophic denitrifiers are mainly represented by *Pseudomonas* and *Bacillus* [50,52]. Both nitrification and denitrification contribute to the release of N_2O and NO, contributing to global warming [45,49]. Particularly, during nitrification, N_2O is produced as a by-product of the oxidation of NH_4^+, resulting from the chemical decomposition of NH_4^+ to NO_2^-, or NH_2OH to NO_2^- [53–55]. In contrast to nitrification, N_2O is a direct intermediate product of the denitrification process [56].

In addition to the generation of greenhouse gases, substantial amounts of feed organic carbon and high aeration energy are necessary for effective N-removal treatment, leading to elevated operating costs [57–59]. Recent progress in wastewater treatment emphasizes the development of advanced, highly efficient processes and technologies for C, N, and P removal, including partial nitritation-anammox (PN/A) [32–35], microalgal-bacterial wastewater treatment systems [36–40], simultaneous nitrification denitrification and P removal (SNDPR) [41,42] and shortcut SNDPR [43,44].

The anammox process involves the oxidation of NH_4^+ coupled with the reduction of NO_2^- to N_2 by autotrophic anaerobic ammonium oxidizing bacteria (AAO) [60]. While

the PN/A process offers significant benefits, such as a 60% reduction in aeration energy, a 90% reduction in sludge production, and minimal reliance on organic carbon, a major hurdle is long-term NOB inhibition [32,61]. This challenge makes the maintenance of optimal N removal efficiencies over time difficult to achieve [34,57]. The treatment of wastewater through the interaction of microalgae and bacteria represents a compelling alternative due to its significant potential to achieve carbon neutrality, its advanced treatment capabilities, and the production of bio-energy [39,62]. Bacteria benefit from the O_2 released during algal photosynthesis, and algae in turn absorb the CO_2 produced by bacteria. This dynamic promotes a symbiotic relationship between the two organisms that is mutually beneficial to both. However, the most significant constraint on this technology is the lengthy startup and the influence of climatic variables such as low solar irradiance and temperature [63–65].

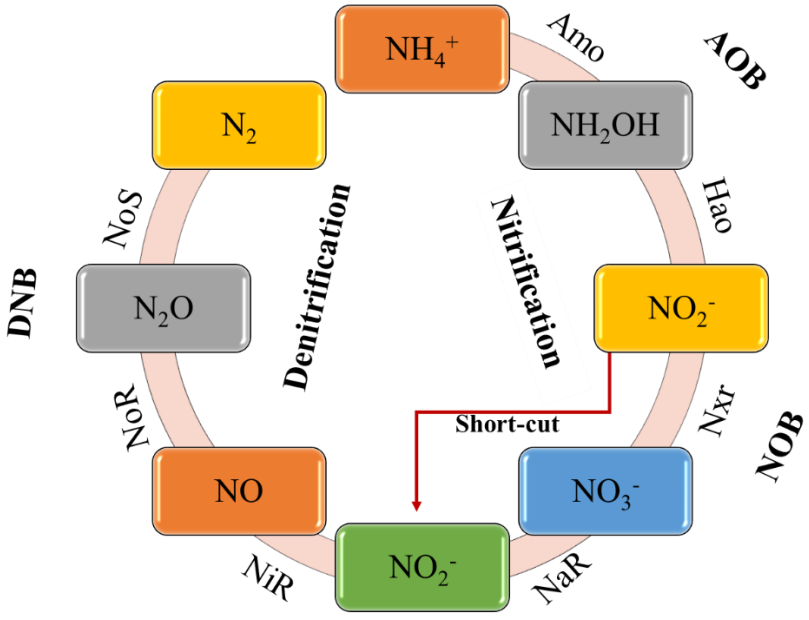

Figure 1. Overview of the main biological processes in the nitrogen cycle. AOB, ammonium-oxidising bacteria; NOB, nitrite-oxidising bacteria; DNB, denitrifying bacteria; Amo,

ammonia monooxygenase; Hao, hydroxylamine oxidoreductase Nxr, nitrite oxidoreductase; NaR, nitrate reductase; NiR, nitrite reductase; NoR, nitric oxide reductase; NoS, nitrous oxide reductase.

1.2 Simultaneous nitrification and denitrification process

The SND process refers to the simultaneous execution of the aerobic nitrification and anoxic denitrification processes under the same operating conditions within a single treatment unit [66]. The process offers several advantages, including a smaller plant footprint [67], lower capital and operating costs, reduced carbon requirements and sludge production [68], and lower energy requirements for the aeration process [69]. Up to now, the SND process has been investigated in different bioreactor configurations, such as the sequencing batch reactor (SBR) [70–72], moving bed SBR (MBSBR) [73,74], microalgae-bacteria SBR [75,76], sequencing batch biofilm reactor (SBBR) [77–81], moving bed biofilm reactor (MBBR) [21,82–85], bioelectrochemical systems (BESs) [86–90], and aerobic granular sludge (AGS) system [42,91–93].

In general, biofilm-based systems foster the co-occurrence of diverse microbial communities, also enabling a higher concentration of active biomass. This approach also minimizes space requirements and reduces sludge production in comparison to suspended-floc systems like the conventional activated sludge (CAS) and modified Ludzack–Ettinger (MLE) [94]. The SND process could be coupled with P removal (SNDPR), providing an efficient process for biological nutrient removal from wastewater with a lower carbon demand and DO consumption than the conventional biological phosphorus removal [68,95].

Recent studies have also focused on the short-cut SND pathway, which involves nitritation and denitritation processes. Specifically, the short-cut SND process can significantly improve N and P removal efficiency, especially when the influent carbon source is insufficient [96]. **Table 1.1** shows a comparative analysis of the SND performance of different bioreactors under various operating conditions.

Table 1.1. A comparative investigation of simultaneous nitrification and denitrification (SND) removal efficiencies (REs) in different bioreactor configurations and operating conditions. Sequencing batch reactors (SBRs), aerobic granular sludge SBR (AGS-SBR), moving bed SBR (MBSBR), membrane bioreactors (MBRs), microalgae-bacteria SBR, sequencing batch biofilm reactors (SBBRs), hybrid SBBRs, electrolysis-SBBR, moving bed biofilm reactors (MBBRs), intermittent aeration MBBRs, anaerobic/intermittently-aerated MBBR, integrated fixed film activated sludge (IFAS), bioelectrochemical systems (BESs), biological aerated filter (BAF) and biological folded non-aerated filter (BFNAF).

Urban wastewater characteristics		**Reactor configuration**	**Process conditions**	**Scale**	**$N\text{-}NH_4^+$ RE %**	**COD RE %**	**TN RE %**	**TP RE %**	**References**
Real	COD = 360-520 $mg \cdot L^{-1}$	SBR	HRT = 6-24 h	Lab-scale V= 3.3 L	97-99	33-98	/	10-100 (as $P\text{-}PO_4^{3-}$)	[70]
Synthetic	COD=120-660 $mg \cdot L^{-1}$ $N\text{-}NH_4^+$=40 $mg \cdot L^{-1}$ $P\text{-}PO_4^{3-}$=5 $mg \cdot L^{-1}$	SBR	C/N = 3-16.5	Lab-scale V= 2 L	90-99	85-95	45-98	10-99 (as $P\text{-}PO_4^{3-}$)	[71]
Real and synthetic	/	SBR	T=10 °C	Lab-scale V=18 L	/	90-98	91	92	[72]
Synthetic	$N\text{-}NH_4^+$= 40 $mg \cdot L^{-1}$ $P\text{-}PO_4^{3-}$= 4 $mg \cdot L^{-1}$	SBR	DO=1.0-4.0 $mg \cdot L^{-1}$	Lab-scale V=3.2 L	95	/	35-62	/	[93]
Synthetic	COD= 250-260 $mg \cdot L^{-1}$ $N\text{-}NH_4^+$= 39-41 $mg \cdot L^{-1}$	SBR	DO=0.4-1.2 $mg \cdot L^{-1}$	Lab-scale V= 25 L	/	63-72	63-72	/	[16]
Synthetic	COD= 200-300 $mg \cdot L^{-1}$ $N\text{-}NH_4^+$= 20-24 $mg \cdot L^{-1}$ TP = 3-4 $mg \cdot L^{-1}$	SBR	Aeration time= 60,75,90 min	Lab-scale V= 2.2 L	95-99	90-91	66-71 (as TIN)	97	[97]
Synthetic	COD= 241 $mg \cdot L^{-1}$ $N\text{-}NH_4^+$= 43 $mg \cdot L^{-1}$ TP = 4.6 $mg \cdot L^{-1}$	SBR	C/N= 7-11	Lab-scale V= 2.3 L	46-85	77-91	/	27-94	[98]

Urban wastewater characteristics		Reactor configuration	Process conditions	Scale	$N\text{-}NH_4^+$ RE %	COD RE %	TN RE %	TP RE %	References
Synthetic	COD= 200-350 $mg \cdot L^{-1}$ $N\text{-}NH_4^+$= 250-330 $mg \cdot L^{-1}$	AGS	/	Lab-scale V=3 L	98	/	/	/	[42]
Synthetic	COD= 331-582 $mg \cdot L^{-1}$ TN= 33-44 $mg \cdot L^{-1}$ TP = 3.3-5.4 $mg \cdot L^{-1}$	AGS	DO=0.5-6.0 $mg \cdot L^{-1}$	Lab-scale V=13 L	/	/	13-65	/	[92]
Synthetic	COD= 200-1000 $mg \cdot L^{-1}$ TN= 10-50 $mg \cdot L^{-1}$ TP = 2-10 $mg \cdot L^{-1}$	AGS	Intermittent aeration	Lab-scale V=4.3 L	99-100	75-90	80-98	/	[99]
Synthetic	COD= 400 $mg \cdot L^{-1}$ TN= 20-80 $mg \cdot L^{-1}$ TP = 10 $mg \cdot L^{-1}$	AGS	DO=4.0-5.0 $mg \cdot L^{-1}$ C/N= 5-20	Lab-scale V=7 L	84-98	96-97	74-89	85-88	[100]
Synthetic	COD= 200 $mg \cdot L^{-1}$ TN= 10-40 $mg \cdot L^{-1}$ TP = 4 $mg \cdot L^{-1}$	AGS	C/N= 5-20	Lab-scale V=3.6 L	99	88-92	/	92	[101]
Synthetic	COD=300-1000 $mg \cdot L^{-1}$	MBSBR	HRT=1.5-3.5 h	Pilot-scale V=30 L	/	86-95	73-99	48-72	[73]
Synthetic	COD= 295-312 $mg \cdot L^{-1}$ $N\text{-}NH_4^+$=27-60 $mg \cdot L^{-1}$ TN=27-31 $mg \cdot L^{-1}$	MBSBR	DO=1.5-5.5 $mg \cdot L^{-1}$ pH=6.5-8.5 HRT=6-12 h	Lab-scale V=6.5 L	25-98	92	40-80	/	[102]
Synthetic	COD= 536-591 $mg \cdot L^{-1}$ $N\text{-}NH_4^+$= 19-31 $mg \cdot L^{-1}$ TP = 4.6-6.7 $mg \cdot L^{-1}$	MBR	DO=0.5-3.0 $mg \cdot L^{-1}$	Lab-scale V= 2.7 L	60-100	/	70-91	/	[103]
Synthetic	COD= 157 $mg \cdot L^{-1}$ $N\text{-}NH_4^+$=26 $mg \cdot L^{-1}$ TN=26 $mg \cdot L^{-1}$ TP=2.9 $mg \cdot L^{-1}$	Microalgae-bacteria SBR	DO=3.2 $mg \cdot L^{-1}$ HRT=8 h Light-intensity = 200 $\mu mol \cdot m^{-2}$	Lab-scale V=2.8 L	97	/	67	/	[75]

Urban wastewater characteristics		Reactor configuration	Process conditions	Scale	$N\text{-}NH_4^+$ RE %	COD RE %	TN RE %	TP RE %	References
Synthetic	COD= 150-250 $mg \cdot L^{-1}$ $N\text{-}NH_4^+$=24-30 $mg \cdot L^{-1}$ TN=22-29 $mg \cdot L^{-1}$	SBBR	DO=3-4 $mg \cdot L^{-1}$ T=15-35 °C	Lab-scale V=16 L	/	/	56-92	/	[77]
Synthetic	TOC= 126 $mg \cdot L^{-1}$ $N\text{-}NH_4^+$=38 $mg \cdot L^{-1}$ TN=39 $mg \cdot L^{-1}$ TP=9 $mg \cdot L^{-1}$	SBBR	DO=2.2-5.5 $mg \cdot L^{-1}$ Salinity=0-9 $g \cdot L^{-1}$	Lab-scale V=9 L	95-99	46-69	/	/	[78]
Synthetic	COD=230 $mg \cdot L^{-1}$ $N\text{-}NH_4^+$=13-40 $mg \cdot L^{-1}$ $P\text{-}PO_4^{3-}$=27 $mg \cdot L^{-1}$	SBBR	DO=5.4-6.8 $mg \cdot L^{-1}$	Lab-scale V=20 L	72-94	/	/	98 (as $P\text{-}PO_4^{3-}$)	[79]
Synthetic	COD*=525 $mg \cdot L^{-1}$ $N\text{-}NH_4^+$*=107 $mg \cdot L^{-1}$ $P\text{-}PO_4^{3-}$*=2 $mg \cdot L^{-1}$	Hybrid-SBBR	Salinity = 1-3 %	Lab-scale V=13.3 L	38-90	96-100	84	/	[80]
Synthetic	COD=400 $mg \cdot L^{-1}$ $N\text{-}NH_4^+$=40 $mg \cdot L^{-1}$	Hybrid-SBBR	Salinity = 0-2.4 %	Lab-scale V=7 L	/	87-92	74-83	/	[104]
Synthetic	COD=48-118 $mg \cdot L^{-1}$ $N\text{-}NH_4^+$=32 $mg \cdot L^{-1}$ $P\text{-}PO_4^{3-}$=5 $mg \cdot L^{-1}$	Electrolysis-SBBR	C/N = 1.5-3.5	Lab-scale V=5 L	99	74-83	70-84	98	[81]
Real	COD= 98-280 $mg \cdot L^{-1}$ $N\text{-}NH_4^+$=30-70 $mg \cdot L^{-1}$	MBBR	DO=0.6-0.8 $mg \cdot L^{-1}$ C/N= 1.4-5	Lab-scale V=12.6 L	79-92	/	44-72	/	[105]
Synthetic	COD=222 $mg \cdot L^{-1}$ $N\text{-}NH_4^+$=16 $mg \cdot L^{-1}$ $P\text{-}PO_4^{3-}$=15 $mg \cdot L^{-1}$	MBBR	Carrier filling ratio= 20-60 % HRT=4-8 h	Lab-scale V=2.5 L	56-89	65-82	/	18-42	
Synthetic	TOC=110-120 $mg \cdot L^{-1}$ $N\text{-}NH_4^+$=28-33 $mg \cdot L^{-1}$ TP=2.7-3.5 $mg \cdot L^{-1}$	MBBR	DO=5.0-6.5 $mg \cdot L^{-1}$	Lab-scale V=12 L	/	/	75-84	/	[106]

Urban wastewater characteristics		Reactor configuration	Process conditions	Scale	$N\text{-}NH_4^+$ RE %	COD RE %	TN RE %	TP RE %	References
Synthetic	COD=231-509 $mg \cdot L^{-1}$ $N\text{-}NH_4^+$=31-63 $mg \cdot L^{-1}$ $P\text{-}PO_4^{3-}$=14 $mg \cdot L^{-1}$	MBBR	DO=1.0 $mg \cdot L^{-1}$ HRT=1-2 d C/N = 2.7-5.6	Lab-scale V=2.2 L	/	80-100	32-68	66-72	[82]
Synthetic	COD=40-400 $mg \cdot L^{-1}$ $N\text{-}NH_4^+$=20 $mg \cdot L^{-1}$ $P\text{-}PO_4^{3-}$=6.8 $mg \cdot L^{-1}$	MBBR	DO=0.8-3.5 $mg \cdot L^{-1}$ HRT=40 h C/N = 2-20	Lab-scale V=1.5 L	98-100	90-95	79-95	55-67	[107]
Synthetic	DOC= $mg \cdot L^{-1}$ $N\text{-}NH_4^+$= $mg \cdot L^{-1}$ $P\text{-}PO_4^{3-}$= $mg \cdot L^{-1}$	Intermittent aeration MBBR	DO=0.2-4 $mg \cdot L^{-1}$ HRT=1 d C/N = 2.8-4.2	Lab-scale V=2.0 L	/	100 (as DOC)	40-82 (as TIN)	16-81	[21]
Synthetic	DOC= 90-136 $mg \cdot L^{-1}$ $N\text{-}NH_4^+$= 24-48 $mg \cdot L^{-1}$ $P\text{-}PO_4^{3-}$= 4-10 $mg \cdot L^{-1}$	Intermittent aeration MBBR	DO=0.2-3 $mg \cdot L^{-1}$ HRT=1 d C/N = 1.4-3.5	Lab-scale V=1.5 L	68-100	100 (as DOC)	69-88	62-95 (as $P\text{-}PO_4^{3-}$)	[83]
Synthetic	COD= 103-132 $mg \cdot L^{-1}$ $N\text{-}NH_4^+$= 29-33 $mg \cdot L^{-1}$	Anaerobic/intermittently-aerated MBBR	DO=0.1-6 $mg \cdot L^{-1}$ C/N = 3-5	Lab-scale V=5 L	/	90	51-90	20-74	[84]
Synthetic	COD= 1000 $mg \cdot L^{-1}$ $N\text{-}NH_4^+$= 50 $mg \cdot L^{-1}$	MBBR	OLR=0.45-0.95 kg $COD \cdot m^{-3} \cdot d^{-1}$	Lab-scale V=7.5 L	93-100	82-98	/	/	[85]
Synthetic	COD= 350 $mg \cdot L^{-1}$ $N\text{-}NH_4^+$= 35 $mg \cdot L^{-1}$ $P\text{-}PO_4^{3-}$= 10 $mg \cdot L^{-1}$	MBBR	DO=1.0-5.0 $mg \cdot L^{-1}$	Lab-scale V= 1.8 L	49-94	88	41-68	/	[108]
Synthetic	COD= 300 $mg \cdot L^{-1}$ TN= 55 $mg \cdot L^{-1}$ TP = 5 $mg \cdot L^{-1}$	IFAS	DO=0.5-4.5 $mg \cdot L^{-1}$	Lab-scale V= 5 L	91-95	81-96	83	/	[109]
Synthetic	$N\text{-}NH_4^+$= 600 $mg \cdot L^{-1}$	BES	Applied voltage= 1.2-1.8 V	Lab-scale V=400 mL	21-48	/	20-45	/	[110]
Synthetic	COD= 1500-2000 $mg \cdot L^{-1}$ $N\text{-}NH_4^+$= 100 $mg \cdot L^{-1}$	BES	DO=0.6-1.2 $mg \cdot L^{-1}$	Lab-scale V=1 L	38-65	98	50-71	/	[87]

Urban wastewater characteristics		Reactor configuration	Process conditions	Scale	$N\text{-}NH_4^+$ RE %	COD RE %	TN RE %	TP RE %	References
Synthetic	COD= 192-303 $mg \cdot L^{-1}$ $N\text{-}NH_4^+$= 51-53 $mg \cdot L^{-1}$	BES	DO=0.5-4.0 $mg \cdot L^{-1}$	Lab-scale V=951 mL	90-99	80-90	44-84	/	[89]
Synthetic	COD= 0-293 $mg \cdot L^{-1}$ $N\text{-}NH_4^+$= 65 $mg \cdot L^{-1}$	BES	COD/N=0-4.5	Lab-scale V=2.8 L	/	93-98	30-84	/	[90]
Synthetic	COD= 2000 $mg \cdot L^{-1}$ $N\text{-}NO_3^-$= 200-375 $mg \cdot L^{-1}$	BES	C/N = 2-3.75	Lab-scale V= 3 L	65-90 (as $N\text{-}NO_3^-$)	60-76	/	/	[111]
Synthetic	$N\text{-}NH_4^+$= 600 $mg \cdot L^{-1}$	BES	Voltage = 1.2-1.8 V	Lab-scale V=400 mL	45-48	/	/	/	[110]
Real	COD= 271 $mg \cdot L^{-1}$ TN= 42 $mg \cdot L^{-1}$	BAF	DO=0.5-2.0 $mg \cdot L^{-1}$ HRT=8-20 h	Lab-scale V= 3.5 L	/	71-90	47-72	/	[69]
Synthetic	COD= 121-182 $mg \cdot L^{-1}$ $N\text{-}NH_4^+$= 31-46 $mg \cdot L^{-1}$	BFNAF	HRT=8-12 h C/N = 4-10	Lab-scale V= 40 L	27-92	42-79	11-66	/	[112]

*Stoichiometrically calculated.

1.3 Main factors influencing the SND and SNDPR process

SND and SNDPR removal efficiencies depend on several factors such as temperature, pH, DO, feed carbon-to-nitrogen (C/N) ratio, source of organic carbon, hydraulic retention time (HRT), electron acceptor used to sustain the denitrifying phosphorus-accumulating organisms (DPAO) and salinity [57,113].

- **Temperature**

Temperature is a key factor in the nitrification and denitrification process as it alters the metabolic activity of the microbial community and the rate of biological reactions [49,57]. Overall, the specific growth rates of AOB and NOB undergo significant changes depending on the temperature. At relatively higher temperatures (>25 °C), AOBs tend to compete with NOBs due to their higher specific growth rate [114], whereas NOBs prevail over AOBs at temperatures below 15 °C [115]. On the other hand, high temperatures (>20°C) can lead to a deterioration of the P-removal performance. This can reduce the population and substrate affinity of PAOs in the biomass [116].

Zhang et al. [77] evaluated the effects of different temperatures (15, 21, 26, 31, and 35 °C) on the TN removal rate and nitrite accumulation in the short-cut SND process using an SBBR. The highest TN removal of 91.9% was at 31 °C with DO in the range of 3-4 $mg \cdot L^{-1}$ [77]. According to other studies [117], the NH_4^+ oxidation rate exhibits a positive correlation with temperature within the 15-31 °C range. Additionally, the composition of the bacterial community can vary with increasing temperature [118]. Biological N removal is difficult at low temperatures because microbial activity is considerably reduced, resulting in decreasing nitrification and denitrification rates. Nonetheless, high N and P removal efficiencies can also be achieved at a temperature of 10 °C, as reported by Li et al. [119] and Bai et al. [72]. Despite this, lower temperatures can lead to increased

emissions of NO and N_2O during denitrification due to a general enzymatic slowdown or disruption of the pathway [49].

- **pH**

Conventional biological N removal is known to be sensitive to pH changes. It is generally accepted that nitrification by AOB and NOB is optimal under slightly alkaline conditions. In contrast, anaerobic denitrifiers thrive in slightly acidic environments. Wang et al. [102] investigated the effect of different pH values (6.5, 7.0, 7.5, 8.0, and 8.5) on the performance of SND in a MBSBR. The research shows that while COD removal was optimal at all pH values, NH_4^+ removal has peaked at 94% at pH 8 [102]. Generally, maintaining a pH between 7.5 and 8.5 is beneficial for NO_2^- accumulation [120].

- **DO concentration**

DO concentration plays a crucial role in influencing SND as it serves as the electron acceptor in nitrification reactions [121]. Conventionally, SNDPR may be obtained at low DO concentrations (0.05 - 2 $mg \cdot L^{-1}$) [57]. The occurrence of anoxic microenvironments within sludge flakes or biofilms is attributed to DO concentration gradients caused by limited DO diffusion. This creates a scenario where heterotrophic DNB dominate the biofilm interior while nitrifiers remain active on the biofilm surface, providing a favorable environment for SND [122]. Specifically, the nitrification rate increases with increasing DO concentrations but remains stable as the biofilm thickness increases. However, high DO concentrations can significantly inhibit the development of the denitrification capacity of a biofilm, but this effect is strongly reduced once a certain biofilm thickness is exceeded [123]. Therefore, for both nitrification and denitrification, an intermediate DO level must be found [124]. Recently, the effect of DO concentration on the performance and mechanism of SND in the integrated fixed-film activated sludge (IFAS)

system was investigated by Jin et al. [109], showing that the highest SND efficiency (88.5 %) was achieved at a DO concentration of 0.5 $mg \cdot L^{-1}$. Additionally, a DO concentration of 4.5 $mg \cdot L^{-1}$ was reported to significantly inhibit the denitrification process, confirming that DO strongly affects biomass and microbial activity [109]. Zhang et al. [125] evaluated the N and P removal in a plant-scale multistage-activated sludge-membrane bioreactor system at different DO concentrations (0.6-4.0 $mg \cdot L^{-1}$), reporting that reducing DO levels (0.6-0.7 $mg \cdot L^{-1}$) improved N removal efficiency from 82.4 to 94.3% [125], thus promoting SND. Moreover, the biodegradability of the effluent can be improved under oxygen-limited conditions, which favors the predominant growth of nitrifying and denitrifying bacteria in the SND process [126]. In contrast to continuous aeration, intermittent aeration (IA) proves to be cost and energy-effective as it establishes a sequence of continuous aerobic-anoxic-anaerobic phases within the reactor, which favors the SND process [58]. Ma et al. [97] investigated the effect of aeration time (90, 75, 60, 45, and 30 min) on anaerobic/oxic/anoxic (AOA) SNDPR finding that moderate aeration time of 45-60 min is the most beneficial for N and P removal. Recent studies have shown that although *Nitrobacter* and *Nitrosomonas* are the main AOBs involved in the nitrification process, *Nitrosomonas* is the most abundant AOB species in SND systems due to its lower sensitivity under oxygen-limiting conditions [103,108,126]. Conversely, *Nitrospira* was typically the dominant NOB species in the SND process [108]. Since a high DO concentration is favorable for *Nitrospira*, this means that NO_2^- can accumulate in the SND process under low DO conditions [124].

- **Feed carbon-to-nitrogen ratio**

The C/N ratio in wastewater treatment is an important parameter that influences the growth and activities of microorganisms, consequently affecting N removal. Although

the optimal C/N ratio for N removal is approximately 8-12 [127], municipal wastewater generally has a low C/N ratio, which may lead to incomplete denitrification and high NO_3^- levels in the effluent. [111,128,129]. The conventional approach is the addition of a carbon source (such as methanol, ethanol, glucose, or sodium acetate) to provide electron donors for denitrification [130]. Variations in the feed C/N ratio affect the kinetics of heterotrophic and autotrophic biomass. [131]. Iannacone et al. [82] assessed the SNDPR process in a continuous-flow microaerobic MBBR operated at different feed C/N ratios (2.7, 4.2, and 5.6). Stable TN removal was attained at a feed C/N ratio of 4.2, while a feed C/N ratio of 5.6 resulted in excessive growth of heterotrophic aerobic bacteria (HAB), suppressing nitrification [82]. On the contrary, insufficient organic carbon can lead to a decrease in denitrification efficiency, as reported by Chang et al. [112]. Furthermore, in a study conducted by Zhu et al. [132], it was observed that a C/N ratio of 5 increased the storage of PHA in the system, thus providing more energy for P uptake and allowing for high removal efficiencies of TN and TP, reaching 66% and 96%, respectively.

- **Source of organic carbon**

The selection of the proper carbon source strongly influences the efficiency of N and P removal during wastewater treatment. Although sodium acetate is the most widely used carbon source, much research has focused on finding alternative carbon sources. For instance, Hagman et al. [133] demonstrated that a mixture of methanol and acetate as a carbon source can enhance denitrification efficiency. Concerning P removal, the choice of carbon source significantly influences the presence of volatile fatty acids (VFAs), which in turn influence the presence of polyphosphate accumulating organisms (PAOs) and glycogen (GAOs) [134]. Shen et al. [135] tested acetate and propionate as carbon sources to evaluate P removal performance and microbial communities in two SBRs,

reporting that more stable P removal was observed with acetate as the sole carbon source. Conversely, He et al. [136] utilized a combination of sodium acetate and succinate as a mixed carbon source in the operation of the AGS-SNDPR system. The study reveals that sodium succinate is more favorable for biomass enrichment and sludge settleability in AGS compared to sodium acetate [136]. Additionally, different synthetic biodegradable polymers (BDPs) have been used as carbon sources, improving N removal efficiency [137]. Recent studies report the use of plant-based waste biodegradable materials as a natural carbon source to improve the feasibility of the SND process in the presence of low C/N ratio domestic wastewater due to its good biodegradability, low cost, and easy availability [69,98,138]. For instance, in a study by Chen et al. [98], acid-pretreated pistachio shells were utilized as carbon sources to assess the impact of carbon-source dosage on SNDPR, achieving high removal efficiencies for TN and TP of 84 and 94 %, respectively, after 25 d of reactors operation.

- **Hydraulic retention time**

Hydraulic retention time (HRT) plays an important role in influencing microbial distribution and wastewater treatment performance. Chang et al. [112] evaluated the N removal via SND in a biological folded non-aerated filter at different HRTs (4, 8, and 12 h). By increasing the HRT up to 10.83 h, higher NH_4^+, COD, and TN removal efficiencies equal to 88.62 ± 0.81%, 76.12 ± 0.57%, and 50.48 ± 1.02%, respectively can be achieved. On the contrary, a lower HRT of 4 h does not promote the contact between the degradation of pollutants and the biofilm, leading to a deterioration of the nitrification performance [112], in agreement with other study [70,139].

- **Salinity**

In biological wastewater treatment, elevated salinity can reduce cellular activity and induce cell plasmolysis, affect sludge floc structure and settling characteristics, and extracellular polymeric substances (EPS) production and composition [80]. However, the inhibitory effect can be overcome as a result of biomass adaptation [140]. As reported by Luo et al. [141] an increase in salinity has a significant impact on microbial species composition, flora richness, and dominant species. Similarly, Xia et al. [104] reported that, among AOBs, the presence of *Nitrosomonas* increased with increasing salinity, while among NOBs, *Nitrospira* showed significant sensitivity to salinity variation. In general, it was reported that AOBs are more salt-tolerant than NOBs [142].

1.4 Short-cut SND

Short-cut SND, also called simultaneous partial nitrification and denitrification (SPND) or SND via nitrite, consists of a direct coupling of nitritation and denitritation phase achieved by inhibiting the NOB activity and only promoting the growth of AOBs.

Compared to the SND process, short-cut SND has several advantages, such as a) an approximately 25% reduction in aeration consumption, leading to energy savings [143]; b) a nearly 40% reduction in carbon requirements for denitrification [144]; c) a reduction in sludge yield, simplifying sludge disposal [145]; d) the ability to reduce reactor volume and save space due to the shorter reaction time [146]. However, the main challenge of this process is related to the instability of NOB inhibition [147].

By leveraging the variations in the growth of AOBs and NOBs, different operational strategies can be implemented to hinder and subsequently eliminate NOBs. These strategies include a) operating the bioreactors at high pH (>7.5) and temperatures (>25 °C) [148,149]; sludge retention time (SRT) control [150]; b) setting the DO level between

1 and 2 mg $O_2 \cdot L^{-1}$ [151]; c) maintaining free ammonia (FA i.e. NH_3) and free nitrous acid (FNA i.e. HNO_2) concentrations within ranges that inhibit NOB and tolerate AOB [60]. Although both AOBs and NOBs are aerobic organisms, they have different affinities for oxygen. In particular, some studies have shown that AOBs tend to have a higher affinity for oxygen than NOBs [152,153]. This suggests that AOBs may become dominant under low DO conditions, allowing the accumulation of NO_2^-. Conversely, other studies have shown that certain genera of NOBs have a higher affinity for oxygen, allowing them to adapt to low DO conditions [154,155]. Duan et al. [156] examined the kinetic parameters of AOBs and NOBs under different DO concentrations ranging from 0.6 to 5.0 mg $O^2 \cdot L^{-1}$. The results reveal that AOBs showed limited adaptability to DO variation, with a decrease in oxygen affinity observed in the presence of high DO levels (4.0-5.0 mg $O^2 \cdot L^{-1}$). In contrast, under low DO (0.3-0.8 mg $O^2 \cdot L^{-1}$), the main NOB genus, *Nitrospira*, dominated the nitrifying community.

In addition, both AOBs and NOBs are found to be sensitive to FA. The inhibition thresholds are different and range from 10-605 mg $N \cdot L^{-1}$ for AOBs [157] to 0.04-5 mg $N \cdot L^{-1}$ for NOBs [158–160]. In addition, FNA concentrations ranging from 0.42 to 1.72 mg $N \cdot L^{-1}$ resulted in a 50% reduction in the AOBs activity. In contrast, lower FNA concentrations of 0.026 to 0.22 mg $N \cdot L^{-1}$ could completely inhibit NOBs [148,161]. Chen et al. [162] used 250 mg $N \cdot L^{-1}$ of $N\text{-}NH_4^+$ and $N\text{-}NO_2^-$ to evaluate the performance of FA/FNA treatment on NOB suppression, confirming that nitritation could be achieved by temporary FA/FNA treatment. Similarly, Qian et al. [163] reported that increasing the FA concentration from 0 to 16.8 mg $N \cdot L^{-1}$ resulted in a greater decrease in NOB activity compared to AOBs. In addition, Zhou et al. [164], achieved complete NOB suppression

by a combination of high FA (26.2 mg $N \cdot L^{-1}$) concentration and low DO levels (0.12 mg $O^2 \cdot L^{-1}$).

Many studies have shown that IA can be a rapid and effective method to accumulate AOB and inhibit NOB, while also saving energy [165–167]. Particularly, the optimization of the operational approach for IA is crucial, as maintaining prolonged anoxic phases during IA not only increases operational costs, leading to lower N removal rates but also leads to increased operational complexity [165]. Xu et al. [168], combining IA using an aeration period of 20 min with a DO concentration of 0.5 mg $O_2 \cdot L^{-1}$, achieved an 80-89 % N removal. Recently, Luan et al. [169] studied the N removal pathway in an intermittently aerated activated sludge system by adding iron-chitosan (Fe-CS) beads achieving 93.9 % TN removal efficiency and an inhibitory effect on the NOB growth. Iannacone et al. [83] investigated the feasibility of short-cut SNDPR in continuous-flow intermittently-aerated MBBR. NOB suppression within the MBBR was efficiently achieved by maintaining a pH of 8.2, an SRT of 4 days, a T between 26 and 28 °C, and using IA (0.2-3.0 mg $O_2 \cdot L^{-1}$). Alternatively, Chang et al. [170] achieved a short-cut SND in the hybrid membrane aerated biofilm reactor for treating low COD/N ratio (3.3-5.3) using an aeration pressure of 0.01 Mpa, temperature of 30 °C, and a pH of 8.

1.5 SND applications in MBBR and AGS reactor

SND can be effectively integrated into various wastewater treatment systems, including activated sludge, AGS, biofilm reactors, and other bio-configurations [57]. Biofilm-based systems foster the coexistence of diverse microbial communities, enabling efficient biodegradation of various pollutants. Additionally, these systems concentrate active biomass, resulting in faster reaction rates and smaller reactor footprints [171].

Conversely, AGS forms self-organizing microbial aggregates similar in structure to biofilms, but without requiring external inert support. This technology combines the efficient degradation of suspended-growth systems with the compact structure and reduced sludge production of biofilms, offering potential benefits for wastewater treatment [172,173].

1.5.1 Moving bed biofilm reactors

MBBR technology is an efficient wastewater treatment solution. The use of mobile carriers facilitates the development of a stratified biofilm, characterized by the presence of different bacterial communities that are influenced by the composition of the treated wastewater and the operating conditions [174]. The type of biocarrier therefore plays a key role in the stable operation of an MBBR. The widely employed carriers for MBBRs are plastic-based and are commercially accessible in diverse shapes and sizes. These include chip-type media, characterized by flat or curved plastic discs (such as the Z-carrier by AnoxKaldnes, Lund, Sweden), mesh-type media, resembling chip-type but permitting flow through mesh openings (i,e. BiofilmChip by AnoxKaldnes), porous or sponge-type media, and media featuring internal tubular channels (such as K3 media from AnoxKaldnes) [175]. Other specific types of carriers used were lignite-activated coke [176], polyvinyl chloride rings [177], polypropylene (PPE) pall rings [178], and polyurethane foam [179]. Among the options mentioned, polyurethane sponge stands out as an optimal growth medium due to its high mechanical strength, large specific surface area, robust surface, and excellent adhesion to microorganisms [180]. An additional advantage of polyurethane sponge is its advanced capability for SND due to the well-developed DO gradient within the biofilm [181]. **Table 1** lists the operational parameters

and SND performance of MBBR. Song et al. [106] developed a new MBBR with zeolite powder-based polyurethane sponges as carriers to evaluate the SND and also to compare the results with those obtained using conventional polyurethane sponges as carriers. The study showed that the use of zeolite powder-based polyurethane sponges as biocarriers not only increased the TN removal efficiency by 10% but also promoted the presence of 1.3 times more biofilm attached to the new biocarriers than the conventional polyurethane sponges with a higher abundance of denitrifying bacteria. Shi et al. [85] comparing the effects of four soft polyurethane biocarriers with different sizes and a hard polypropylene biocarrier on the performance of SND for coking wastewater treatment in an MBBR, found that soft polyurethane biocarriers can help prevent nitrifying bacteria from washing out under shock loading. Recently, Lu et al. [182] identified that novel flocking 0.5 mm biocarriers composed of polypropylene fibers can enhance the SND process showing a 52% removal of TN and promoting the formation of EPS, resulting in increased microbial community stability. In addition, according to Yang et al. [183] agricultural wastes (cellulose, hemicellulose, lignin) can be used as carbon sources and biological carriers. In a study by Loh et al. [69] a novel biodegradable *Cocos nucifera* fiber was used as biofilter media evaluating the performance of the system based on the biofilm concentrations, SND efficiencies, and COD and N removal efficiencies. The study shows that under the best operating conditions of DO 1.5 mg $O_2 \cdot L^{-1}$ and HRT 16 h, an average COD and TN removal efficiency of 90.9% and 71.1% were achieved, respectively. In addition, the *Cocos nucifera* fiber media degraded by only 0.8% after 176 days of continuous operation, indicating an expected life of over 5 years.

In addition, a suitable filling fraction must be defined to ensure effective hydrodynamic properties without limiting mass transfer [151]. However, the filling fraction of the

carriers must not exceed 70% of the total reactor volume [184]. The selection of the loading ratio can impact the efficiency and effectiveness of the bioreactor system, thereby influencing the overall operating costs incurred, including energy consumption and the procurement of carriers [58]. Recently, Pratap et al. [174] investigated the effect of three high-density polyethylene (HDPE) and PPE filling ratios (20, 40, and 60 %) on biofilm formation and MBBR performance in both batch and continuous setups using real municipal wastewater. The highest COD and TN removal efficiencies were found to be 77 and 75 and 89 and 91 % with HDPE and PPE, respectively, and a carrier filling ratio of 40 %, which confirms previous literature reports [185,186].

Recent studies have shown that, under certain operating conditions, the SNDPR process can also be implemented in MBBRs. Pan et al. [107] reveal that 99.6, 63.6 78.9, and 59.6 % of $N\text{-}NH_4^+$, $N\text{-}NO_3^-$, TN and TP were removed at C/N ratio, HRT, and carrier film amount equal to 5, 40 h and 1.2 $mg \cdot g^{-1}$. Shao et al. [187] evaluated the SNDPR process by manganese redox cycling in MBBR at a C/N ratio of 5 obtaining removal efficiencies of TN, $N\text{-}NH_4^+$, TP, and Mn^{2+} of 65.1, 92.7, 51.6 and 68.1 %, respectively, using sodium succinate as the denitrifying carbon source. Luan et al. [84] found TN and TP removal efficiencies were 90 and 74 %, 88 and 59 % with a C/N of 3 and for short and long aeration, respectively, noting that different aeration times can alter the nutrient degradation pathway, biofilm characteristics, microbial community, and functional metabolic pathways. In particular, the short aeration also provided a more stable biofilm structure and facilitated the cultivation of denitrifying glycogen-accumulating organisms (DGAOs). Similarly, Iannacone et al. [21] obtained average dissolved organic carbon (DOC), total inorganic carbon (TIN), and $P\text{-}PO_4^{3-}$ efficiencies of 100, 62 and 75 % at a DO range of 0.2-3.0 mg $O_2 \cdot L^{-1}$, thus alternating microaerobic-aerobic conditions favoring

the coexistence of key species involved in nitrification, denitrification, and phosphorus accumulation.

1.5.2 Aerobic granular sludge reactor

AGS technology represents an innovative approach for the treatment of both domestic and industrial wastewater, primarily due to its significantly reduced footprint and energy consumption compared to conventional activated sludge systems [188,189]. AGS are characterized by a dense biofilm comprised of self-mobilized cells, eliminating the necessity for support material. Compared to CAS, AGS can reduce bioreactor volume by 30% and energy consumption by up to 63%, while their compact and heavy structure facilitates faster settling, reducing the time required for settling without the use of flocculants [190]. Additionally, the presence of multiple layers promotes the coexistence of nitrifying organisms in the outer layers and denitrifying and anaerobic organisms toward the center of the granules, enabling SND implementation [189,191]. However, AGS has some limitations, including instability, and long granule cultivation time [57]. In general, the main requirements for the aerobic granulation process are a) distinct feast-famine periods during operation, b) a short settling time, and c) a high aeration intensity [192]. In contrast, several parameters such as C/N ratio, aeration intensity, and organic loading rate (OLR) can influence the long-term stability of AGS [193]. Further parameters including granule size, DO, and microbial community can affect SND in AGS reactors [194]. **Table 1.1** provides a comprehensive overview of the operation of the AGS reactor. Granule size selection is an important control variable in achieving and maintaining efficient nutrient removal [195]. As both small and large granules are exposed to the same mass DO concentration, the smaller granules have a higher aerobic

volume fraction with a limited anoxic zone, promoting the growth of nitrifiers but negatively affecting the SND [92]. Conversely, the larger granules have a higher anoxic volume fraction, facilitating the proliferation of denitrifying bacteria [196]. Although aerobic granular sludge has been successfully cultured in sizes ranging from 0.02 mm to 9.0 mm, it is usually characterized by average diameters between 0.1 mm and 3.0 mm [197]. Quoc et al. [196] evaluated the optimal granule size fractions ranging from 0.2 to > 2.0 mm for SND in an AGS pilot plant. Particle sizes within the range of 0.2 to 0.6 mm show the highest rates of nitrification and P removal at DO values ranging from 1.0 to 3.0 mg $O_2 \cdot L^{-1}$ due to the greater aerobic volume fraction resulting in higher abundances of PAO and AOB. Conversely, larger granules (>1 mm) demonstrate significantly lower ammonia oxidation rates, ranging from 1.4 to 4.7 times lower than the smaller granule sizes, consistent with their lower AOB abundance relative to the granule biomass. Therefore, for a DO concentration of 2.0 mg $O_2 \cdot L^{-1}$, the choice of size fractions in the range of 0.2 - 1.0 mm can result in higher N removal capacity and energy savings. Additionally, control of the aeration process is a valuable tool for optimizing the AGS granulation process and increasing SND treatment efficiency.

In general, a high DO level, while beneficial for complete nitrification, can lead to a deterioration of denitrification in the SND process [16]. On the other hand, an adequate aerobic rate and a low DO content favor the formation of a short-cut SND process in the AGS [198]. Huang et al. [99] reported that IA contributed to higher removal efficiencies of organics, N and P, faster granulation process, larger particle size, and more microbial communities than continuous aeration. The C/N ratio is an important parameter that influences the stability of the AGS technology and the SNDPR process. Su et al. [100] investigated the effect of different C/N ratios (20, 15, 10, 5) on the SNDPR process in

SBR-AGS and found that a C/N ratio of 10 favors the maintenance of a more compact structure of the granule sludge, whereas at a C/N ratio of 5 leads to granule disintegration. Furthermore, the results showed that different C/N ratios have a significant effect on the N removal rate of AGS but have little effect on the organic matter and P removal rate, in agreement with Zhou et al. [101]. Chen et al. [199] achieved a short-cut SND process in an AGS-SBR for the treatment of low COD/TN (≈4) ratio wastewater by tapered aeration. However, at a low COD/TN ratio, the P removal performance of the AGS-SBR can be unstable and require the addition of an external carbon source.

1.6 SND in bioelectrochemical systems

Bioelectrochemical systems (BES) have been proposed as a technology to revolutionize conventional energy-intensive processes into integrated systems that simultaneously recover energy, nutrients, and other value-added products [200]. BES use microorganisms to catalyze oxidation and reduction reactions at electrodes. The microorganisms can engage directly with the electrode, improving electron transfer efficiency and increasing cell activity. Electric field stimulation also promotes the formation of electrochemically active bacteria (EAB) [201]. Typically, anaerobic bacteria oxidize organic matter in wastewater to CO_2, using the anode as a terminal electron acceptor. As organic matter is degraded, electrons are released and transported by extracellular transport mechanisms to the anode, which is at a higher potential than the organic substrate. These electrons then traverse an external circuit, passing through a load (resistor) to reach the cathode. Finally, the electrons are consumed in the reduction of electron acceptors such as O_2, NO_3^-, and metal ions at the cathode [202].

BES can be broadly categorized into microbial fuel cells (MFCs), microbial electrosynthesis cells (MESs), and microbial electrolysis cells (MECs) [203]. A MFC

combines the oxidation of a substrate at a low redox potential with the reduction of an electron acceptor at a higher redox potential to produce electricity. One or both reactions are catalyzed at the electrode surface by microorganisms [204]. A MES is a sustainable and cost-effective biotechnology for efficiently converting pollutants, carbon dioxide (CO_2), and waste into useful chemicals [205]. In MECs, electrons and protons are generated at the anode by the degradation of organic substrates and transferred to the cathode via an external circuit containing a power supply and an ion-exchange membrane, respectively [206]. At the cathode, hydrogen (H_2) is produced by the reduction of protons or water [207].

Watanabe et al. [208] investigated the performance of SND in BES consisting of anode and cathode electrodes to which nitrifying and denitrifying biofilms were adhered, respectively. The results showed that the nitrification rate can improve as the applied current increases, even at lower DO concentrations. This suggests that nitrification takes place within the anodic biofilm, using the oxygen generated by the electrolysis of the water and that present in the suspended liquid. Furthermore, the denitrification rate remained consistently high at high DO concentrations due to the addition of H_2 in the cathodic biofilm. Recently, Song et al. [86] proposed a stainless steel tube as an anaerobic single-chamber MEC for investigating autotrophic SND under different voltages (1.8 V, 1.5 V, 1.2 V) applied by DC power, using ammonia as the only electron donor. The authors showed that when the voltage was applied at 1.5 V, a TN removal efficiency of 45% can be achieved, indicating a direct dependence between the reactions at the applied potential, as reported also by Zheng et al. [209]. In contrast, several studies have reported SND in MFCs showing also a linear relationship between TN removal performance with energy production [204,210]. In a recent study, San-Martín et al. [211] explored the SND

process in a 150 L BES-based pilot plant comprising five autonomous modules connected hydraulically and electrically in parallel. The initial step involves feeding the fresh waste effluent to the anodic side of each module to facilitate the oxidation of organic matter. Subsequently, the effluent is directed to a packed-bed column reactor to facilitate the conversion of ammonia into nitrate. Finally, the effluent from the column is directed to the cathodic side of each module to undergo denitrification. The results showed that although the removal rates of total organic carbon (TOC) and TN averaged 80% and 70%, respectively, with a specific energy consumption of 0.18 $kWh \cdot m^{-3}$, the external nitrification reactor was not able to convert all the ammonia to nitrate, limiting the denitrification process to the cathode.

1.7 Mathematical modeling of SND in biofilm reactors

Modeling is an effective tool for better understanding the interrelationships between different operating conditions, analyzing different treatment scenarios, and optimizing the processes involved in WWTPs [212]. To date, several models have been developed to evaluate the SND process in different biological reactors. Activated sludge models (ASM) are the most commonly used in optimization studies for municipal and industrial wastewater treatment plants, as they represent microbial development and substrate utilization in an activated sludge system. They are integrated into most of the currently used simulation software, e.g. Simba# (Ifak GmbH, Magdeburg, Germany), GPS-X^{TM} (Hamilton, Ontario), AQUASIM® (EAWAG, Switzerland), BioWin (Envirosim Associates Ltd.) and WEST (MKE DHI®) [213]. Dolatshah et al. [214] used GPS-X software to predict influent and effluent COD concentrations while operating an IFAS for the SND process, treating industrial wastewater under various operational conditions. The

congruence between experimental and calibrated data indicates that GPS-X accurately models the IFAS system and establishes it as a reliable tool for predicting effluent quality by adjusting operational parameters. Baek et al. [215] developed a mathematical model using AQUASIM 2.0 for the SND process in an MBR for the treatment of diluted municipal wastewater under low DO conditions (< 0.6 mg $O_2 \cdot L^{-1}$) using ASM No. 1 (ASM1). The model showed that the most sensitive coefficients are related to the growth of heterotrophic biomass, indicating its predominance in the total biomass. In addition, a decrease in AOB and NOB was also observed as a result of the decrease in the DO concentration. The dynamic simulations using BioWin software 3.0 were also used to evaluate the effect of SND on N removal performance and filamentous microorganism diversity of an MBR [216].

CHAPTER 2

Modeling complete and shortcut simultaneous nitrification and denitrification coupled to phosphorus removal in moving bed biofilm reactors

This Chapter has been published as:

Lanzetta A., Mattioli D., Di Capua F., Minieri V., Papirio S., Esposito G. Modeling complete and shortcut simultaneous nitrification and denitrification coupled to phosphorus removal in moving bed biofilm reactors, Journal of Water Process Engineering, Volume 59, 2024, 105022, ISSN 2214-7144, https://doi.org/10.1016/j.jwpe.2024.105022.

Nomenclature

μ_{AOB}	maximum specific growth rate AOB [d^{-1}]
$b_{AOB,aerobic}$	aerobic decay rate AOB [d^{-1}]
$b_{AOB,anoxic/anaerobic}$	anoxic/anaerobic decay rate AOB [d^{-1}]
$K_{SB,AOB}$	substrate half saturation AOB [mg $N \cdot L^{-1}$]
$K_{O2,AOB}$	ammonia oxidizing DO half saturation [mg $O_2 \cdot L^{-1}$]
μ_{NOB}	maximum specific growth rate NOB [d^{-1}]
$b_{NOB,aerobic}$	aerobic decay rate NOB [d^{-1}]
$b_{NOB,anoxic/anaerobic}$	anoxic/anaerobic decay rate AOB [d^{-1}]
$K_{SB,NOB}$	substrate half saturation NOB [mg $N \cdot L^{-1}$]
$K_{O2,NOB}$	nitrite-oxidizing biomass DO half saturation [mg $O_2 \cdot L^{-1}$]
μ_H	maximum specific growth rate OHO [d^{-1}]
Y_H	heterotrophic biomass yield [mg COD·mg COD^{-1}]
$b_{H,aerobic}$	aerobic decay rate OHO [d^{-1}]
$b_{H,anoxic}$	anoxic decay rate OHO [d^{-1}]
$K_{SB,OHO}$	substrate half saturation OHO [mg $COD \cdot L^{-1}$]
μ_{PAO}	maximum specific growth rate PAO [d^{-1}]
Y_{PAO}	PAO biomass yield [mg COD·mg COD^{-1}]
$b_{PAO,anaerobic}$	anaerobic decay rate PAO [d^{-1}]
$b_{PAO,anoxic/aerobic}$	anoxic/aerobic decay rate PAO [d^{-1}]
$K_{SB,PAO}$	substrate half saturation PAO [mg $COD_{PHB} \cdot$mg COD_{PAO}^{-1}]
$K_{O2,PAO}$	phosphorus accumulating DO half saturation [mg $O_2 \cdot L^{-1}$]
$K_{P\ uptake}$	phosphate uptake half saturation constant [mg $P \cdot L^{-1}$]
Diff. N-NH_4^+	biofilm diffusivity of N-NH_4^+ [$m^2\ d^{-1}$]

Diff. N-NO_3^-	biofilm diffusivity of N-NO_3^- [$m^2\ d^{-1}$]
Diff. N-NO_2^-	biofilm diffusivity of N-NO_2^- [$m^2\ d^{-1}$]
Diff. oxygen	biofilm diffusivity of oxygen [$m^2\ d^{-1}$]
Diff. acetate	biofilm diffusivity of acetate [$m^2\ d^{-1}$]
Diff. acetate	biofilm diffusivity of acetate [$m^2\ d^{-1}$]
Diff. neta	80% of the specified effective diffusivities [-]
FZno	fraction of total influent COD which is nitrite-oxidizing organisms [g COD·g COD^{-1}]
L1	Film surface area to media area ratio – max [μm]

2.1. Introduction

The removal of nitrogen (N) and phosphorus (P) from wastewater is of crucial importance in controlling the eutrophication process, which is responsible for the excessive growth of algae and, consequently, a depletion of dissolved oxygen (DO) in the receiving water bodies [217–220]. Conventionally, biological N removal (BNR) in wastewater treatment plants (WWTPs) includes autotrophic nitrification and heterotrophic denitrification implemented in sequence according to different possible configurations [221]. During the first step of nitrification, ammonium is oxidized to nitrite (NO_2^-) by ammonia-oxidizing bacteria (AOB) by consuming 1.5 mol of O_2. Specifically, NH_4^+ is first oxidized to hydroxylamine (NH_2OH) by the enzyme ammonia monooxygenase (AMO). Next, NH_2OH is oxidized to NO_2^- by hydroxylamine oxidoreductase (HAO) [45]. In the nitratation step carried out by nitrite-oxidizing bacteria (NOB), the NO_2^- produced during nitritation is rapidly converted to NO_3^- through the catalysis of the enzyme nitrite oxidoreductase (NXR) with the consumption of 0.5 mol of O_2. Heterotrophic denitrification consists of nitrate (NO_3^-) reduction to dinitrogen gas (N_2) under anoxic conditions with organic carbon as the electron donor [222]. However, this approach results in energy-intensive aeration [15], high capital and operating costs, a large footprint, and high sludge production [121].

Phosphorus removal primarily relies on methods such as adsorption, chemical precipitation, or biological processes [7–9]. Compared to the other P removal systems, enhanced biological phosphorus removal (EPBR) with activated sludge systems is a cost-effective and environmentally sustainable alternative to chemical treatment [10, 14]. The EBPR process achieves P removal by cycling anaerobic-aerobic metabolisms of phosphate-accumulating organisms (PAO) [25].

Simultaneous nitrification and denitrification (SND) is considered a promising alternative to conventional nitrification and denitrification processes for N removal within a single bioreactor, as it offers several advantages mainly associated with a lower footprint, carbon demand, sludge production, and oxygen requirement [58]. Moreover, no recirculation of nitrified effluent is needed, which simplifies the process scheme and reduces the energy requirement. One of the main factors affecting the successful occurrence of SND is the oxygen diffusion limitation, which leads to the formation of an anoxic microenvironment in the inner parts of sludge flocs or adhered biofilms and allows the coexistence of autotrophic nitrifying and heterotrophic denitrifying microorganisms at different layers of the same stratified structure [122].

Recent studies showed that the SND process can be coupled to successful phosphorus removal [18,68]. According to Zaman et al [68], the simultaneous nitrification, denitrification, and phosphorus removal (SNDPR) process requires less organic matter and DO consumption than the conventional biological phosphorus removal. Recent research has also focused on the shortcut (or partial) SND pathway involving partial nitrification or *nitritation* (NH_4^+ oxidation to NO_2^-) and *denitritation* (NO_2^- reduction to N_2) instead of complete nitrification and denitrification pathways. By eliminating the NO_2^- oxidation (*nitratation*) step, the shortcut pathway is advantageous compared to the complete pathway as less organic carbon and oxygen are needed for BNR. However, suppression of NOB activity is needed, which can be pursued via several strategies, including strict control of DO, pH, solid retention time (SRT), temperature, and concentrations of free ammonia and nitrous acid [58].

To date, various bioreactor configurations have been tested for SND processes, including the sequential batch reactor (SBR) [95,224], membrane bioreactor (MBR) [103], moving

bed biofilm reactor (MBBR) [12–14], and aerobic granular sludge (AGS) reactor [15, 16]. Compared with suspended-growth systems, biofilm-based technologies have shown several advantages, including higher biomass concentration, lower space requirements, shorter retention time, reduced sludge production, and more stable performances [225].

The growing interest in biofilm-based treatment processes has been accompanied by an increasing focus on their numerical analysis and biofilm modeling studies. Mathematical modeling is an important tool to predict the performance of a biological treatment, determine important variables and critical parameters, and aid in troubleshooting [226]. Additionally, the use of simulations during modeling can improve the WWTP design by providing different bioreactor operation scenarios [227]. Many biofilm models are incorporated in most of the currently used simulation software, such as Simba# (Ifak GmbH, Magdeburg, Germany), AQUASIM® (EAWAG, Switzerland), BioWin (Envirosim Associates Ltd.), and WEST (MIKE DHI®) [213]. The dynamic mixed-culture biofilm model implemented in BioWin belongs to the class of 1D models, as described by Wanner and Reichert [228,229]. In summary, the mathematical model of mixed-culture biofilms consists of a series of 1D mass balance equations that allow to model the progression of biofilm thickness as well as the spatial distribution and development over time of various dissolved (nutrients, electron donors, and electron acceptors) and particulate components (microbial cells, extracellular polymeric substances, organic and inorganic particles) in a biofilm as a function of transport and transformation processes [228,230].

Compared to the previous multispecies biofilm models [231], the dynamic mixed-culture biofilm model of BioWin permits a more flexible description of the transport of dissolved components in the biofilm and considers the diffusive transport of particulate components

in the biofilm solid matrix, changes in the biofilm liquid phase volume fraction (porosity), and simultaneous detachment and attachment of cells and particles at the biofilm surface [228]. The process model integrated with the biofilm model in BioWin is the activated sludge/anaerobic digestion model (ASDM), which allows to simulate the complex interactions occurring in the aerobic, anoxic, and anaerobic layers of the biofilm. Despite the growing interest in SND processes and the empirical mathematical models supporting their successful implementation, calibrated models using experimental data are scarce in the literature [25, 26]. Specifically, none of the abovementioned studies include the modeling of the complete and shortcut SNDPR processes.

The present study contributes to filling the existing gap in this field by modeling complete and shortcut SNDPR in MBBRs based on the data collected from two different experimental campaigns conducted at a laboratory scale by Iannacone et al. [21,83]. The main objective of this work is to assess whether a calibrated and validated model could accurately predict the experimental results. By using the BioWin software, different operating conditions, including dissolved oxygen (DO), feed carbon-to-nitrogen (C/N) ratio, and hydraulic retention time (HRT), were simulated with the aim of investigating the main impacts on the process in terms of removal of the main wastewater contaminants (i.e., COD, ammonium, oxidized nitrogen species, and phosphate) and evolution of the dominant functional groups (i.e., AOB, NOB, ordinary heterotrophic organisms (OHO), and PAO). Additionally, the validated model from the second experimental campaign was used to test alternative scenarios to improve nutrient removal efficiencies, thus representing an important aid for potential future successful implementation and scale-up of the process.

2.2. Materials and methods

2.2.1. Experimental data

The experimental data from two different campaigns [21,83] were used to calibrate and validate the biofilm model implemented in BioWin 6.0. Specifically, the studies were based on long-term (shortcut) SNDPR in continuous-flow MBBRs under different operational conditions, involving changes in C/N, HRT, and DO concentration, as reported in **Table 2.1.**

Table 2.1. Main operational conditions in terms of dissolved oxygen (DO), hydraulic retention time (HRT) and carbon-to-nitrogen (C/N) ratio of the two modeled experimental campaigns [21,83].

	Experimental campaign I				**Experimental campaign II**			
Period	Days	DO [mg $O_2 \cdot L^{-1}$]	HRT [d]	Feed C/N	Days	DO [mg $O_2 \cdot L^{-1}$]	HRT [d]	Feed C/N
P1	0-13	0.2-2.0	1	4.2±0.3	0-41	0.2-3.0	1	3.5±0.3
P2	14-30	0.2-2.0	1	2.8±0.5	42-69	0.2-3.0	1	3.0±0.3
P3	31-58	0.2-3.0	1	2.9±0.3	70-83	0.2-2.0	1	3.4±0.1
P4	59-76	0.2-4.0	1	2.8±0.1	84-95	0.2-3.0	1	3.3±0.1
P5	77-89	0.2-3.0	1	2.8±0.1	96-125	0.2-3.0	1	4.0±0.2
P6	90-140	0.2-3.0	1	3.6±0.4		/	/	/

The MBBRs were fed exclusively with synthetic wastewater containing acetate, NH_4^+, and PO_4^{3-} as the main sources of organic carbon, nitrogen, and phosphorus, respectively. DO, pH, and HRT were monitored as reported by Iannacone et al. [21,83].

The first experimental campaign lasted 137 days and was divided into 6 experimental periods (P1-P6). The continuous-flow MBBR (intermittent-aeration MBBR, IAMBBR)

was operated under alternating microaerobic and aerobic conditions with the aim of removing carbon, nitrogen, and phosphorus through SNDPR [21]. The HRT was set to 1 day and different DO conditions and C/N ratios were tested. The values of the input parameters used in BioWin for the simulations are reported in **Table 2.2**. The input flow rate was constant for the entire calibration and validation periods and equal to 0.02 $m^3 \cdot d^{-1}$ in accordance with the HRT value of 1 day. The fractionation of total COD (tCOD), TKN, total phosphorous (TP), and total sulfur (TS) used in the BioWin model are reported in **Table 2.3**. In particular, the fraction of acetate was set to the maximum value allowed of 0.97 to simulate the presence of only readily biodegradable organic matter in the influent. The temperature was set at 22°C according to the experimental campaign, while to reproduce the DO profiles of the microaerobic-aerobic cycles applied during the experimental campaign [21] an oxygen time trend based on the experimental DO profiles was considered for the simulations (**Table 2.4**). For the first two experimental periods (P1 and P2), as detailed experimental data were not available, the DO concentration trend used for the simulation was reproduced considering the experimental DO ranges, while for P3-P6 a cyclic variation in oxygen over time was reconstructed based on the experimental DO profiles.

Table 2.2. Experimental data set used for calibration of first experimental campaign in terms of total chemical demand (tCOD), total Kjendahl nitrogen (TKN), total phosphorus (TP), total sulfur (TS), $N\text{-}NO_3^-$, pH, alkalinity, total inorganic suspended solid (tISS), calcium (Ca^{2+}) and magnesium ions (Mg^{2+}).

Days	tCOD (mgCOD L^{-1})	TKN (mgN L^{-1})	TP (mgP L^{-1})	TS (mgS L^{-1})	N-NO_3^- (mgN L^{-1})	pH	Alkalinity (mmol L^{-1})	tISS (mgISS L^{-1})	Ca^{2+} (mg L^{-1})	Mg^{2+} (mg L^{-1})
3	338	30.1	11.6	3.0	1.0	7.95	21.7	2.0	117.6	42.9
4	322	33.7	11.7	3.0	1.0	8.01	21.0	2.0	117.6	42.9
5	324	34.0	11.9	3.0	1.0	7.80	20.6	2.0	117.6	42.9

Days	tCOD (mgCOD L^{-1})	TKN (mgN L^{-1})	TP (mgP L^{-1})	TS (mgS L^{-1})	N-NO_3^- (mgN L^{-1})	pH	Alkalinity (mmol L^{-1})	tISS (mgISS L^{-1})	Ca^{2+} (mg L^{-1})	Mg^{2+} (mg L^{-1})
6	334	34.0	11.9	3.0	1.0	7.79	20.7	2.0	117.6	42.9
9	313	43.7	11.1	3.0	1.0	7.95	20.6	2.0	117.6	42.9
10	360	32.1	11.2	3.0	1.0	7.78	20.5	2.0	117.6	42.9
11	349	34.0	11.1	3.0	1.0	7.66	21.9	2.0	117.6	42.9
12	431	31.6	11.5	3.0	1.0	7.67	22.3	2.0	117.6	42.9
13	283	32.0	10.2	3.0	1.0	7.69	20.7	2.0	117.6	42.9
16	250	35.3	8.9	3.0	1.0	7.72	22.3	2.0	117.6	42.9
17	242	35.1	9.8	3.0	1.0	7.82	22.3	2.0	117.6	42.9
18	250	34.3	8.4	3.0	1.0	7.88	22.2	2.0	117.6	42.9
19	218	36.2	9.8	3.0	1.0	7.85	21.2	2.0	117.6	42.9
20	223	32.8	11.3	3.0	1.0	7.85	20.8	2.0	117.6	42.9
23	231	32.8	10.8	3.0	1.0	7.76	20.9	2.0	117.6	42.9
24	231	32.1	10.8	3.0	1.0	7.84	21.4	2.0	117.6	42.9
25	231	33.1	10.4	3.0	1.0	7.94	21.5	2.0	117.6	42.9
26	231	33.4	10.4	3.0	1.0	8.03	20.9	2.0	117.6	42.9
27	231	34.9	10.4	3.0	1.0	7.83	20.9	2.0	117.6	42.9
30	231	34.7	8.6	3.0	1.0	7.83	20.5	2.0	117.6	42.9
31	231	34.3	10.5	3.0	1.0	7.83	20.6	2.0	117.6	42.9
32	281	35.1	10.1	3.0	1.0	7.90	21.2	2.0	117.6	42.9
33	275	35.1	10.5	3.0	1.0	7.86	21.3	2.0	117.6	42.9
34	252	35.1	10.5	3.0	1.0	7.94	20.6	2.0	117.6	42.9
37	228	33.2	10.8	3.0	1.0	7.84	21.2	2.0	117.6	42.9
38	252	34.5	12.9	3.0	1.0	7.79	18.5	2.0	117.6	42.9
39	252	34.7	11.1	3.0	1.0	7.81	21.4	2.0	117.6	42.9
40	252	33.3	10.9	3.0	1.0	7.85	21.0	2.0	117.6	42.9
41	252	32.3	10.5	3.0	1.0	7.93	21.6	2.0	117.6	42.9
44	229	32.5	11.1	3.0	1.0	7.84	20.9	2.0	117.6	42.9
45	281	32.1	11.5	3.0	1.0	7.94	21.0	2.0	117.6	42.9
46	230	33.5	12.1	3.0	1.0	7.84	20.4	2.0	117.6	42.9
47	281	31.2	10.4	3.0	1.0	7.83	20.7	2.0	117.6	42.9
48	275	33.1	10.6	3.0	1.0	7.86	20.8	2.0	117.6	42.9
51	208	30.5	11.5	3.0	1.0	7.98	21.6	2.0	117.6	42.9
52	237	32.4	10.8	3.0	1.0	8.11	19.7	2.0	117.6	42.9
53	237	32.0	11.5	3.0	1.0	7.77	20.1	2.0	117.6	42.9
54	237	32.5	11.5	3.0	1.0	7.77	0.0	2.0	117.6	42.9
55	237	32.2	11.5	3.0	1.0	8.02	20.3	2.0	117.6	42.9
58	237	34.4	11.4	3.0	1.0	8.20	21.4	2.0	117.6	42.9
59	237	33.9	11.0	3.0	1.0	7.89	21.2	2.0	117.6	42.9
60	195	34.4	11.0	3.0	1.0	8.06	20.1	2.0	117.6	42.9
61	195	33.1	11.1	3.0	1.0	7.82	20.7	2.0	117.6	42.9
62	195	31.5	11.0	3.0	1.0	8.03	20.1	2.0	117.6	42.9
65	195	33.5	10.9	3.0	1.0	7.96	20.0	2.0	117.6	42.9
66	195	34.6	10.9	3.0	1.0	8.05	21.2	2.0	117.6	42.9
67	195	34.6	10.7	3.0	1.0	7.93	21.2	2.0	117.6	42.9
68	195	32.3	10.8	3.0	1.0	7.90	20.2	2.0	117.6	42.9
69	195	33.0	10.7	3.0	1.0	7.89	20.2	2.0	117.6	42.9
72	195	32.4	11.1	3.0	1.0	8.06	21.0	2.0	117.6	42.9
73	195	34.9	9.4	3.0	1.0	7.80	21.3	2.0	117.6	42.9
74	237	34.1	10.7	3.0	1.0	7.82	21.6	2.0	117.6	42.9
75	237	33.4	9.9	3.0	1.0	7.84	21.1	2.0	117.6	42.9
76	237	34.4	9.8	3.0	1.0	7.88	21.4	2.0	117.6	42.9
79	237	35.0	9.3	3.0	1.0	7.83	21.4	2.0	117.6	42.9
80	244	32.7	9.9	3.0	1.0	7.87	21.6	2.0	117.6	42.9
81	244	32.1	11.2	3.0	1.0	7.69	20.8	2.0	117.6	42.9

Days	tCOD (mgCOD L^{-1})	TKN (mgN L^{-1})	TP (mgP L^{-1})	TS (mgS L^{-1})	N-NO_3^- (mgN L^{-1})	pH	Alkalinity (mmol L^{-1})	tISS (mgISS L^{-1})	Ca^{2+} (mg L^{-1})	Mg^{2+} (mg L^{-1})
82	244	33.0	10.8	3.0	1.0	7.58	19.4	2.0	117.6	42.9
83	244	33.2	10.1	3.0	1.0	7.67	19.5	2.0	117.6	42.9
86	244	33.8	9.4	3.0	1.0	7.74	19.8	2.0	117.6	42.9
87	325	33.5	10.3	3.0	1.0	7.70	20.4	2.0	117.6	42.9
88	286	34.1	10.7	3.0	1.0	7.81	20.5	2.0	117.6	42.9
89	281	33.0	11.2	3.0	1.0	7.84	20.4	2.0	117.6	42.9
90	273	33.0	10.8	3.0	1.0	7.91	20.7	2.0	117.6	42.9
94	273	32.0	10.8	3.0	1.0	7.97	21.0	2.0	117.6	42.9
95	299	32.7	10.8	3.0	1.0	7.72	20.5	2.0	117.6	42.9
96	296	33.5	10.8	3.0	1.0	7.73	20.3	2.0	117.6	42.9
97	286	33.0	11.1	3.0	1.0	7.79	20.5	2.0	117.6	42.9
109	344	33.9	10.2	3.0	1.0	7.82	22.5	2.0	117.6	42.9
110	326	33.5	10.3	3.0	1.0	7.81	21.0	2.0	117.6	42.9
112	326	33.5	10.3	3.0	1.0	7.90	21.6	2.0	117.6	42.9
116	286	33.5	10.8	3.0	1.0	7.79	21.0	2.0	117.6	42.9
117	322	33.5	10.8	3.0	1.0	7.80	21.3	2.0	117.6	42.9
118	299	33.5	10.8	3.0	1.0	7.83	21.0	2.0	117.6	42.9
119	269	33.5	10.8	3.0	1.0	7.94	21.2	2.0	117.6	42.9
122	273	33.5	10.8	3.0	1.0	7.94	21.6	2.0	117.6	42.9
123	341	32.7	11.1	3.0	1.0	7.92	21.9	2.0	117.6	42.9
124	308	34.7	10.5	3.0	1.0	7.92	23.4	2.0	117.6	42.9
125	248	33.6	10.5	3.0	1.0	7.94	23.5	2.0	117.6	42.9
126	308	33.7	10.2	3.0	1.0	7.94	22.8	2.0	117.6	42.9
129	308	30.7	11.1	3.0	1.0	7.87	22.5	2.0	117.6	42.9
130	248	31.1	11.1	3.0	1.0	7.85	21.9	2.0	117.6	42.9
131	237	32.4	11.1	3.0	1.0	7.89	21.4	2.0	117.6	42.9
132	348	31.7	11.1	3.0	1.0	7.71	21.3	2.0	117.6	42.9
133	308	32.4	11.1	3.0	1.0	8.00	21.4	2.0	117.6	42.9
136	341	33.9	11.1	3.0	1.0	7.83	21.0	2.0	117.6	42.9
137	325	33.3	11.1	3.0	1.0	7.94	21.2	2.0	117.6	42.9

Table 2.3. Wastewater fractions used in BioWin models.

Components	Unit	Period I
Fbs – readily biodegradable organic matter (including acetate) *	gCOD g total COD $^{-1}$	0.9700
Fac- acetate*	gCOD g readily biod. COD^{-1}	1.0000
Fxsp – Non colloidal slowly biodegradable*	gCOD g slowly biod. COD^{-1}	0
Fus – Unbiodegradable soluble COD*	gCOD g total COD^{-1}	0
Fup – unbiodegradable particulate COD*	gCOD g total COD^{-1}	0
Fcel – Cellulose fraction of unbiodegradable particulate	gCOD gCOD^{-1}	0.5000
Fna – Ammonia*	gNH_4-N gTKN^{-1}	0.9700
Fnox – Particulate organic nitrogen	gN g Organic N^{-1}	0.5000
Fnus - Soluble unbiodegradable TKN*	gN gTKN^{-1}	0
FupN N:COD ratio for unbiodegradable part. COD	gN gCOD^{-1}	0.0700
Fpo4 – Phosphate*	gPO_4-P gTP^{-1}	0.9700
FupP – P:COD ratio for unbiodegradable part. COD	gP gCOD^{-1}	0.0220
Fsr – Reduced sulfur [H_2S]	gS gS^{-1}	0.1500
FZbh – Ordinary heterotrophic COD fraction	gCOD g total COD^{-1}	0.0200
FZbm – Methylotrophic COD fraction	gCOD g total COD^{-1}	0.0001
FZao – Ammonia oxidizing COD fraction*	gCOD g total COD^{-1}	0.001
FZno – Nitrite oxidizing COD fraction*	gCOD g total COD^{-1}	0.001
FZaao – Anaerobic ammonia oxidizing COD fraction	gCOD g total COD^{-1}	0.0001
FZppa – Phosphorus accumulating COD fraction	gCOD g total COD^{-1}	0.0001
FZpa – Propionic acetogenic COD fraction	gCOD g total COD^{-1}	0.0001
FZam – Acetoclastic methanogenic COD fraction	gCOD g total COD^{-1}	0.0001
FZhm – Hydrogenotrophic methanogenic COD fraction	gCOD g total COD^{-1}	0.0001
FZso – Sulfur oxiding COD fraction	gCOD g total COD^{-1}	0.0001
FZsrpa – Sulfur reducing propionic acetogenic COD fraction	gCOD g total COD^{-1}	0.0001
FZsra – Sulfur reducing acetotrophic COD fraction	gCOD g total COD^{-1}	0.0001
FZsrh – Sulfur reducing hydrogenotrophic COD fraction	gCOD g total COD^{-1}	0.0001
FZe – Endogenous products COD fraction	gCOD g total COD^{-1}	0

* Modified from BioWin default values

Table 2.4. Trend of DO concentration (mg $O_2 \cdot L^{-1}$) used during the dynamic calibration for each period of the modeled second experimental campaign to simulate the experimental DO concentrations.

Time (min)	P1	P2	P3	P4	P5	P6
0	0.20	0.20	0.20	0.20	0.20	0.20
5	0.65	0.65	0.76	0.96	0.90	0.90
10	1.10	1.10	1.32	1.72	1.60	1.60
15	1.55	1.55	1.88	2.48	2.30	2.30
20	2.00	2.00	2.44	3.24	3.00	3.00
25	1.82	1.82	3.00	4.00	2.25	2.23
30	1.65	1.65	2.44	3.25	1.50	1.45
35	1.47	1.47	1.87	2.50	0.75	0.68
40	1.30	0.52	1.31	1.75	0.64	0.58
45	1.02	1.02	0.74	1.00	0.53	0.49
50	0.75	0.75	0.18	0.25	0.42	0.39
55	0.47	0.47	0.19	0.23	0.31	0.30
60	0.20	0.20	0.19	0.22	0.20	0.20
65	0.20	0.20	0.20	0.20	0.20	0.20
70			0.20	0.20		
75			0.20	0.20		
80				0.20		
85				0.20		
90				0.20		

The second experimental campaign lasted 125 days and investigated the feasibility of coupling shortcut SND with biological P removal in two continuous-flow IAMBBRs alternating microaerobic and aerobic conditions and fed with two different carbon sources, i.e., ethanol and acetate [83].

The reactors were operated at an HRT of 1 day, DO ranges of 0.2-3.0 mg $O_2 \cdot L^{-1}$, and feed C/N ratios between 3.6 and 4.0 in both reactors (**Table 2.1**) [13]. NOB activity was inhibited by cultivating the biomass at a temperature of 26-28°C, a pH of 8.2±0.2, and an SRT of 4 days before MBBR inoculation. The input dataset used in BioWin for the

simulations is reported in **Table 2.5**. The input flow rate was constant for the entire calibration and validation periods in accordance with the calibration of the first experimental campaign. The temperature value set in the model was higher than the temperature during the first experimental campaign and equal to 30°C (on average), according to the temperature measured during the experiment (in the range of 26-32°C). To reproduce the experimental aeration conditions [83], a time trend of the DO based on the experimental data was considered during the dynamic simulations (**Table 2.6**). In the absence of experimental data, BioWin's default values were used to set the initial values, and a steady-state simulation was performed. This simulation generated the initial values of the main active biomasses used in the dynamic simulation of both experimental campaigns.

Table 2.5. Experimental data set used for the calibration of second experimental campaign in terms of total chemical demand (tCOD), total Kjeldahl nitrogen (TKN), total phosphorus (TP), total sulfur (TS), N-NO_3^-, pH, alkalinity, total inorganic suspended solid (tISS), calcium (Ca^{2+}) and magnesium ions (Mg^{2+}).

Days	tCOD (mgCOD L^{-1})	N-TKN (mgN L^{-1})	TP (mgP L^{-1})	TS (mgS L^{-1})	N-NO_3^- (mgN L^{-1})	pH	Alkalinity (mmol L^{-1})	tISS (mgISS L^{-1})	Ca^{2+} (mg L^{-1})	Mg^{2+} (mg L^{-1})
1	246	26	8.9	3.0	1.0	7.73	23.8	2.0	117.6	42.9
4	259	27	8.7	3.0	1.0	8.11	23.3	2.0	117.6	42.9
5	276	27	9.0	3.0	1.0	8.11	23.9	2.0	117.6	42.9
6	228	28	8.6	3.0	1.0	8.20	24.4	2.0	117.6	42.9
8	234	27	9.1	3.0	1.0	7.65	23.5	2.0	117.6	42.9
11	236	27	10.5	3.0	1.0	7.80	24.1	2.0	117.6	42.9
12	190	26	8.1	3.0	1.0	7.91	24.0	2.0	117.6	42.9
14	222	26	7.5	3.0	1.0	7.94	23.3	2.0	117.6	42.9
15	263	26	8.5	3.0	1.0	7.75	23.4	2.0	117.6	42.9
18	255	27	8.6	3.0	1.0	7.89	24.1	2.0	117.6	42.9
19	272	27	8.6	3.0	1.0	7.88	22.3	2.0	117.6	42.9
20	218	26	8.7	3.0	1.0	7.95	25.4	2.0	117.6	42.9
21	234	26	8.5	3.0	1.0	7.85	23.0	2.0	117.6	42.9
23	250	26	8.1	3.0	1.0	8.14	23.9	2.0	117.6	42.9
27	248	26	7.7	3.0	1.0	8.18	23.5	2.0	117.6	42.9
32	243	26	8.1	3.0	1.0	8.00	24.5	2.0	117.6	42.9
35	214	26	7.7	3.0	1.0	7.80	24.0	2.0	117.6	42.9

Days	tCOD (mgCOD L^{-1})	N-TKN (mgN L^{-1})	TP (mgP L^{-1})	TS (mgS L^{-1})	N-NO_3^- (mgN L^{-1})	pH	Alkalinity (mmol L^{-1})	tISS (mgISS L^{-1})	Ca^{2+} (mg L^{-1})	Mg^{2+} (mg L^{-1})
37	222	26	8.9	3.0	1.0	8.11	25.0	2.0	117.6	42.9
39	222	26	8.8	3.0	1.0	7.90	24.0	2.0	117.6	42.9
41	215	26	8.4	3.0	1.0	7.94	24.0	2.0	117.6	42.9
43	202	25	3.6	3.0	1.0	7.90	24.0	2.0	117.6	42.9
46	205	25	4.3	3.0	1.0	8.12	24.5	2.0	117.6	42.9
47	209	25	4.3	3.0	1.0	8.24	24.5	2.0	117.6	42.9
49	243	27	4.0	3.0	1.0	8.24	24.3	2.0	117.6	42.9
50	216	26	4.1	3.0	1.0	8.07	25.0	2.0	117.6	42.9
53	207	26	4.2	3.0	1.0	8.20	25.8	2.0	117.6	42.9
55	207	26	4.6	3.0	1.0	8.06	24.3	2.0	117.6	42.9
56	207	26	4.4	3.0	1.0	8.06	24.3	2.0	117.6	42.9
57	197	25	4.2	3.0	1.0	7.99	24.0	2.0	117.6	42.9
60	221	24	4.2	3.0	1.0	8.22	25.0	2.0	117.6	42.9
61	208	26	3.7	3.0	1.0	8.22	25.0	2.0	117.6	42.9
62	203	25	4.0	3.0	1.0	8.22	25.0	2.0	117.6	42.9
64	205	25	4.0	3.0	1.0	8.22	25.0	2.0	117.6	42.9
68	198	26	4.4	3.0	1.0	8.22	24.5	2.0	117.6	42.9
69	208	26	4.4	3.0	1.0	8.22	24.3	2.0	117.6	42.9
71	236	26	10.1	3.0	1.0	7.85	26.0	2.0	117.6	42.9
77	257	26	9.2	3.0	1.0	8.15	23.9	2.0	117.6	42.9
78	248	27	9.5	3.0	1.0	8.15	24.0	2.0	117.6	42.9
82	244	26	9.1	3.0	1.0	8.01	23.5	2.0	117.6	42.9
83	234	26	8.5	3.0	1.0	8.23	23.8	2.0	117.6	42.9
84	226	26	8.5	3.0	1.0	8.20	23.8	2.0	117.6	42.9
85	202	26	8.4	3.0	1.0	8.25	24.0	2.0	117.6	42.9
88	226	26	8.5	3.0	1.0	8.22	24.3	2.0	117.6	42.9
91	229	26	8.4	3.0	1.0	8.20	24.3	2.0	117.6	42.9
92	222	26	9.1	3.0	1.0	8.15	25.3	2.0	117.6	42.9
95	231	26	8.3	3.0	1.0	8.25	24.0	2.0	117.6	42.9
97	259	26	8.9	3.0	1.0	7.97	24.0	2.0	117.6	42.9
99	287	26	7.9	3.0	1.0	7.99	25.3	2.0	117.6	42.9
103	260	26	8.1	3.0	1.0	8.19	25.5	2.0	117.6	42.9
104	283	25	8.2	3.0	1.0	7.91	25.7	2.0	117.6	42.9
106	275	26	8.3	3.0	1.0	8.06	26.0	2.0	117.6	42.9
109	237	25	8.0	3.0	1.0	8.19	25.3	2.0	117.6	42.9
111	289	26	8.4	3.0	1.0	8.00	24.8	2.0	117.6	42.9
113	289	25	8.4	3.0	1.0	8.08	24.5	2.0	117.6	42.9
118	263	27	8.0	3.0	1.0	8.25	25.0	2.0	117.6	42.9
119	300	27	8.9	3.0	1.0	8.30	25.0	2.0	117.6	42.9
122	270	28	8.9	3.0	1.0	8.33	24.8	2.0	117.6	42.9
125	287	28	8.5	3.0	1.0	7.92	24.8	2.0	117.6	42.9

Table 2.6. Oxygen time variation (mg $O_2 \cdot L^{-1}$) of the dynamic simulation for each period of the modeled second experimental campaign.

Time (min)	P1	P2	P3	P4	P5	P6
0	0.20	0.20	0.20	0.20	0.20	0.20
5	1.05	0.50	0.90	1.10	0.50	1.5
10	3.00	1.25	1.20	2.00	1.10	3
15	1.05	3.00	3.00	1.20	3.00	1.60
20	0.50	1.20	1.25	0.60	1.10	1.05
25	0.20	0.70	0.80	0.40	0.60	0.60
30	0.20	0.40	0.50	0.20	0.30	0.20
35	0.20	0.20	0.20	0.20	0.20	0.20
40	0.20	0.20	0.20	0.20	0.20	0.20
45	0.20	0.20	0.20		0.20	0.20
50		0.20	0.20		0.20	0.20
55			0.20			

2.2.2. Biofilm model calibration

Model calibration can be described as an iterative process to reproduce the observed values by adjusting input model parameters. The calibration procedure followed in this study was based on six main stages as proposed by Rieger [234], including 1) the identification of different calibration and validation datasets, 2) refinement of the stop criteria based on data quality and availability, 3) initial run of the model using default kinetics and stoichiometric parameter values on BioWin, 4) sensitivity analysis to obtain the reproduction of the biofilm models and optimize the efficiency of the calibration procedure, 5) calibration, and 6) validation.

The sensitivity analysis allows to check the sensitivity of the output variables to varying parameters, inputs, or initial conditions. The sensitivity analysis of the biofilm parameters was carried out using the normalized sensitivity coefficient ($S_{i,j}$), where *i* and *j* represent the input and output parameters, respectively. This coefficient is defined as the ratio between the output variable (Y_i) and the input variable (X_i) (**Eq. 1**), as reported by Eldyasti et al. [213].

$$S_{i,j} = \left| \frac{\Delta Y_i / Y_i}{\Delta X_i / X_i} \right| \quad (1)$$

The influence of the parameters was interpreted as proposed by Julien et al. [235]. If $S_{i,j}$ is equal to zero, the parameters have no influence. For $S_{i,j} < 0.25$, the influence of the parameter is not considered to be significant. If $0.25 < S_{i,j} < 1$, the parameter is influential. If $S_{i,j} > 1$, the parameters are very influential. The sensitivity analysis was carried out only for the first experimental campaign by increasing the selected parameter values by 5% compared to the default values and recording the effect on several output variables. Only the most influential parameters were considered for the calibration procedure. The analysis comprised 21 kinetic parameters of AOB, NOB, OHO, and PAO biomass, 5 diffusion coefficients, and 4 biofilm parameters.

The model calibration of the first experimental campaign was carried out using the monitoring data collected from periods P1 to P4 (**Table 2.1**). For the second experimental campaign, the model calibration was also performed using the monitoring data collected from periods P1 to P4 (**Table 2.1**) starting with the calibrated model from the previous experimental campaign. During the cultivation phase of the second experimental campaign, NOB growth in the MBBR was successfully inhibited by setting specific SRT, pH, and temperature conditions, as described in Section 2.1. To simulate the same conditions in the model, the μ_{NOB} and *FZno* parameters were set to 0 during a preliminary steady-state step.

To compare the measured and simulated data in the calibration and validation procedure, the absolute variance S_{ai} was chosen as the acceptance criterion **(Eq. 2)**:

$$S_{ai} = |\overline{y_s} - \overline{y_m}| \quad (2)$$

where y_s is the average simulated data and y_m is the average measured data.

For each experimental campaign, the absolute variance S_{ai} must be lower than 5% of y_m. A maximum S_{ai} value ($S_{ai,max}$) of 2.5 mg N·L^{-1} was considered acceptable for N-NH_4^+, N-NO_3^-, and N-NO_2^- concentrations. For COD and total P concentrations, maximum values of 20 mg COD·L^{-1} and 1.0 mg P·L^{-1} were considered. Furthermore, Thiel's inequality coefficient (*TIC*), as suggested by Hvala [236], (**Eq. 3**), and the normal objective function (*NOF*), as shown in **Eq. 4** [27], were chosen as additional acceptance criteria.

$$TIC = \frac{\sqrt{\sum_i (y_i - y_{m,i})^2}}{\sqrt{\sum_i y_i^2} + \sqrt{\sum_i y_{m,i}^2}} \quad (3)$$

.

$$NOF = \sqrt{\frac{\sum_i (y_i - y_{m,i})^2}{N}} \frac{N}{\sum_i y_i} \quad (4)$$

y_i represents the measured data points, $y_{m,i}$ represents the simulated data points, and N is the number of data points [237].

TIC values should be between 0 and 1, with values closer to 0 indicating a better model validity [27]. Zeng et al. [237] suggested that the values of *TIC* that do not exceed 0.3 are usually considered evidence of good agreement between the time series. Moreover, *NOF* values < 1 reveal good reproducibility between the experimental and modeled data.

2.3. Results and discussion

2.3.1. Modeling complete and shortcut SND in continuous-flow IAMBBR

2.3.1.1. Sensitivity analysis

The significant results of the sensitivity analysis for the soluble COD, $N\text{-}NH_4^+$, $N\text{-}NO_3^-$, $N\text{-}NO_2^-$, and $P\text{-}PO_4^{3-}$ concentrations, as well as for biomass thickness, are reported in **Figure 2.1**.

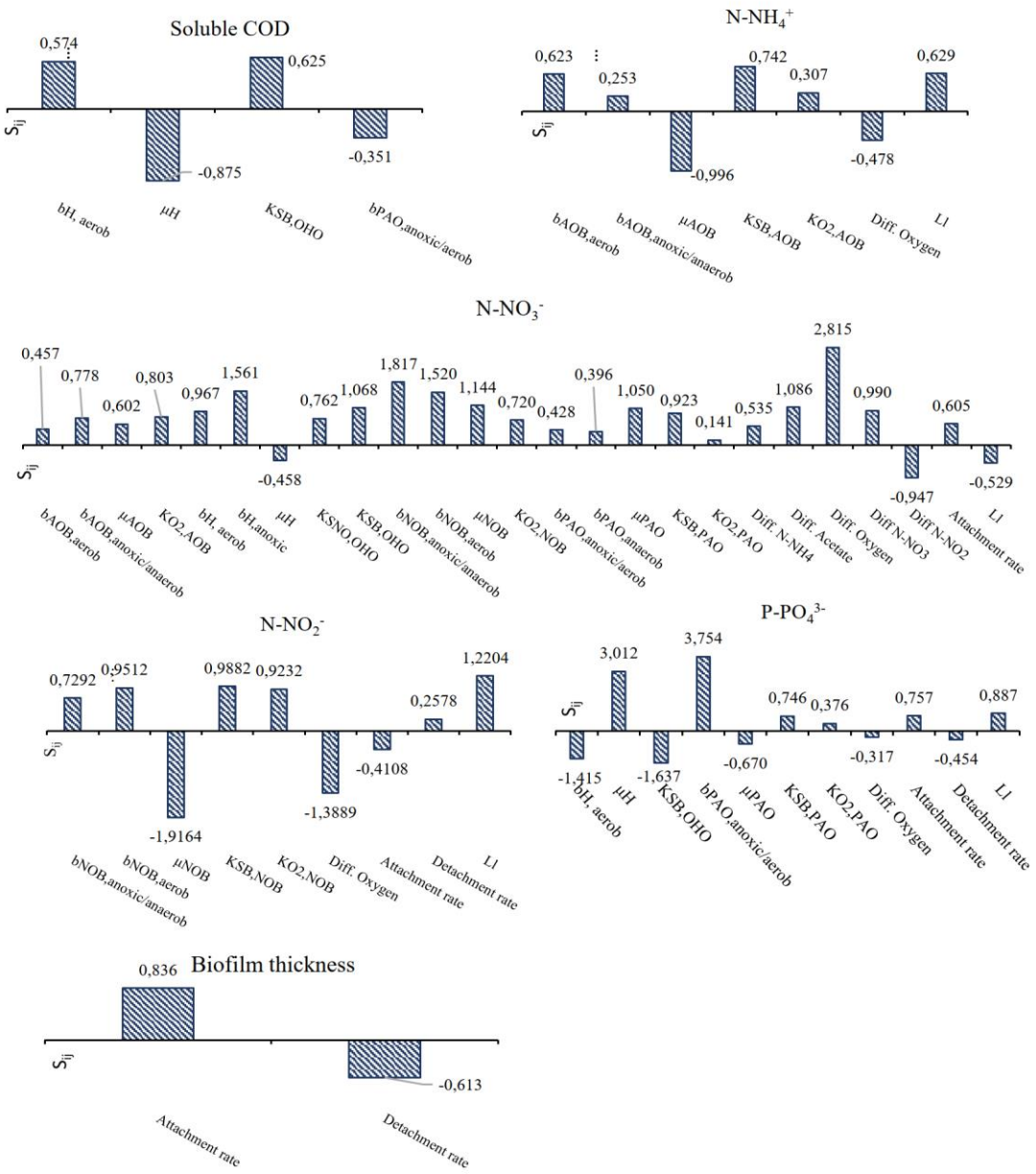

Figure 2.1. Influence of the main process parameters on the soluble COD, N-NH_4^+, N-NO_3^-, N-NO_2^-, P-PO_4^{3-} concentrations trend and modeled biomass thickness obtained in the first experimental campaign

The sensitivity analysis showed that the significant factors for COD and N-NH_4^+ abatement were linked to the growth of the heterotrophic and autotrophic biomass (i.e., μ_H and μ_{AOB}), respectively (**Figure 2.1**). The N-NO_3^- concentration was influenced by the

kinetic parameters of NOB (i.e., $b_{NOB,aerobic}$ and $b_{NOB,anoxic/anaerobic}$), OHO ($b_{H,anoxic}$), PAO (μ_{PAO}), and mainly by oxygen diffusivity in the biofilm, which can be ascribed to high sensitivity of denitrifiers to oxygen. Typically, the presence of oxygen has a detrimental effect on denitrifying activity through enzyme inhibition or alteration of their gene expression [238]. The NO_2^- concentration was mainly sensitive to changes in the kinetic parameters of NOB ($b_{aerobic,\,NOB}$, $b_{anaerobic,\,NOB}$, μ_{NOB}, $K_{SB,NOB}$) and oxygen diffusivity in the biofilm. For typical BNR, the NO_2^- generated from NH_4^+ oxidation is subsequently oxidized to NO_3^- by NOB under aerobic conditions [120]. Therefore, a DO limitation could lead to NOB inhibition and a subsequent increase in NO_2^- concentration. For P-PO_4^{3-} concentration, the most significant variations were related to the change of the kinetic parameters of OHO ($b_{H,aerobic}$, μ_H, $K_{SB,OHO}$) and PAO ($b_{PAO,anoxic/aerobic}$) due to substrate competition between PAO and denitrifiers [239]. Furthermore, changing the attachment and detachment rates significantly affected the biofilm thickness. Precisely, particulate attachment and detachment rates have a major role in establishing biofilm thickness, dynamics, and biomass activity in the system [230]. Particulate detachment in this model is influenced by bulk particulate concentration. Detachment is a composite function that takes into account key variables that affect film detachment, including film thickness, EPS strength coefficient, and the effects of N_2 or CH_4 gas generation in the deeper layers of the film. Biofilm development is determined by a combination of physical and physiological processes, including attachment, cell growth, endogenous decay, and detachment [240]. The particulate attachment rate in BioWin is related to the bulk particulate concentration, while the detachment rate is a combined function reflecting the most important variables affecting film detachment, such as film thickness, extracellular polymerase substances (EPS) strength coefficient, and the effect of N_2 or

CH_4 gas generation inside the deeper film layers. **Figure 2.2** shows the sensitivity analysis conducted on the average biomass concentrations of the main microbial functional groups present in the bioreactor, including AOB, NOB, OHO, and PAO. The results of the sensitivity analysis confirmed that attachment and detachment rates had a significant impact on the growth of microorganisms. Specifically, an increased detachment rate results in a higher concentration of the active biomass in the biofilm. This can be explained by the fact that in systems with a high detachment (or shear) force, the biofilm becomes more compact, with less filamentous structure growth [241]. This results in an increase in biomass in the biofilm.

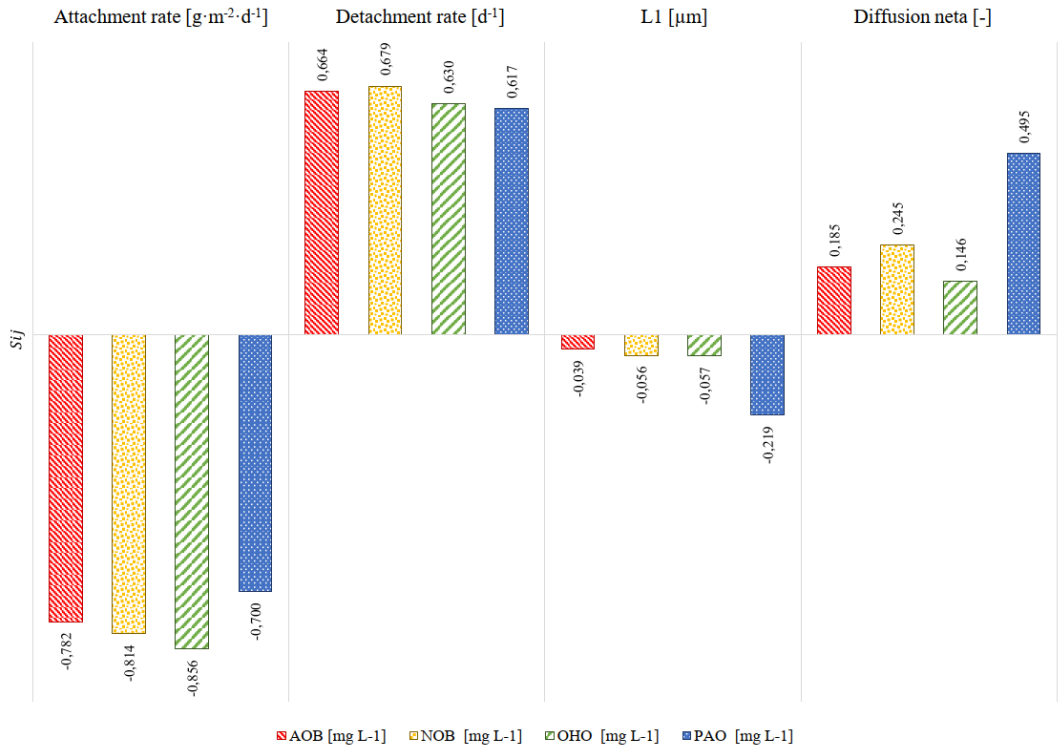

Figure 2.2. Sensitivity analysis results of the average biomass concentrations of the main functional groups present in the biofilm obtained for the first experimental campaign.

2.3.1.2. Model calibration

Table 2.7 shows the kinetic, stoichiometric, and biofilm parameters used in the dynamic model calibration for the two experimental campaigns compared with their default values in BioWin and literature values.

Table 2.7. Calibration of the parameters of the dynamic models of the two experimental campaigns.

	Unit	**Experimental campaign I**	**Experimental campaign II**	**BioWin Default**	**Literature Range**	**Reference**
Detachment rate	d^{-1}	4000	4000	8000	-	This study
Y_H	mg COD·mg COD^{-1}	0.540	0.540	0.666	0.21-0.90	[27, 40]
Y_{PAO}	mg COD·mg COD^{-1}	0.520	0.520	0.639	0.625-0.821	[243]
$b_{H,anoxic}$	d^{-1}	0.62	0.62	0.233	0.2-0.6	[22, 33], [35, 38]
$K_{SB,\ OHO}$	mg COD·L^{-1}	5	5	5	5-20	[245]
$K_{O2,OHO}$	mg O_2·L^{-1}	0.15	0.15	0.15	0.05-0.20	[15, 17], [39]
Anoxic growth factor, $_{OHO}$	-	0.2	0.2	0.5	-	This study
$b_{PAO,anoxic/anaerob}$	d^{-1}	0.20	0.10	0.10	0.15-0.20	[31, 41]
$K_{P\ uptake}$	mg P·L^{-1}	0.5	0.2	0.15	-	This study
$K_{O2,\ PAO}$	mg O_2·L^{-1}	0.025	0.025	0.05	-	This study
$K_{SB,AOB}$	mg N·L^{-1}	1.20	1.20	0.7	1	[248]
μ_{AOB}		0.7	0.9	0.9	0.77- 1	[27, 31]
$K_{O2,\ AOB}$	mg O_2·L^{-1}	1.09	1.3	0.25	0.2-0.75	[234]
$K_{SB,NOB}$	mg N·L^{-1}	1.0	0.7	0.1	-	This study
$K_{O2,NOB}$	mg O_2·L^{-1}	0.89	1.10	0.5	0.2-0.75	[27, 31]

According to Eldyasti et al. [213] and Boltz et al. [249], three sequential calibration changes should be followed in biofilm processes to fit the experimental data: (1) the biofilm thickness (by setting the appropriate values of the attachment and/or detachment

rates), (2) the biomass stoichiometry parameters, and finally (3) the kinetics. In biofilm models, the biofilm thickness is predominantly governed by the detachment rate. Therefore, the first step was to calibrate the biofilm thickness by gradually reducing the detachment rate up to 50% compared to its default value. According to the model results, as the detachment rate decreases, the biofilm thickness tends to increase. The reduction was made not to exceed a biofilm thickness of 1.5 mm, a value consistent with experimental observations [21,83]. After the adjustment of biofilm thickness, in accordance with the calibration procedure [213], the default values of stoichiometric coefficients of OHO and PAO, i.e., Y_H and Y_{PAO}, were calibrated and reduced from 0.666 to 0.540 and 0.639 to 0.520 mg COD·mg COD^{-1}, respectively. Other studies on experimental biofilms [250] have reported even lower yields than those used in this study. In a previous study, Eldyasti et al. [213] observed a Y_H value of 0.36 mg COD·mg COD^{-1} in fluidized bed respirometers. In another study aimed at modeling the process of partial nitrification and denitrification in a hybrid biofilm reactor, a Y_H value of 0.52 mg COD·mg COD^{-1} was found. Furthermore, for the application of biofilm mathematical models, Trojanowicz et al. [242] recommend Y_H values ranging from 0.206 to 0.900 mg COD·mg COD^{-1}.

Regarding the calibration of kinetic parameters, it was necessary to intervene on the heterotrophs by reducing the anoxic growth factor of OHO, which in the model represents the fraction of microorganisms capable of growing under anoxic conditions, and/or by reducing the growth rate under anoxic conditions, while at the same time increasing the default value of $b_{H,anoxic}$. These modifications are consistent with the consideration that the high SRTs of attached growing systems are compatible with higher decay rates compared to the activated sludge process. Specifically, the anoxic factor of OHO biomass

and $b_{H,anoxic}$ were set at 0.2 and 0.62 d^{-1}, respectively. Other changes involved a reduction in PAO growth kinetics. To better match the experimental and calibrated results of the first experimental campaign, the decay coefficient $b_{PAO,Anoxic/aerob}$ was increased from 0.1 to 0.2 d^{-1} according to Henze [246]. These changes were made considering that in the absence of a specific anaerobic phase, typical PAO does not develop in the reactor. Indeed, microbial community analyses performed on the carrier-attached biomass collected from the experimental reactor showed high relative abundances of atypical P-accumulating denitrifiers (e.g. *Hydrogenophaga*) [21] characterized by accumulation rates lower than those of typical PAO bacteria [251]. Hence, $K_{Puptake}$ was increased from 0.15 to 0.50 mg $P \cdot L^{-1}$ in the first and to 0.20 mg $P \cdot L^{-1}$ in the second experimental campaign. This parameter stops the growth of PAO biomass with polyphosphate storage at low soluble P concentration, thus impacting the concentration of soluble effluent P. In addition, to accurately reproduce experimentally measured N removals at low concentrations, other parameters that were acted upon are $K_{O2,\ AOB}$ and $K_{O2,\ NOB}$, which were increased from 0.25 to 1.09 and 0.89 mg $O_2 \cdot L^{-1}$ in the first experimental campaign and from 0.5 to 1.3 and 1.1 mg $O_2 \cdot L^{-1}$ in second experimental campaign in order to limit NH_4^+ and NO_2^- oxidation respectively by AOB and NOB at low DO conditions [230]. The difference in calibration between the two experimental campaigns is acceptable due to the different biomass cultivation methods and operational conditions [21,83].

2.3.1.3. Model validation

After calibration, the model of the first experimental campaign was validated using data from different periods (P5-P6) than those used for calibration (P1-P4) (**Table 2.1**). **Figure 2.3** shows the simulations performed on both the calibration and validation periods.

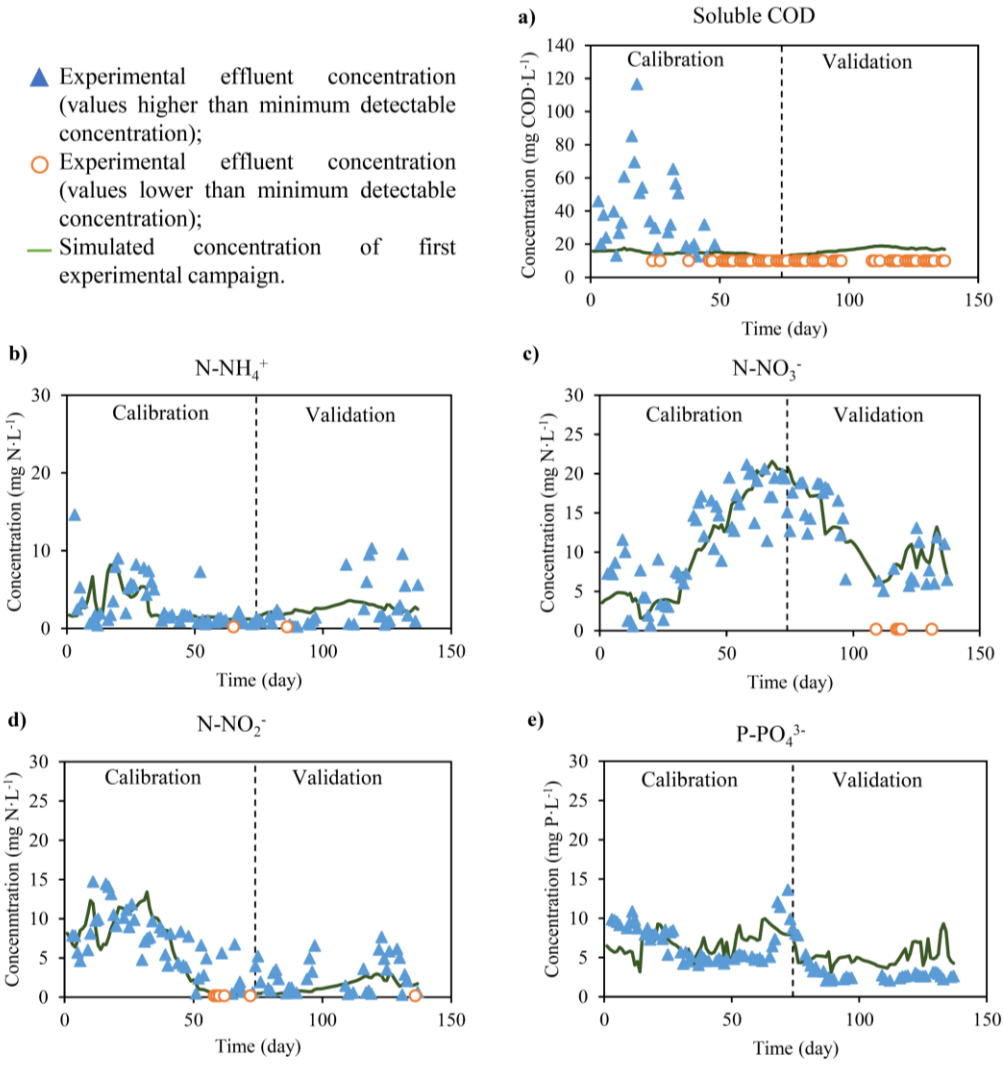

Figure 2.3. Comparison of measured and simulated effluent concentrations of soluble COD, N-NH_4^+, N-NO_3^-, N-NO_2^-, and P-PO_4^{3-} obtained during the first experimental campaign. The minimum detectable concentrations were equal to 10 mg·L^{-1} for COD and 0.2 mg·L^{-1} for N-NH_4^+, N-NO_3^-, N-NO_2^-, and P-PO_4^{3-}.

Table 2.8 reports the absolute variance S_{ai} as well as the *TIC* and *NOF* indicators used for the calibration and validation of the model.

Table 2.8. Absolute variance S_{ai}, Thiel's inequality coefficient (*TIC*), and the normal objective function (*NOF*) used as acceptance criteria in the calibration and validation processes of the first experimental campaign.

Calibration model			
	S_{ai} **[mg·L^{-1}]**	***TIC***	***NOF***
Soluble COD	9.5	-	-
N-NH_4^+	0.2	0.42	1.10
N-NO_3^-	1	0.14	0.32
N-NO_2^-	0.4	0.23	0.55
P-PO_4^{3-}	0.0	0.19	0.40
Validation model			
	S_{ai} **[mg·L^{-1}]**	***TIC***	***NOF***
Soluble COD	-	-	-
N-NH_4^+	0.0	0.43	1.10
N-NO_3^-	1	0.19	0.44
N-NO_2^-	1.2	0.50	0.95
P-PO_4^{3-}	1.8	0.33	0.92

S_{ai} = average value in the calibration and validation periods.

The indicators show a good correspondence between experimental and modeled values, and the soluble COD, N-NH_4^+, N-NO_3^-, N-NO_2^-, and P-PO_4^{3-} concentrations showed a similar trend compared to the experimental data (**Figure 2.3**, **Table 2.8**). The higher discrepancy observed in the fit of the data was related to the concentration of soluble COD in P1. Specifically, for the soluble COD, it was not possible to evaluate the concentrations because all measured data were below the analytical detection limit (<10 mg COD·L^{-1}). For N-NH_4^+ and N-NO_2^- concentrations, the obtained *TIC* and *NOF* values during calibration and validation can be accepted due to the low effluent NH_4^+ and NO_2^- concentrations. It should be noted that the acceptance indicators refer to the relative

difference. Therefore, a small absolute variation could produce a significant relative deviation if values are low. The other acceptance indicators are perfectly within the literature ranges. Consequently, the results obtained for all analyzed parameters showed a good simulation of data by the calibrated model.

The validation procedure of the second experimental campaign was also carried out using a different dataset (P5-P6) instead of calibration periods (P1-P4) (**Table 2.1**). **Figure 2.4** shows the results obtained from the calibration and validation steps.

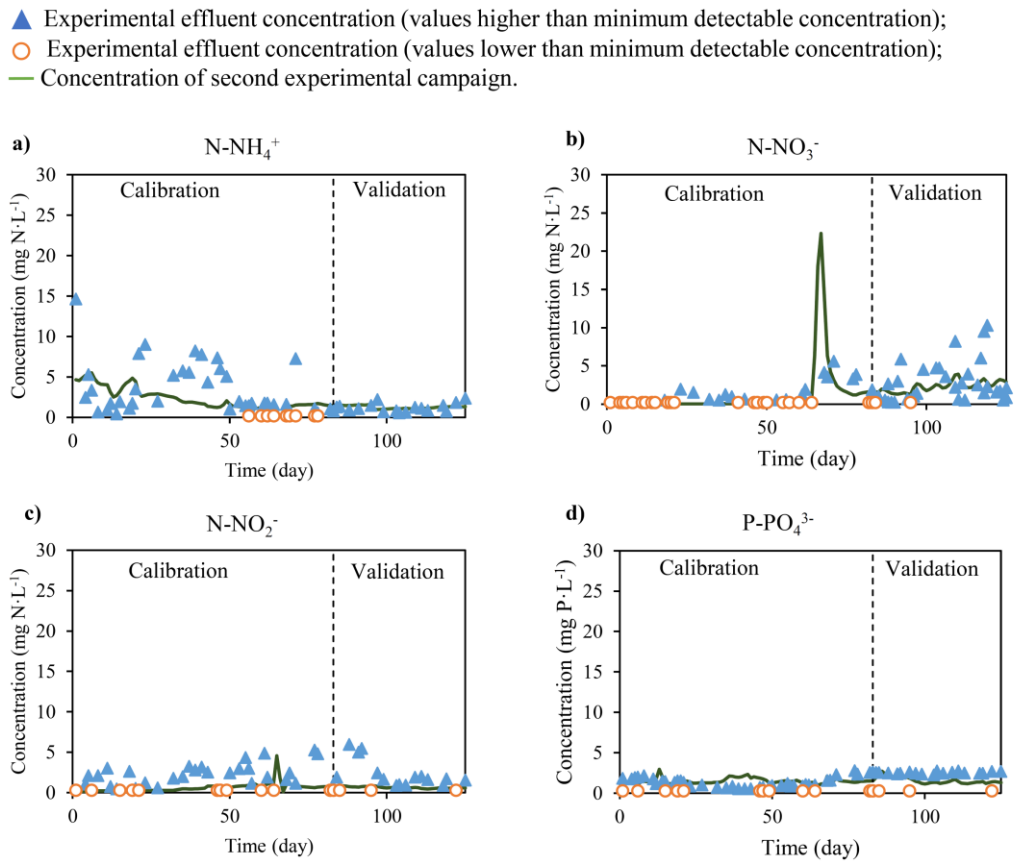

Figure 2.4. Comparison of measured and simulated concentrations in terms of $N\text{-}NH_4^+$, $N\text{-}NO_3^-$, $N\text{-}NO_2^-$, and $P\text{-}PO_4^{3-}$ for the second experimental campaign. The minimum detection values for the ion concentrations were equal to 0.2 $mg \cdot L^{-1}$.

The measured COD values were lower than the detection values, thus it was not possible to compare them to the simulated data. The calibrated model showed a good reproduction of the measured data for all analyzed parameters (**Figure 2.4**). The peak in the plot of the $N\text{-}NO_3^-$ concentration was caused by a sudden change in aeration patterns from microaerobic to aerobic conditions with the aim of reproducing the reactor operating conditions (**Figure 2.4**b). Indeed, due to a malfunctioning of the DO control system, on day 69 an increase in DO concentration to approximately 5 $mg \cdot L^{-1}$ was observed and lasted for two days, resulting in an unexpected growth of NOB biomass [83]. For these days only, the DO concentration in the model was set to the fixed value of 5 $mg \cdot L^{-1}$ to reproduce the experimental conditions.

Table 2.9 shows the results of S_{ai}, *TIC*, and *NOF* used as acceptance criteria in the calibration and validation processes of the second experimental campaign.

Table 2.9. Absolute variance S_{ai}, Thiel's inequality coefficient (*TIC*), and the normal objective function (*NOF*) used as acceptance criteria in the calibration and validation processes of the second experimental campaign. The measured COD values could not be compared with the simulated data due to the COD value being lower than the detection value.

Calibration model			
	S_{ai} **[mg L^{-1}]**	***TIC***	***NOF***
$N\text{-}NH_4^+$	0.0	0.38	0.98
$N\text{-}NO_3^-$	0.2	0.46	2.33
$N\text{-}NO_2^-$	1.1	0.64	1.12
$P\text{-}PO_4^{3-}$	0.1	0.25	0.56
Validation model			
	S_{ai} **[mg L^{-1}]**	***TIC***	***NOF***
$N\text{-}NH_4^+$	0.8	0.48	0.95
$N\text{-}NO_3^-$	0.3	0.33	0.69
$N\text{-}NO_2^-$	1.3	0.66	1.10
$P\text{-}PO_4^{3-}$	0.9	0.25	0.40

S_{ai} = average value in the calibration and validation periods.

For the $N\text{-}NH_4^+$ and $N\text{-}NO_2^-$ concentrations, even if TIC and NOF are higher than the acceptance threshold, the calibrated model can be accepted due to the low absolute variance values. For the $N\text{-}NO_3^-$ and $P\text{-}PO_4^{3-}$ concentrations, the *TIC* and *NOF* indicators are perfectly within the literature ranges, thus indicating the goodness of fit of the calibrated and validated mathematical model.

2.3.2. Evolution of microbial functional groups in the biofilm

The trends of the biomass composing the microbial biofilm within the MBBRs for the two modeled campaigns are shown in **Figure 2.5**.

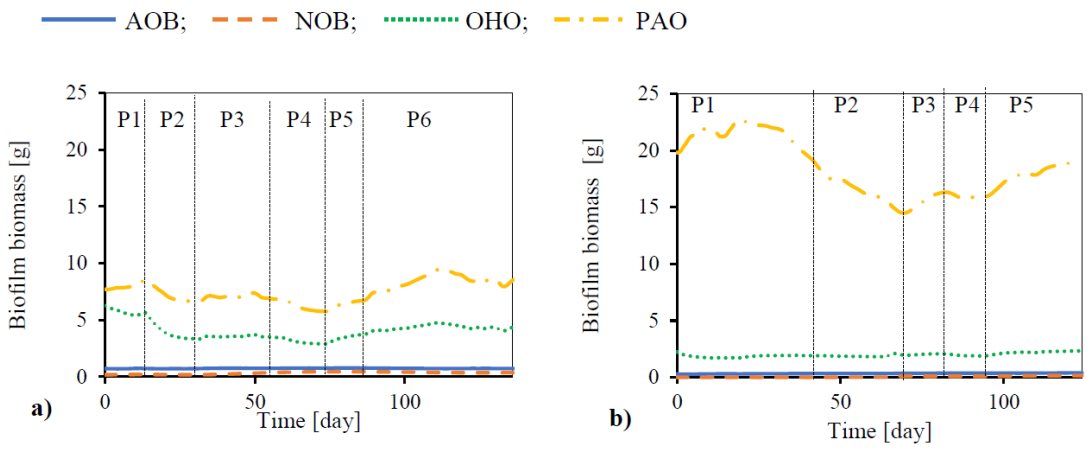

Figure 2.5. Biofilm biomass trend during the first (a) and second (b) modeled campaign.

Biomass trends for the first campaign (**Figure 2.5**a) showed a slight growth of AOB biomass, except in P6, as confirmed by Iannacone et al. [21]. The trend of NOB biomass was quite steady, with a gradual increase during P4 due to the higher value of DO (**Table 2.1**). As expected, the trend in OHO and PAO biomass was dependent on the change in COD concentration. During P2-P5, there was a slight decrease in the concentrations of OHO and PAO biomass due to the lower COD levels in the system, while an increase in OHO and PAO biomass was observed during P6 in accordance with the higher COD concentrations in the experimental data [21].

The simulated trends of AOB and NOB biomass during the second campaign are shown in **Figure 2.5**b. The NOB and AOB biomass trends agree with the experimental results. From day 65, due to the increase in DO concentration in the reactor, the NOB biomass increased. Instead, the AOB biomass remained constant in all experimental periods.

2.3.3. Model optimization of the shortcut SND process

The experimental results of the second campaign confirmed the advantages of the shortcut SND process over complete SND in terms of removal efficiency for the various contaminants. For this reason, the validated model of this campaign was used to test alternative scenarios to improve N removal while ensuring successful NOB inhibition. The modeled scenarios involved changes in the aeration conditions, pH, and HRT, as shown in **Table 2.10**.

Table 2.10. Modeled scenarios for the shortcut SND process with different aeration patterns, pH, and HRT.

Scenario	Proposed actions
1	1.0 Intermittent aeration without DO failure (0.2-3.0 mg $O_2 \cdot L^{-1}$)
	1.1 DO range equal to P4 period of second campaign (0.2-2.0 mg $O_2 \cdot L^{-1}$)
	1.2 DO concentration = 0.8 mg $O_2 \cdot L^{-1}$
	1.3 DO concentration = 0.6 mg $O_2 \cdot L^{-1}$
2	2.1 pH value = 8.1 (starting condition)
	2.2 pH value = 6.5
	2.3 pH value = 8.4
	2.4 pH value = 9.0
3	3.1 HRT value = 1.0 d
	3.2 HRT value = 0.9 d
	3.3 HRT value = 0.75 d
	3.4 HRT value = 0.5 d

First, the shortcut SND in the MBBR was modeled without considering the DO control malfunctioning during days 65-67 in order to assess the potential of intermittent aeration conditions to inhibit NOB growth effectively.

Figure 2.6 illustrates the results in terms of N-NH_4^+, N-NO_3^-, AOB, and NOB biomass under intermittent aeration conditions.

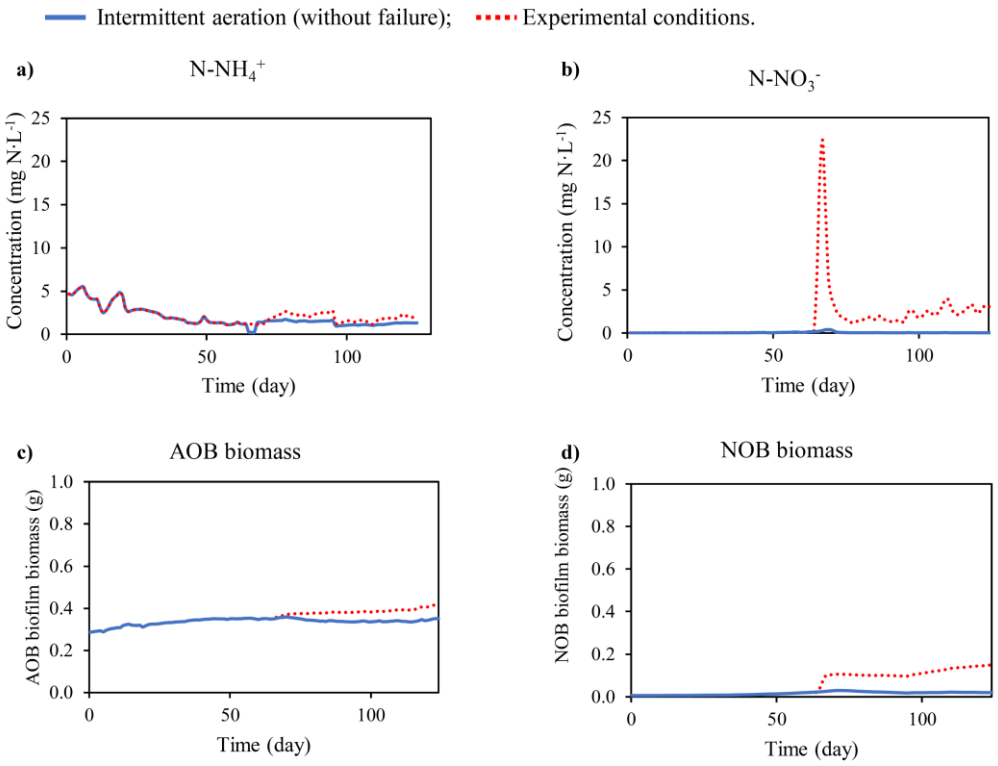

Figure 2.6. Comparison of simulated effluent nitrogen (N-NH_4^+, N-NO_3^-) and biomass (AOB, NOB) concentration trends under experimental and modeled (without DO system failure) intermittent aeration conditions.

The results confirm that intermittent aeration can effectively induce and maintain NOB inhibition. Comparing the experimental and simulated data (intermittent aeration without failure), no significant difference can be noted in N-NH_4^+ removal and AOB biomass concentration. In contrast, the abrupt growth of NOB biomass observed by modeling the experimental data, caused by the DO malfunction, produced an increase in N-NO_3^- concentration, which was completely absent in the simulated data.

The optimization scenarios presented in **Table 2.10** and discussed below use the simulation in the absence of DO control failure as a reference for comparisons. Starting from the validated model of the second campaign, the first step of optimization concerned the simulation of different aeration conditions, as reported in **Table 2.10**. **Figure 2.6** shows the profiles of N-NH_4^+, N-NO_3^-, and N-NO_2^- concentrations for all optimization scenarios considering the starting conditions of pH (8.1) and HRT (1 d).

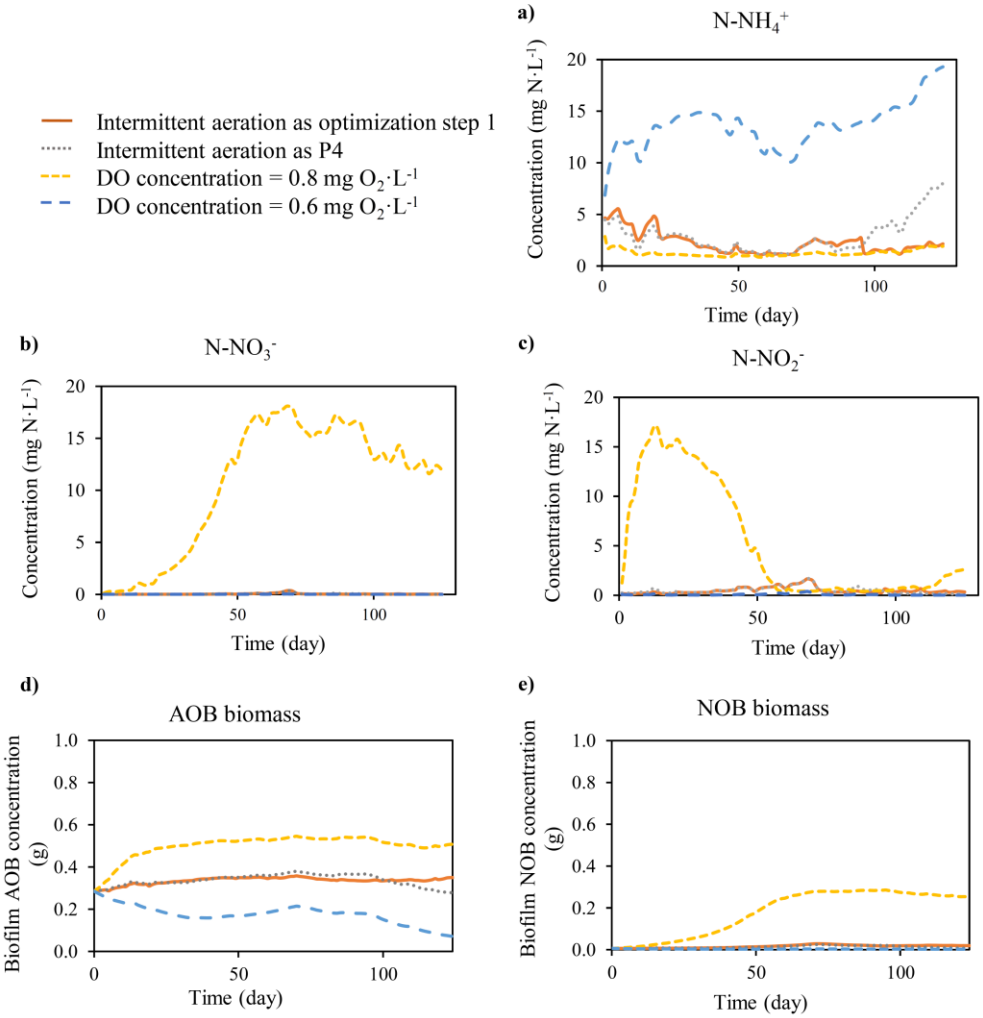

Figure 2.6. Temporal profiles of the simulated concentrations of nitrogenous compounds, AOB, and NOB for the different aeration scenarios.

Specifically, a constant DO concentration of 0.6 mg $O_2 \cdot L^{-1}$ had a negative impact in terms of $N\text{-}NH_4^+$ removal, as it reduced AOB activity. Instead, a constant DO value of 0.8 mg $O_2 \cdot L^{-1}$ caused excessive growth of the NOB biomass, resulting in a breakthrough of NO_3^- and NO_2^- concentrations. By comparing the simulated data in **Figure 2.6**, it is clear that the intermittent aeration conditions (without DO failure) represent the best strategy for the efficient removal of $N\text{-}NH_4^+$, $N\text{-}NO_3^-$ and $N\text{-}NO_2^-$ as it resulted in maximum effluent values below 5.5, 0.4 and 1.7 mg $N \cdot L^{-1}$, respectively.

In a second optimization step, the effect of changing the pH from 9.0 to 6.5 was evaluated, as shown in **Figure 2.7**.

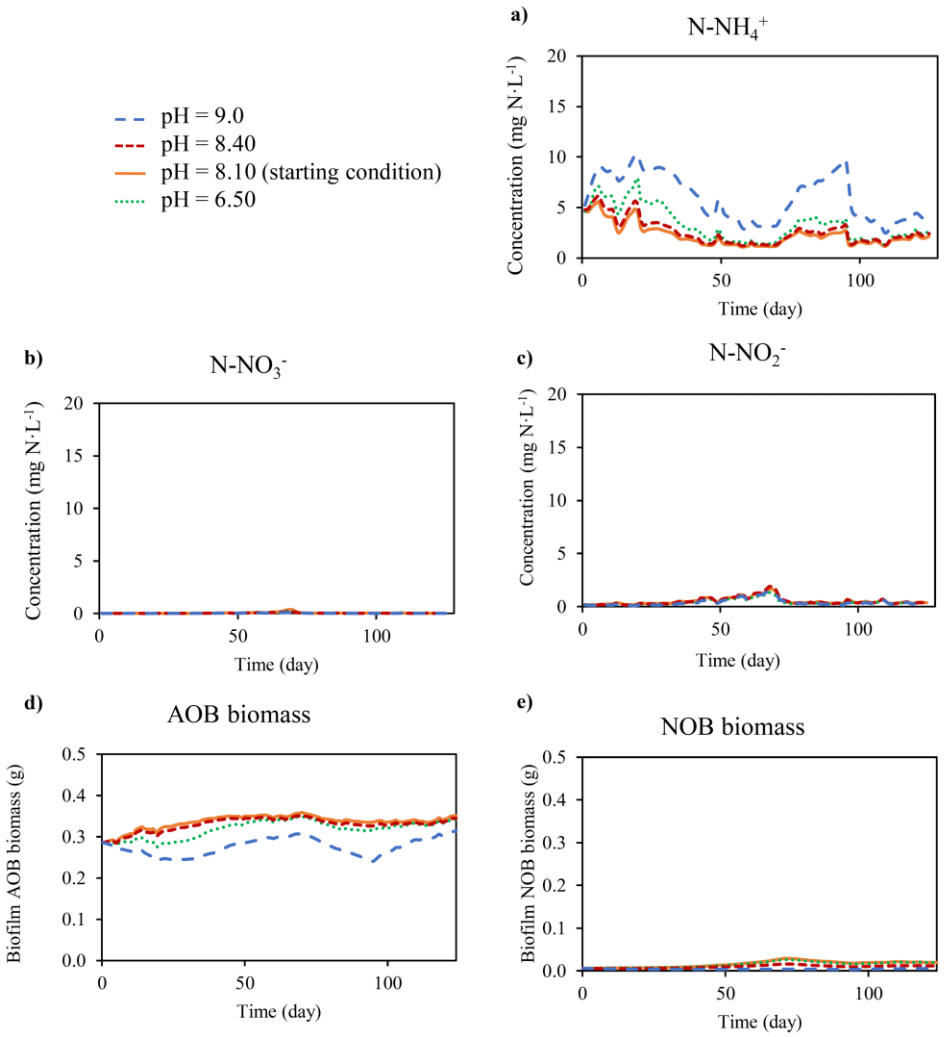

Figure 2.7. Temporal profiles of the simulated concentrations of nitrogenous compounds, AOB, and NOB for different pH values.

According to Rahimi et al. [11], pH values ranging from 7.5 to 8.5 benefit NO_2^- accumulation. Compared to the initial conditions, all proposed pH changes caused an increase in the $N\text{-}NH_4^+$ level in the reactor. In particular, the highest $N\text{-}NH_4^+$ increase was observed at pH 9.0 due to AOB inhibition [252], although this pH also resulted in the highest NOB inhibition [253]. On the other hand, the lowest simulated pH value of 6.5 did not improve N removal, as it led to a slight increase in $N\text{-}NH_4^+$ concentration.

Comparing the results obtained for a pH of 8.4 and 8.1, a higher NOB inhibition was observed at pH of 8.4 with no significant changes in AOB biomass and $N\text{-}NH_4^+$ concentrations. Thus, based on these simulations, a pH value of 8.4 can be considered the best solution to obtain sufficient NOB inhibition and good N removal efficiency, with an average effluent $N\text{-}NH_4^+$, $N\text{-}NO_3^-$ and $N\text{-}NO_2^-$ concentrations of 2.6, 0.04 and 0.5 mg $N{\cdot}L^{-1}$, respectively. Based on the results of the first experimental campaign regarding the benefits of HRT reduction from 2 to 1 d [82], the impact of a further HRT reduction from 1 to 0.5 d was simulated by increasing the influent flow rate (**Figure 2.8**).

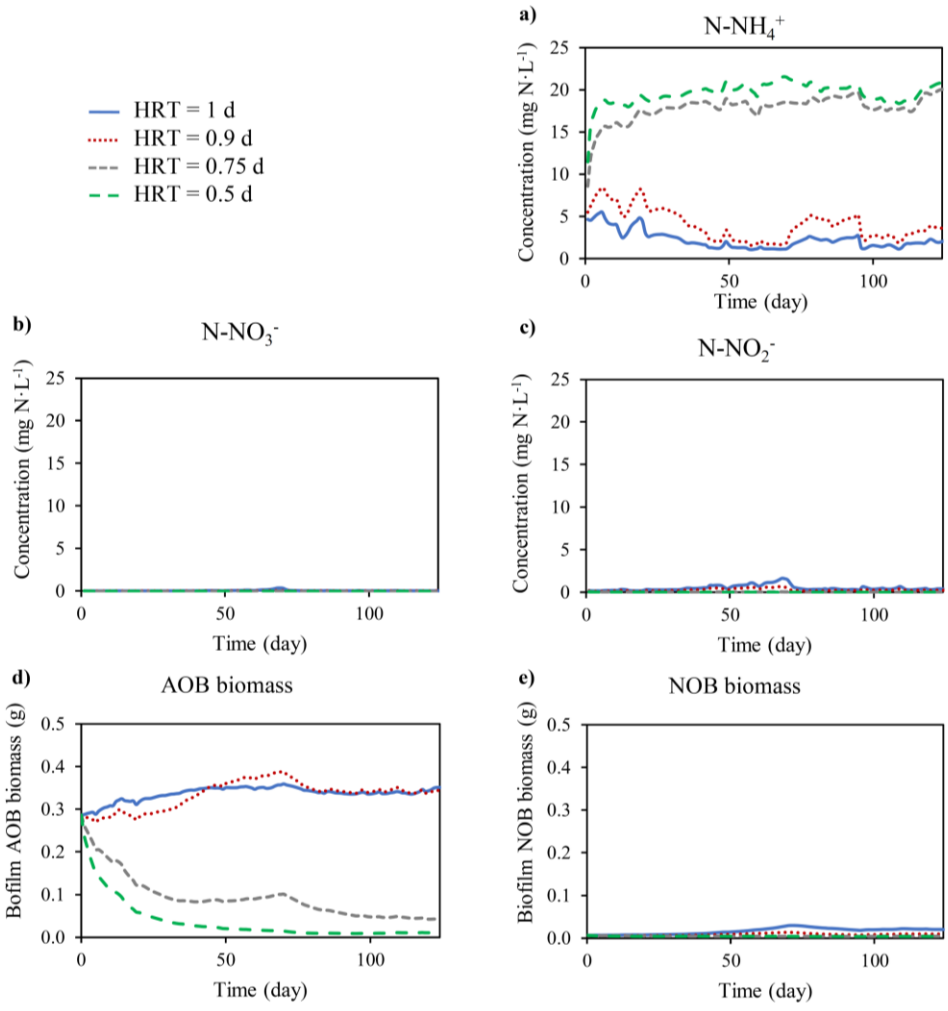

Figure 2.8. Temporal profiles of the simulated concentrations of nitrogenous compounds, AOB, and NOB for different HRTs.

Figure 2.8 shows that an HRT reduction to 0.75 and 0.5 d caused an inhibition of the nitrifying activity. An HRT of 0.5 d led to the maximum decrease in AOB biomass to a value of 0.01 g at the end of the simulation period. Compared to the results obtained at an HRT of 1 d, an HRT reduction to 0.9 d resulted in a higher NOB inhibition and average $N\text{-}NH_4^+$, $N\text{-}NO_3^-$ and $N\text{-}NO_2^-$ concentrations of 4.0, 0.02, and 0.07 $mg \cdot L^{-1}$, respectively, indicating favourable conditions for the shortcut SND process.

2.4. Conclusions

Mathematical modeling successfully reproduced complete and shortcut SND processes in lab-scale MBBRs based on the results obtained from two different experimental campaigns. The sensitivity analysis was an effective tool to identify the most important parameters of the biofilm model. The calibrated and validated models showed a similar trend for $N\text{-}NH_4^+$, $N\text{-}NO_3^-$, $N\text{-}NO_2^-$, and $P\text{-}PO_4^{3-}$ concentrations compared to the experimental data. For all analyzed parameters, the *TIC* values ranged between 0.14 and 0.66 indicating a considerable model validity. Moreover, *NOF* values were almost constantly below 1 revealing an acceptable reproducibility between the experimental and modeled data. On the other hand, higher *TIC* and *NOF* values can be accepted due to the low absolute S_{ai} variance values. Process optimization via model simulation of different scenarios allowed to identify the best operating conditions to maximize N removal through the shortcut SND process. The results confirm that intermittent aeration can effectively induce and maintain NOB inhibition in the reactor with an average $N\text{-}NO_3^-$ concentration of 0.05 mg $N \cdot L^{-1}$. A pH value of 8.4 resulted in sufficient NOB inhibition and a low effluent $N\text{-}NH_4^+$ concentration of 2.57 mg $N \cdot L^{-1}$ (on average). An HRT of 0.9 d can be considered optimal as it resulted in average effluent $N\text{-}NH_4^+$, $N\text{-}NO_3^-$, and $N\text{-}NO_2^-$ concentrations of 4.0, 0.02, and 0.07 $mg \cdot L^{-1}$, respectively.

CHAPTER 3

Impact of Influent Composition and Operating Conditions on Carbon and Nitrogen Removal from Urban Wastewater in a Continuous-Upflow (Micro)Aerobic Granular Sludge Blanket Reactor

This Chapter has been published as:

Lanzetta, A.; Di Capua, F.; Panneerselvam, B.; Mattioli, D.; Esposito, G.; Papirio, S. Impact of Influent Composition and Operating Conditions on Carbon and Nitrogen Removal from Urban Wastewater in a Continuous-Upflow (Micro)Aerobic Granular Sludge Blanket Reactor. Energies 2023,16, 6303. https://doi.org/10.3390/en16176303.

3.1. Introduction

In the last decades, the increasing urbanization and industrialization have caused an increase in wastewater production and discharge of carbonaceous and nitrogenous compounds especially in developing countries, leading to oxygen depletion and eutrophication in surface waters [254]. Biological processes in wastewater treatment plants (WWTPs) are often performed within conventional activated sludge (CAS) systems for the removal of organic matter and within the modified Ludzack-Ettinger (MLE) process, consisting of separate denitrification and nitrification steps, for combined carbon (C) and nitrogen (N) removal. However, current research is looking for alternative solutions to improve treatment efficiencies while minimizing capital and operational costs [172].

In this regard, the simultaneous nitrification and denitrification process (SND) is one of the promising alternatives to the MLE cycle in WWTPs for the treatment of urban wastewaters due to lower carbon demand for denitrification and reduced sludge production [122], lower energy for aeration [233], and smaller footprint [255]. Specifically, SND is capable to completely remove N in a single-stage system under specific operating conditions, thus differently from what occurs in MLE systems. The SND process is affected by environmental and operating factors such as pH, temperature, dissolved oxygen (DO), hydraulic retention time (HRT), feed carbon to nitrogen (C/N) ratio, diffusion limitations inside flocs or biofilm, microbial competition, and type of influent wastewater [58]. These factors play an essential role in regulating the balance between the different bacterial communities as well as the process efficiency [42,255].

Up to now, processes allowing the concomitant removal of C and N, such as SND, have been investigated in different bioreactor configurations, such as the sequencing batch

reactor (SBR) [58,256], moving bed SBR (MBSBR) [74], sequencing batch biofilm reactor (SBBR) [257], moving bed biofilm reactor (MBBR) [83], and aerobic granular sludge (AGS) system [58,255]. Generally, the use of biofilm-based systems promotes the coexistence of different microbial communities and allows higher concentration of active biomass, while reducing space requirements and sludge production compared to suspended-floc systems, such as CAS and MLE [94]. AGS integrates the characteristics of suspended-growth and biofilm systems, as it leads to the formation of microbial aggregates without any support and having a structure similar to biofilms [258]. The different DO gradients and redox profiles within the aerobic granules result in the formation of (micro)aerobic, anoxic, and anaerobic zones, promoting the coexistence of nitrifiers, denitrifiers, and anaerobic organic-degrading bacteria [259], respectively, and enabling concomitant organics and nutrients removal [58].

Granular sludge was first discovered in upflow anaerobic sludge blanket (UASB) systems in the 1980s [260], and has mainly been employed for anaerobic digestion [261] or removal of oxyanions under anoxic conditions [262]. At the end of 1980s, granular sludge was also applied in aerobic reactors to cope with high organic and nutrient loads [263]. Although aerobic granules were first reported in a continuous upflow aerobic granular sludge blanket (UAGSB) system [58,95], in recent years AGS has mainly been cultivated in SBRs and stood out as a reliable technology at laboratory [258], pilot [264] and full scale [265]. Nonetheless, a continuous-flow AGS system might be advantageous over SBRs for large-scale operations due to the lower installation costs and easier operation, maintenance, and control [122,260]. However, aerobic granule formation is a complex process influenced by some parameters. Several studies have reported that selection pressure is the primary factor for successful aerobic granulation [266,267]. The main

selection pressures affecting the development of aerobic granules include shear force, volumetric exchange ratio, settling time and aeration intensity [202]. Weak selection pressures, such as low shear and long settling times, can inhibit granulation, whereas strong selection pressures are required to initiate aerobic granule development [268]. In addition, one of the main challenges for an effective continuous-flow AGS operation is the long-term physical stability of the granules, which is affected by several factors such as the C/N ratio, aeration intensity, as well as organic and nitrogen loading rates [193]. Hence, a fundamental aspect to be further investigated in continuous-flow AGS systems is represented by C and N removal at different DO concentrations, feed C/N ratios and HRTs [188]. A proper DO control strategy is a requirement for the selection and maintenance of key bacteria for the SND process, such as ammonia oxidizing bacteria (AOB) and nitrite oxidizing bacteria (NOB) [269] and also for achieving the alternation of feast and famine phases which is an essential factor for the start-up of the AGS continuous-flow reactor [270]. Decreasing aeration requirements for wastewater treatment is crucial to limit the carbon footprint and operational costs of WWTPs. In fact, studies have shown that aeration system energy consumption can account for 30-76 % of total energy consumption in sewage treatment plants [220,271–275].

Besides, wastewater composition and the HRT can strongly influence the performance of continuous-flow AGS systems and their influence under different DO conditions should be assessed. Typically, high C/N ratios (> 10) are beneficial for the long-term operation of AGS systems in terms of both the granular integrity and efficiency [276]. The HRT of continuous-flow AGS should be chosen appropriately to avoid the wash-out of the granules and system instability [277,278].

Although the use of continuous-flow conditions in AGS systems have been reported to make granulation less favorable, the good performance and properties of this technology, along with the fact that most large-scale plants are operated in a continuous mode, encourage further research and development [279]. Only a few studies have focused on defining optimal operating conditions to achieve high removal efficiencies in terms of organic matter and nitrogen (**Table 3.1**). Also, previous continuous-flow AGS bioreactor experiences lasted less than 100 d [280], indicating that limited information regarding long-term AGS bioreactor operations can be drawn. Studies assessing the influence of different operating conditions and long-term operation on the system performance are necessary to promote large-scale application while trying to reduce the operating costs for urban wastewater treatment.

Hence, in this work the performance of a continuous-flow double-column UAGSB reactor was studied for a period of 306 days to investigate the effect of different DO concentrations, feed C/N ratios and HRTs on the COD, N-NH_4^+ and total inorganic nitrogen (TIN) removal as well as on the evolution of the different N species. Batch activity tests were also run to assess the denitrification activity in the bioreactor. Moreover, a first estimation of the capital and operating costs associated with the UAGSB reactor was performed to better evaluate whether the process could result in economic savings as compared to a MLE system.

Table 3.1. COD, TIN, and N-NH_4^+ removal efficiencies (REs) for synthetic and real urban wastewater in continuous-flow aerobic and anaerobic granular sludge reactors.

Urban wastewater characteristics		Reactor configuration	Process conditions	Scale	NH_4^+ – N RE (%)	COD RE (%)	TN RE (%)	Reference
Synthetic	COD = 144 – 628 mg·L^{-1} N-NH_4^+= 20-72 mg·L^{-1}	Micro-aerobic granular sludge reactor	DO_{influx} = 0.11 – 0.25 g·L^{-1}· d^{-1} HRT = 5 – 10 h	Lab-scale, V = 18 L	40 – 86	93 – 95	51 – 82	[276]
Real	COD = 150 – 300 mg·L^{-1}	UASB	HRT = 10 – 48 h T= 20°C	Lab-scale, V = 8 L	/	82 – 86	/	[32]
Real	COD = 602 – 866 mg·L^{-1} N-NH_4^+= 48 mg·L^{-1}	UASB	HRT = 8.8 – 24 h T = 25 – 30°C	Pilot-scale, V = 2.75 m^3	/	60 (as sCOD)	/	[33]
Real	COD = 450 – 8150 mg·L^{-1} N-NH_3^+= 31.2-141.9 mg·L^{-1}	UASB	HRT = 24.85–106.85 h T = 22.4–30.7°C	Real-scale, 7800 m^3	/	45 – 88	25.3	[34]
Synthetic	COD = 500 mg·L^{-1} TN = 50 – 56 mg·L^{-1}	UASB	HRT = 9 – 22 h T=25-35°C	Lab-scale, V = 0.9 L	/	84 – 94	<73	[35]
Synthetic	N-NH_4^+= 512 – 594 mg·L^{-1}	Continuous-flow airlift reactor (ALR)	HRT = 5.41 – 22.8 h	Lab-scale, V = 9.2 L	94.4 – 100	/	/	[281]
Synthetic	Organic loading rate (OLR) = 7.0 kg COD·m^{-3}·d^{-1} N-NH_4^+*= 21 mg·L^{-1}*	Continuous flow aerobic granular sludge reactor	HRT = 24 h	Lab-scale, V= 6.8 L	/	83 – 84	/	[282]
Real	COD = 200 – 400 mg·L^{-1} N-NH_4^+= 30 – 40 mg·L^{-1}	Modified oxidation ditch (MOD)	HRT = 3 h	Lab-scale, V = 60 L	95	90 (as BOD_5)	/	[265]
Synthetic	COD* = 514 mg·L^{-1} N-NH_4^+*= 63 mg·L^{-1}	Continuous flow aerobic granular sludge reactor	DO = 0.3 -3.5 mg O_2·L^{-1} HRT = 10 h	Lab-scale, V = 890 mL	/	85	/	[283]
Synthetic	COD = 350 – 1500 mg·L^{-1} N-NH_4^+*= 53.3 mg·L^{-1}	Continuous flow aerobic granular sludge reactor	DO = 7.0 mg O_2·L^{-1}	Lab-scale V= 11.9 L	6 – 60	90 – 97	/	[284]

Urban wastewater characteristics		Reactor configuration	Process conditions	Scale	NH_4^+ – N RE (%)	COD RE (%)	TN RE (%)	Reference
Synthetic	COD = 195 – 604 $mg \cdot L^{-1}$ $N\text{-}NH_4^+$= 37.9 – 45.3 $mg \cdot L^{-1}$	Continuous upflow aerobic granular sludge blanket	DO = 0.01 – 6.0 mg $O_2 \cdot L^{-1}$ C/N = 4.7 – 13.5 HRT = 6 – 24 h	Lab-scale, V = 600 mL	63 – 100	61 – 88	28 – 88 (as TIN)	This study

* Stoichiometrically calculated

3.2. Materials and Methods

3.2.1. Wastewater composition and source of inoculum

The synthetic wastewater used as influent for the UAGSB reactor was prepared by using two different liquid media (A and B) [285], a trace element solution [286] and tap water. Medium A was composed of 3.32-13.3 $g \cdot L^{-1}$ of sodium acetate trihydrate ($CH_3COONa \cdot 3H_2O$) as organic carbon source and 0.912 $g \cdot L^{-1}$ of magnesium sulfate eptahydrate ($MgSO_4 \cdot 7H_2O$). Medium B contained 1.98 $g \cdot L^{-1}$ of ammonium chloride (NH_4Cl) as $N\text{-}NH_4^+$ source, 0.555-5.226 $g \cdot L^{-1}$ of dipotassium hydrogen phosphate (K_2HPO_4) as $P\text{-}PO_4^{3-}$ source and 0.175 $g \cdot L^{-1}$ of potassium chloride (KCl). The influent was prepared by mixing 150 mL of medium A, 150 mL of medium B, 10 mL of trace element solution, and 1300 mL of tap water. Acetate supplementation was varied along the study, resulting in an influent COD concentration ranging from 195 to 617 mg $COD \cdot L^{-1}$ and a feed C/N ratio ranging from 4.7 to 13.6 (**Table 3.2**). Furthermore, the feed phosphorus (P) concentration was maintained in the range of 56.4-79.4 $mg \cdot L^{-1}$ (on average) during the batch phase and the first period of the continuous phase to stimulate biomass growth, while lower P concentrations in the range of 6.7-11.8 $mg \cdot L^{-1}$ were maintained in the feed during the remaining periods to simulate P levels in a real municipal wastewater (**Table 3.2**). The influent NH_4^+ concentration was maintained stable throughout the UAGSB operation at a value of 40.7 ± 5.0 mg $N \cdot L^{-1}$. The inoculum

used for the start-up of the bioreactor was composed of AGS collected from a 1 L lab-scale SBR operated by Sguanci et al. [287].

Table 3.2. Operating conditions and duration of each experimental period during the continuous-flow operation of the UAGSB reactor.

Period	Duration (days)	DO range ($mg \cdot L^{-1}$)	HRT (h)	Feed P-PO_4^{3-} ($mg \cdot L^{-1}$)	Feed COD ($mg \cdot L^{-1}$)	Feed N-NH_4^+ ($mg \cdot L^{-1}$)	Feed C/N
I	0-30	4.0-6.0	24	56.4±25.0	552±55	38.8±6.4	12.1±1.4
II	31-37	2.0-4.0	24	7.5±1.8	604±62	45.3±2.5	13.3±1.4
III	38-65	1.0-2.0	24	8.2±4.8	543±47	43.3±2.9	12.7±1.5
IV	66-87	0.02-1.60	24	6.6±3.1	571±45	42.6±4.3	13.5±1.4
V	88-130	0.12-2.09	24	8.7±3.1	287±141	39.9±8.5	7.0±2.5
VI	131-160	0.10-2.07	24	6.7±2.2	195±30	42.1±2.0	4.7±0.9
VII	161-193	0.03-1.86	24	9.7±2.7	324±47	40.8±2.2	8.0±1.1
VIII	194-220	0.01-0.30	24	10.5±2.9	560±80	41.5±4.3	13.6±2.2
IX	221-258	0.01-1.22	12	12.7±3.6	472±54	41.4±2.1	11.4±1.4
X	259-306	0.01-0.07	6	10.5±1.8	455±30	37.9±3.3	12.1±1.2

3.2.2. Experimental set-up

As shown in **Figure 3.1**, the experimental set-up included two laboratory scale glass columns (0.6 L each), one used as the main bioreactor and the other as an aeration column. A 205S peristaltic pump (Watson-Marlow, UK) was used for influent feeding and effluent suction from the bioreactor. The aeration was performed in a separate column to avoid the loss of biomass from the top of the reactor and prevent damaging of the granules due to impact with air bubbles [41]. The effluent from the bioreactor was oxygenated in the aeration column and recirculated at the bottom of the bioreactor with a 505U peristaltic pump (Watson-Marlow, UK) at a flow rate between 20 and 40 $mL \cdot min^{-1}$. Air was transferred to the aeration column at a flow rate ranging from 0 to 4.5 $L \cdot min^{-1}$ using an aquarium air pump equipped with tubing and a porous stone. DO was monitored twice a day and maintained at different ranges by manually adjusting the air flow during the initial batch phase and the first three experimental continuous-flow periods. Successively, the

DO concentration was controlled and monitored continuously. Monitoring was performed using a FDO 925 optical probe (WTW, Germany) connected to a multiparameter benchtop meter inoLab® Multi 9620 IDS (WTW, Germany). A Raspberry PI 3 Model B+ single board computer (Raspberry Pi Foundation, UK) coupled with Python software 3.0 (Python Software Foundation, USA) was used to control and automate aeration in the reactor, as described by Iannacone et al. [21]. The portable DO meter was connected via an USB port to the Raspberry PI, which was programmed to switch on and off a 5 V relay connected to the air pump at fixed DO values. Temperature was not controlled during the study to simulate real operating conditions and remained in the range of 14.0–26.5°C during period I-VI, 20.3–30.5°C during period VII-IX and 16.8-28.5°C during period X.

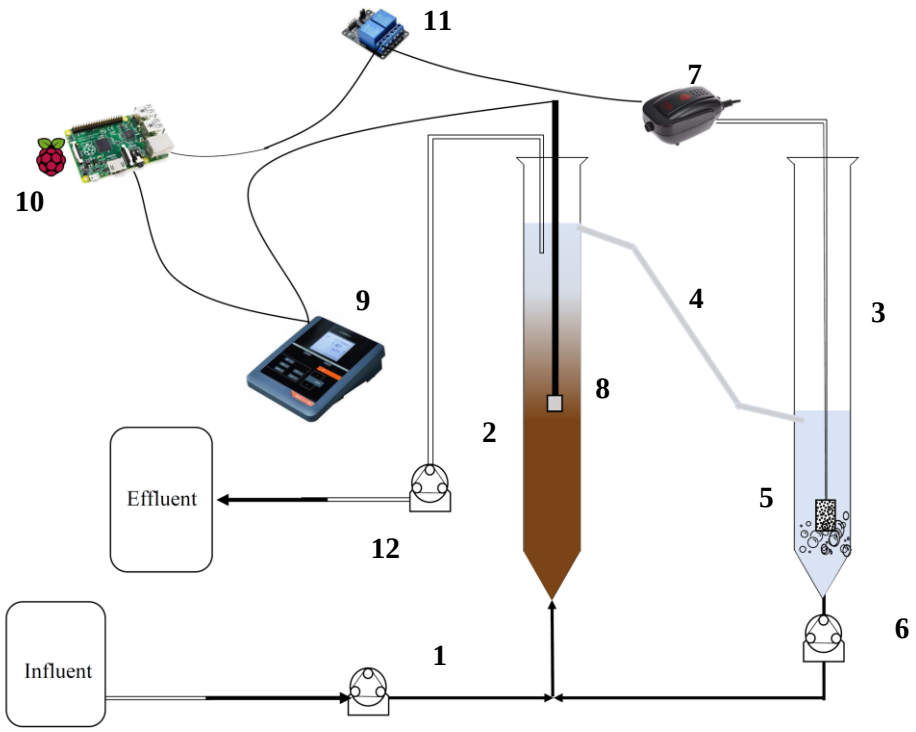

Figure 3.1. Schematic diagram of the UAGSB reactor configuration: 1 inlet pump; 2 bioreactor; 3 aeration column; 4 effluent recirculation; 5 air sparger; 6 recirculation pump; 7 aquarium air pump; 8 DO probe; 9 oxygen benchtop meter; 10 Raspberry PI 3 Model B^{+}; 11 relay 5V; 12 effluent pump

3.2.3. Experimental design

The bioreactor was operated for 21 days in batch mode to promote the acclimation and reactivation of the inoculated AGS biomass. Half of the solution was replaced with fresh synthetic wastewater as soon as the COD and NH_4^+ were completely consumed. In this phase, the DO concentration was monitored twice a day and ranged between 3.0 and 4.0 $mg \cdot L^{-1}$. Subsequently, the bioreactor was operated in continuous mode for 306 days divided into 10 experimental periods, which are outlined in **Table 3.2**. During the first four periods (days 0-87), the DO concentration was progressively reduced from 5.0 to 0.8 $mg \cdot L^{-1}$ (average values) to investigate the impact of reduced oxygenation on organic carbon and TIN removal in the UAGSB reactor. From period V (days 88-130) to VIII (days 194-220), the DO concentration was maintained between 0.03 and 2.09 $mg \cdot L^{-1}$ and the influence of different feed C/N ratios (4.7, 6.9, 7.9, and 13.6 on average) on the system was evaluated. During periods IX and X (days 221-306), the DO range and feed C/N ratio were maintained between 0.01 and 1.22 $mg \cdot L^{-1}$ and 11.8 ± 1.4, respectively, while the HRT was decreased from 24 (periods I-VIII) to 12 (period IX) and 6 h (period X) to investigate the reactor response to increasing organic and N loads.

3.2.4. Anoxic batch activity test

A batch activity test was carried out at the end of period IV to assess the denitrifying activity of the biomass populating the bioreactor [288]. The test was performed in triplicate in 250 mL serum bottles at 20 °C by using a medium composed of NO_3^- (100 $mg \cdot L^{-1}$), sodium acetate trihydrate (600 $mg \cdot L^{-1}$) and nutrients as in the UAGSB reactor influent. Prior to starting the experiment, each bottle was flushed with argon gas for 30 s to ensure anoxic conditions. Mixing was provided by a tilting shaker working at a speed

of 300 rpm. The $N\text{-}NO_3^-$ and $N\text{-}NO_2^-$ concentrations were monitored for 3 h with a sampling interval of 15 min during the first hour and 30 min during the remaining time.

3.2.5. Calculations

The removal efficiencies (REs) of $N\text{-}NH_4^+$, COD, and TIN, the percentage of total influent nitrogen used for biomass growth ($TIN_{inf,\,G}$), the percentage of removed inorganic nitrogen used for biomass growth ($TIN_{rem,\,G}$), and the percentage of total influent inorganic nitrogen being denitrified (TIN_{den}) were calculated by using the following equations (Eqs. 1-6):

$$N\text{-}NH_{4\,RE}^+ = \frac{([N\text{-}NH_{4\,INF}^+] - [N\text{-}NH_{4\,EFF}^+])}{([N\text{-}NH_{4\,INF}^+])} \times 100 \quad (1)$$

$$COD_{RE} = \frac{([COD_{IN}] - [COD_{EFF}])}{([COD_{INF}])} \times 100 \quad (2)$$

$$TIN_{RE} = \frac{([N\text{-}NH_{4\,INF}^+] + [N\text{-}NO_{3\,INF}^-] + [N\text{-}NO_{2\,INF}^-] - [N\text{-}NH_{4\,EFF}^+] - [N\text{-}NO_{3\,EFF}^-] - [N\text{-}NO_{2\,EFF}^-])}{([N\text{-}NH_{4\,INF}^+] + [N\text{-}NO_{3\,INF}^-] + [N\text{-}NO_{2\,INF}^-])} \quad (3)$$

$$TIN_{inf,G} = \frac{0.05 \times ([COD_{INF}] - [COD_{EFF}])}{([N\text{-}NH_{4\,INF}^+] + [N\text{-}NO_{3\,INF}^-] + [N\text{-}NO_{2\,INF}^-])} \times 100 \quad (4)$$

$$TIN_{rem,G} = \frac{0.05 \times ([COD_{INF}] - [COD_{EFF}])}{([N\text{-}NH_{4\,INF}^+] + [N\text{-}NO_{3\,INF}^-] + [N\text{-}NO_{2\,INF}^-] - [N\text{-}NH_{4\,EFF}^+] - [N\text{-}NO_{3\,EFF}^-] - [N\text{-}NO_{2\,EFF}^-])} \quad (5)$$

$$TIN_{den} = [TIN_{RE} - TIN_{inf,G}] \quad (5)$$

where:

- $[N\text{-}NH_4^+{}_{INF}]$ and $[N\text{-}NH_4^+{}_{EFF}]$ are the influent and effluent $N\text{-}NH_4^+$ concentrations, respectively;
- $[COD_{INF}]$ and $[COD_{EFF}]$ are the influent and effluent COD concentrations, respectively;
- $[N\text{-}NO_X^-{}_{INF}]$ and $[N\text{-}NO_X^-{}_{EFF}]$ are the influent and effluent $N\text{-}NO_X^-$ (nitrate- and nitrite-nitrogen) concentrations, respectively.

3.2.6. Analytical methods

Liquid samples were collected daily from the UAGSB reactor and filtered through 0.45 µm syringe filters with polypropylene membranes (VWR, USA) prior to analysis. The COD concentration was determined by the closed reflux colorimetric method [289]. NH_4^+ concentration was determined spectrophotometrically using the indophenol blue method [290]. DO, pH, NO_3^- and NO_2^- concentrations were measured as described by Di Capua et al. [291]. Total suspended solids (TSS) and volatile suspended solids (VSS) concentrations were analyzed according to the Standard Methods [289].

3.2.7. Energy and economic assessment of the UAGSB reactor

To assess the potential energetic and economic benefits of the UAGSB reactor, this was compared with a MLE system, considering for the latter only the denitrification and nitrification steps and assuming to serve a population equivalent (PE) of 10,000 inhabitants for both systems. The operating conditions experimentally identified as the best performing in this study were used to size the UAGSB and MLE systems. The volume of nitrification (V_N) and denitrification (V_D) tanks of the MLE system, the oxygen demand (OD) of nitrification, the operative oxygen capacity (OC) and the number of air diffuser for both plants were calculated as reported by Bonomo [292]. A DO concentration of 2.0 $mg \cdot L^{-1}$ was considered for the MLE system [293], while a DO concentration equal to the upper value of the DO interval of period VIII was used for the UAGSB reactor. The capital expenditure (CAPEX) was assessed taking into account the following equation (Eq. 7), as reported in the local plans of Campania Region (Italy) [294]:

$$CAPEX\ (€ \cdot \mathrm{PE}^{-1}) = 178.45\ PE^{-0.282} \quad (7)$$

Operational costs were based on power use of aerators considering the technical data of a commercial ceramic disc diffusers produced by Xylem Inc. The energy consumption associated with aeration was calculated based on the OD of the nitrification process and the standard aeration efficiency (SAE) of the selected aerators, assuming a continuous aeration in the system, as reported in Eq. 8.

$$Aeration\ energy\ consumption\ (\mathrm{kWh} \cdot \mathrm{year}^{-1}) = \frac{OD}{SAE} \quad (8)$$

3.2.8. Statistical data analysis

A one-way analysis of variance (ANOVA) was performed for data analysis using the Data Analysis Tool of Excel 2016 (Microsoft Corporation, USA). The ANOVA was conducted to determine the statistical differences in the performance parameters in terms of COD, $N\text{-}NH_4^+$ and TIN removal. The significant difference was set at 95% (p<0.05).

3.3. Results and discussion

3.3.1. Effect of DO concentration on COD and N removal efficiencies of the UAGSB reactor

The first four periods were aimed at evaluating the effect of different DO concentrations on the REs of COD, $N\text{-}NH_4^+$ and TIN at feed C/N ratios in the range of 12.1-13.5 (**Table 3.2**). The decrease of DO concentration from period I (4.0-6.0 $mg \cdot L^{-1}$) to period IV (0.02-1.60 $mg \cdot L^{-1}$) resulted in stable (p>0.05) $N\text{-}NH_4^+$ and TIN REs of 95 ± 9 and 85 ± 8% (**Table 3.3**), respectively, with a maximum effluent $N\text{-}NO_3^-$ concentration of 10.6 $mg \cdot L^{-1}$. Additionally, the DO decrease did not negatively affect the COD RE, which remained

stable at 84 ± 5% (p>0.05) in the first four periods (**Table 3.3**), indicating that the UAGSB reactor could be efficiently operated at low DO conditions, thus entailing low aeration costs for the treatment of wastewater.

In a previous study, Liu and Dong [295] observed that reducing the oxygen flow from 0.25 to 0.11 $g \cdot L^{-1} \cdot d^{-1}$ in a continuous-flow AGS system resulted in a decrease of $N\text{-}NH_4^+$ and TIN REs of about 46 and 31%, respectively. This was ascribed to an enhanced competition for DO between AOB and heterotrophic organisms in the outer layer of the granules, combined with a decreased depth of oxygen penetration, which resulted in a decreased nitrification efficiency at lower DO values [296,297]. In contrast with Liu and Dong [295], the $N\text{-}NH_4^+$ and TIN removals were not impaired at decreasing DO concentrations in the UAGSB reactor run in this study. However, it should be pointed out that, according to our calculations, about half of the feed N was removed via biomass growth. Indeed, considering a COD:N ratio of 100:5 for aerobic cell synthesis and that the influent COD concentration and feed C/N ratio were respectively 565 ± 80 $mg \cdot L^{-1}$ and 12.9 ± 1.5 during periods I-IV, the estimated N uptake for microbial growth ($TIN_{inf,\ G}$) accounted for 46-52% of the influent TIN (**Table 3.3**). This percentage increases if the amount of N taken up for microbial growth is calculated on the removed TIN ($TIN_{rem,\ G}$), reaching 51-63% (**Table 3.3**). The remaining fraction of nitrogen (37-49%) not detected in the effluent was likely removed via SND.

The existence of an active denitrifying community in the granular biomass was confirmed by the anoxic batch activity tests carried out at the end of period IV. A gradual $N\text{-}NO_3^-$ reduction was observed over time with a consequent $N\text{-}NO_2^-$ build-up and consumption (**Figure 3.2**).

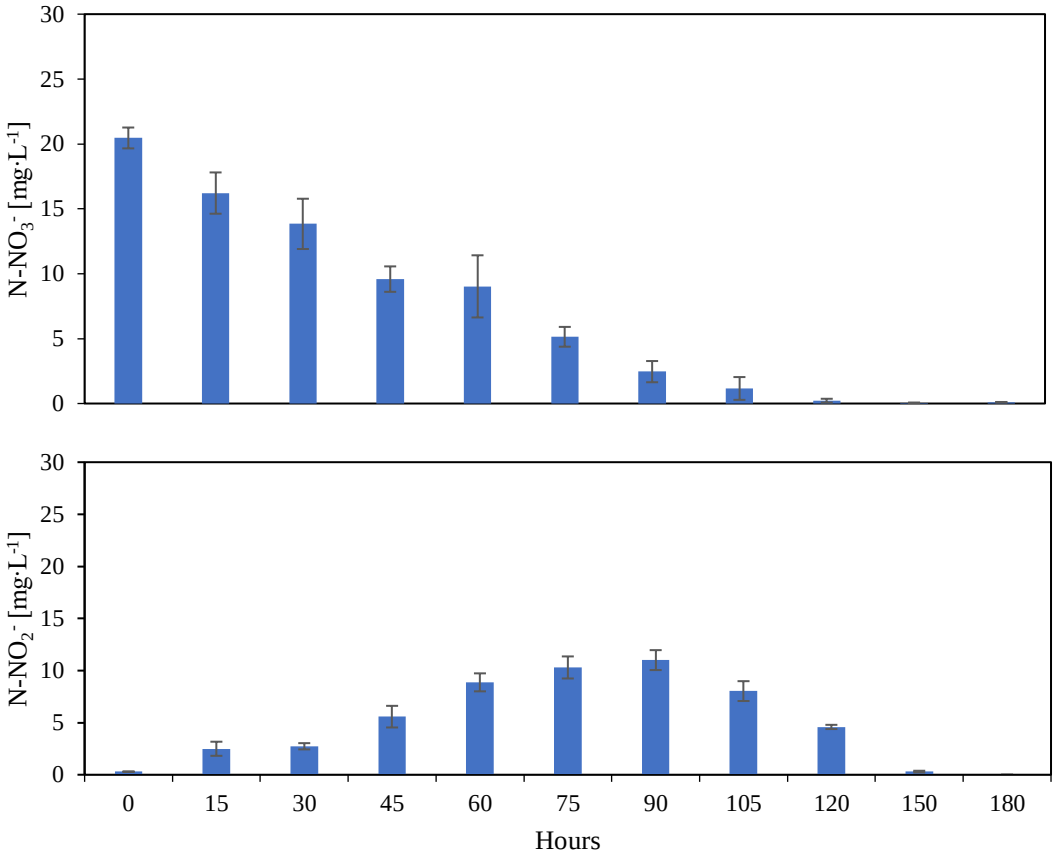

Figure 3.2. Temporal trend of $N\text{-}NO_3^-$ and $N\text{-}NO_2^-$ concentrations ($mg \cdot L^{-1}$) measured during the anoxic batch activity tests carried out at the end of period IV.

After 150 minutes, denitrification ceased as both NO_3^- and NO_2^- concentrations were below the detection limit. In the UAGSB reactor, the average TIN_{den} calculated in periods I-IV (**Eq. 6**) was 36% (**Table 3.3**) with no significant differences at decreasing DO concentrations ($p>0.05$), indicating that denitrification also occurred at high oxygen concentrations ($DO > 1.60\ mg \cdot L^{-1}$).

As shown in **Figure 3.3**, TSS and VSS concentrations in the UAGSB system at the end of period III (day 56) dropped from 2.5 ± 0.7 to $1.1 \pm 0.6\ mg \cdot L^{-1}$ and from 1.7 ± 0.2 to $0.8 \pm 0.3\ mg \cdot L^{-1}$, respectively. However, at the end of period IV (day 70), TSS and VSS concentrations increased up to 2.4 ± 0.3 and $1.1 \pm 0.2\ mg \cdot L^{-1}$, respectively, likely due to the biomass adaptation to lower DO conditions.

Table 3.3. COD, TIN, and N-NH_4^+ removal efficiencies (REs) obtained in the UAGSB reactor at different DO concentrations (periods I-IV), C/N ratios (periods V-VIII) and HRT (periods IX-X). The percentages of total influent and removed nitrogen used for biomass growth ($TIN_{inf, G}$ and $TIN_{rem, G}$, respectively), and of total influent inorganic nitrogen being denitrified (TIN_{den}) were calculated considering a COD:N ratio of 100:5 for aerobic cell synthesis.

Period	NH_4^+ – N RE (%)	TIN RE (%)	COD RE (%)	$TIN_{INF,G}$ (%)	$TIN_{REM,G}$ (%)	TIN_{DEN} (%)
I	93 ± 12	83 ± 12	85 ± 1	46 ± 5	60 ± 8	32 ± 8
II	100 ± 0	88 ± 2	78 ± 4	47 ± 4	54 ± 5	40 ± 5
III	95 ± 6	85 ± 5	84 ± 5	48 ± 7	51 ± 21	42 ± 16
IV	94 ± 8	82 ± 6	88 ± 1	52 ± 5	63 ± 8	30 ± 8
V	97 ± 5	64 ± 19	61 ± 16	20 ± 10	30 ± 15	45 ± 15
VI	99 ± 2	28 ± 8	63 ± 7	14 ± 4	53 ± 18	14 ± 8
VII	97 ± 6	61 ± 12	74 ± 4	28 ± 4	47 ± 12	34 ± 13
VIII	99 ± 2	84 ± 12	86 ± 3	55 ± 9	67 ± 15	29 ± 15
IX	90 ± 13	77 ± 10	75 ± 6	40 ± 6	53 ± 11	37 ± 12
X	63 ± 18	64 ± 15	71 ± 8	41 ± 6	68 ± 10	21 ± 10

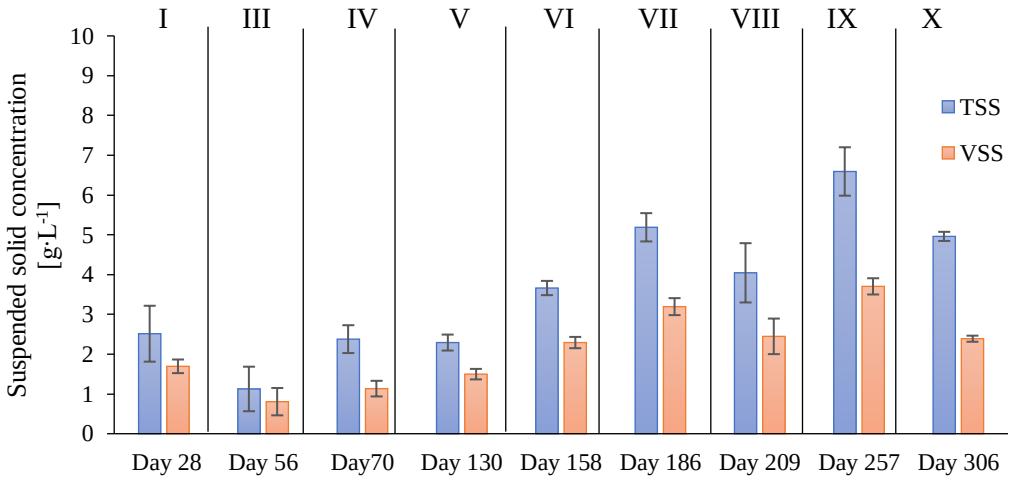

Figure 3.3. Evolution of the mean total (TSS) and volatile suspended solid (VSS) concentrations along the 306 days of the UAGSB reactor operation.

3.3.2. Performance of the UAGSB reactor under different feed C/N ratios

Periods V and VI were characterized by similar DO ranges (**Table 3.2**) and a decrease of the feed C/N ratio from 13.5 (period IV) to 7.0 and 4.7, respectively. The decrease of the C/N ratio did not negatively affect the $N\text{-}NH_4^+$ RE, which remained in the range of 97-99% (p>0.05) (**Table 3.3**). Nevertheless, the mechanisms contributing to $N\text{-}NH_4^+$ removal varied in comparison to the previous experimental periods. The lower feed COD concentration during period V decreased $TIN_{inf,G}$ and $TIN_{rem,G}$ to approximately 20 and 30%, respectively, while nitrification was stimulated as $N\text{-}NO_3^-$ concentration increased from 4.5 ± 2.3 (period IV) to 11.9 ± 5.2 (period V) and 31.1 ± 4.1 (period VI) mg $N{\cdot}L^{-1}$ (**Figure 3.4**), resulting in TIN_{den} values of 45% in period V and 14% in period VI (**Table 3.3**). On the other hand, the reduction in the feed C/N ratio led to insufficient organic carbon to support denitrification, as also reported by Iannacone et al [21]. Consequently, the TIN RE reached a minimum value of 28 ± 8% in period VI (**Table 3.3**) as a consequence of the increased $N\text{-}NO_3^-$ concentrations in the effluent. In contrast, Campo et al. [298] and Wang et al. [299] reported considerably higher TIN REs of about 71 and 78% respectively at feed C/N ratios of 3.8 and 3.5 in SBR, which could be due to the sequence of anaerobic and aerobic phases enhancing the selection and activity of functional microorganisms.

The COD RE decreased from 84 ± 5% (periods I- IV) to 62 ± 13% (periods V-VI) (**Table 3.3**), while the effluent COD concentration did not change significantly (p>0.05) and stayed at 94.7 ± 55.6 $mg{\cdot}L^{-1}$ (**Figure 3.5**). Biomass growth in the system was not affected by the lower COD levels in the feed, as the TSS and VSS concentrations did not change

significantly (p>0.05) in period V and even increased in period VI, reaching 3.66 ± 0.18 mg TSS·L^{-1} and 2.29 ± 0.14 mg VSS·L^{-1}, respectively (**Figure 3.3**).

Periods VII and VIII were characterized by an increase of the feed COD concentration and, therefore, of C/N ratio from 4.7 (period VI) to 8.0 and 13.6, respectively. The increase of feed COD led to lower DO concentrations in the bioreactor (below 1 mg·L^{-1} in period VIII), even though the inlet air flowrate was increased (data not shown). Interestingly, despite the low DO conditions, N-NH_4^+ RE was not affected (p>0.05) and remained stable at 98 ± 5%. In period VIII, more than 50% of the influent TIN was used for the biomass growth (**Table 3.3**). As expected, the feed C/N increase resulted in a gradual reduction of the effluent N-NO_3^- concentration to an average value of 5.30 mg N·L^{-1} in period VIII, suggesting an increase in the denitrifying efficiency of the system that could be favoured by the low DO levels in the bioreactor. TIN_{den} increased from 14% in period VI to 34 and 29% in periods VII and VIII, respectively. However, a gradual increase of the N-NO_2^- concentration up to a value of 3.69 mg N·L^{-1} was observed in period VIII. This suggests that the low DO values probably resulted in a slight inhibition of NOB biomass leading to NO_2^- build-up in the effluent. The COD RE also increased to 74 ± 4% (period VII) and 86 ± 3% (period VIII) (**Table 3.3**). Periods VII-VIII were characterized by a further increase of the TSS and VSS concentrations in the reactor (**Figure 3.3**), likely linked to the higher feed COD concentrations stimulating the growth of the heterotrophic families. The results obtained in this stage confirm that the UAGSB reactor is more efficient at higher C/N ratios even under microaerobic (DO<1 mg·L^{-1}) conditions, which should be taken into account in view of the future upscaling of the system.

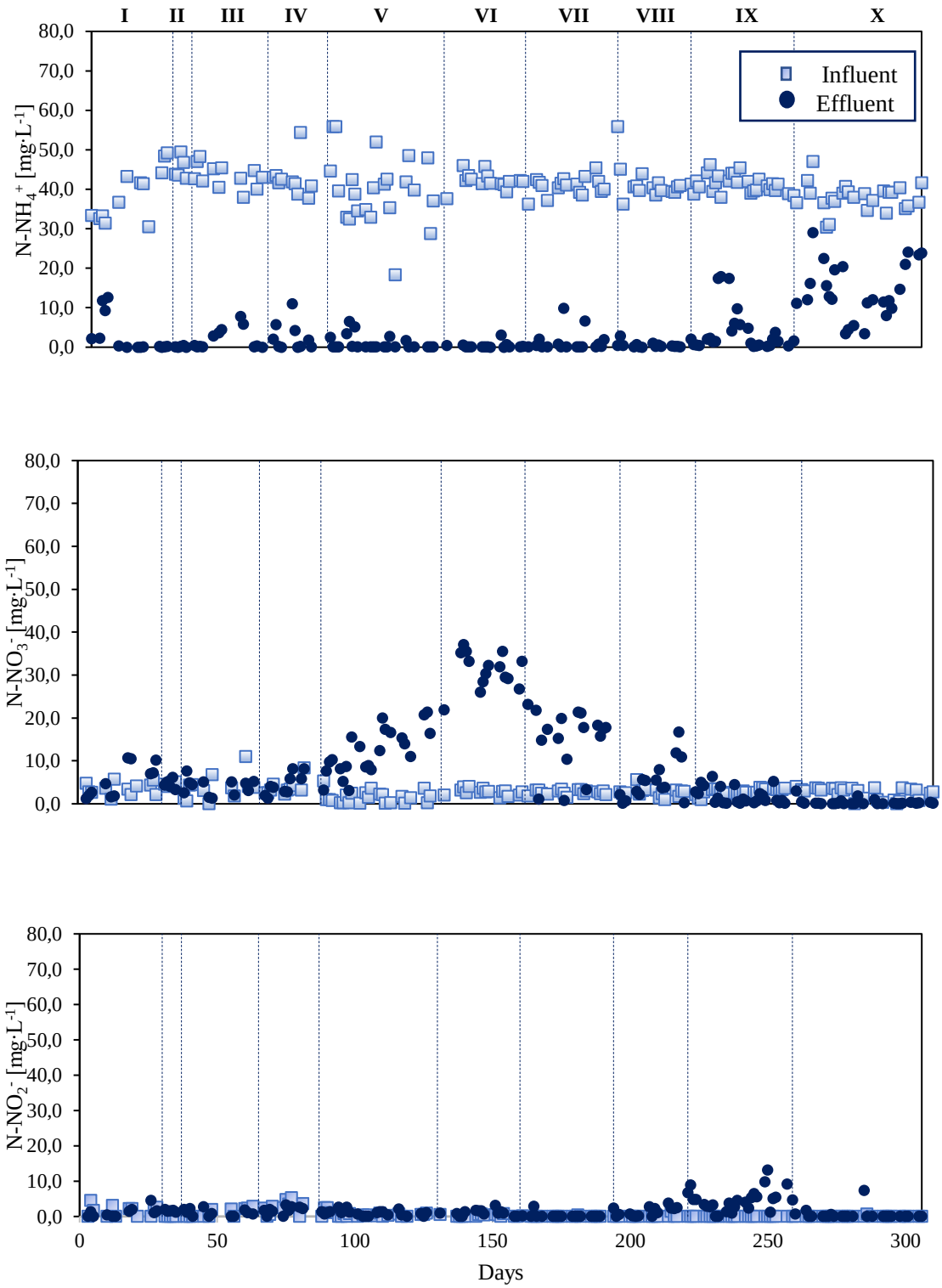

Figure 3.4. Temporal trend of influent and effluent $N\text{-}NH_4^+$, $N\text{-}NO_3^-$ and $N\text{-}NO_2^-$concentrations ($mg \cdot L^{-1}$) measured daily along the ten experimental periods of the UAGSB reactor operation.

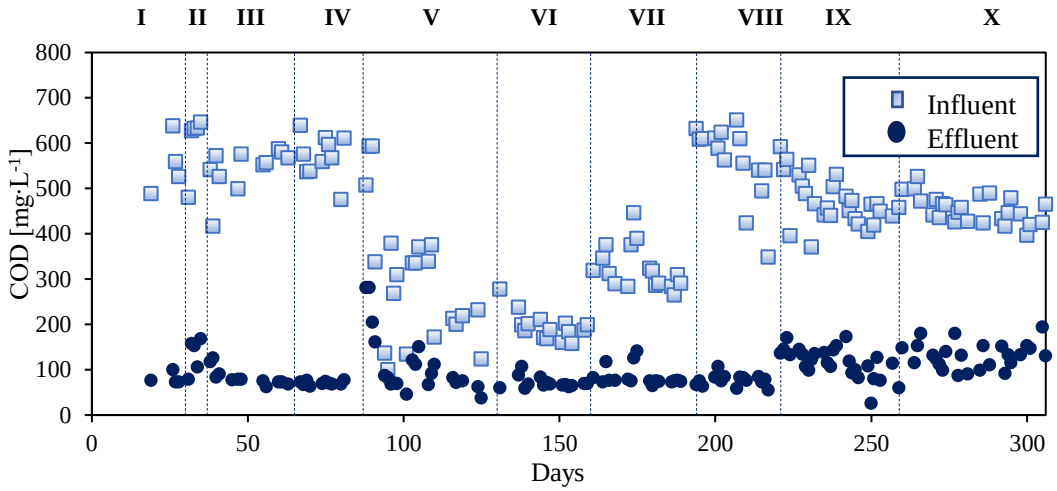

Figure 3.5. Temporal trend of influent and effluent COD concentrations (mg·L^{-1}) along the ten experimental periods of the UAGSB reactor operation.

3.3.3. Effect of HRT on the performance of the UAGSB reactor

At the beginning of period IX (day 221), the HRT was set at 12 h with the objective to evaluate the COD, N-NH_4^+, and TIN REs at increased organic and nitrogen loading rates. HRT decrease from 24 to 12 h resulted in a significant decrease of REs (p<0.05). The effluent N-NH_4^+ concentration (**Figure 3.4**) abruptly increased shortly after HRT decrease (day 231) due to a slow biomass adaptation and a period of interruption of the UAGSB reactor operation due to the summer break (not shown) (**Table 3.3**). From day 236 onwards, the N-NH_4^+ RE increased back up to 90 ± 13 %. Despite this, a significant increase of the effluent N-NO_2^- concentration was observed, as shown in **Figure 3.4**. NO_2^- accumulation indicates that reducing the HRT likely led to a partial nitrification, which can be attributed to a reduced contact time between the biomass and influent NH_4^+ as well as to the already limited DO availability in the bioreactor (0.01-1.22 mg·L^{-1}) (**Table 3.2**). On the other hand, the low DO levels ensured an elevated TIN_{den} in the bioreactor, being equal to 37% (**Table 3.3**). Although lower COD and TIN REs were observed at an HRT of 12 h, the UAGSB performances were still acceptable, being the REs ≥ 75% (on

average) and the effluent COD and TIN concentrations often below the effluent standards (COD=125 $mg \cdot L^{-1}$, TN=15 $mg \cdot L^{-1}$) for safe discharge in water bodies according to the EU legislation (Council Directive 91/271/EEC) for a population equivalent up to 100,000 inhabitants. At the end of period IX, a significant increase of the TSS and VSS concentrations was observed (**Figure 3.3**), which can be attributed to the increased organic loading provided to the system.

In period X (day 259), the HRT was further decreased to 6 h. This led to a gradual reduction of the COD RE to 71 ± 8% (**Table 3.3**). Nevertheless, the most important effect of the lower HRT was observed on $N\text{-}NH_4^+$ and TIN REs, which decreased to average values of 63 and 64%, respectively ($p<0.05$) (**Table 3.3**). Therefore, the HRT reduction led to a deterioration of reactor performance, as also reported by Wan et al. [277]. Considering that the effluent $N\text{-}NO_3^-$ and $N\text{-}NO_2^-$ concentrations were often negligible, the largest N fraction in the effluent remained as $N\text{-}NH_4^+$ (**Figure 3.4**). This suggests that the significant increase in the influent organic and nitrogen loading rates, coupled with the low DO concentrations in the bioreactor, negatively affected nitrification. Consequently, the denitrification performance also drastically decreased, resulting in a TIN_{den} of 21% (**Table 3.3**). This period was also characterized by a significant decrease in terms of TSS and VSS concentrations (**Figure 3.3**). This was due to sludge washout, which occurred for a period of about two weeks right after the HRT decrease and corresponding increase of the influent flow rate, resulting in a biomass loss of about 1.63 $g\ TSS \cdot L^{-1}$.

3.3.4. Preliminary cost evaluation

The continuous-flow UAGSB system investigated in this study during period VIII was able to obtain the highest COD, $N\text{-}NH_4^+$ and TIN REs of 86, 99, and 84%, respectively,

at a maximum DO concentrations of 0.30 mg $O_2 \cdot L^{-1}$, a C/N ratio of 13.6 and an HRT of 24 h. For this reason, the average influent COD and N-NH_4^+ concentrations in period VIII (**Table 3.2**) were used to size both UAGSB reactor and MLE system. The DO concentration was different among the two systems. The main results obtained are shown in **Table 3.4**.

Table 3.4. Main results of the preliminary economic evaluation aimed at evaluating the capital (CAPEX) and operating expenses (OPEX) of a UAGSB reactor and a MLE system both serving a population equivalent (PE) of 10,000 inhabitants.

		MLE	***UAGSB***
Flow rate	$m^3 \cdot year^{-1}$	759,200	759,200
V_N	m^3	1678	2080
V_D	m^3	721	-
OD	kg $O_2 \cdot h^{-1}$	79.2	73.6
N. diffusers	-	270	203
Typical standard aeration efficiency (SAE)	kg $O_2 \cdot kWh^{-1}$	2.5	2.5
Max. power	$kWh \cdot year^{-1}$	277,560	258,020
Max. energetic costs	**€·year^{-1}**	**32,752**	**30,446**
Max. energetic costs	**€·m^{-3}**	0.43	0.40
Construction costs	€	128700	111603
Air diffusers costs	€	5097	3820
Total CAPEX	**€**	**133,797**	**115,422**

Based on the results of this study, the UAGSB reactor could allow an annual energy saving of about 19,540 $kWh \cdot year^{-1}$. Considering the price of the electric energy as given by the Italian Regulatory Authority for Energy Networks and Environment (ARERA) in July 2023, which is equal to 0.118 $€ \cdot kWh^{-1}$, the corresponding economic saving associated is about 2,300 $€ \cdot year^{-1}$. The CAPEX associated with the construction of the MLE and UAGSB systems are about 128,700 and 111,600 €, respectively (**Table 3.4**). By adding the costs of the air diffusers, taking into consideration an approximate cost for each air diffuser of about 19 €, the total CAPEX of MLE and UAGSB systems were about

133,800 and 115,400 €, respectively, with an economic saving of about 18,400 €. These preliminary economic considerations confirm that the UAGSB system could be a more attractive cost-effective technology than the MLE system.

3.4. Practical applications and future research

The results of this study suggest that the UAGSB reactor can be considered as a promising technology for the simultaneous removal of C and N from wastewaters with C/N ratios as high as 11.4-13.6 when operated at HRT > 6 h. Compared to continuous-flow anaerobic and aerobic granular sludge reactors operated in previous studies (**Table 3.1**), the UAGSB reactor herein tested showed comparable or even higher REs under different operating conditions. Further studies should be addressed to a better investigation of the process in the case of low C/N ratios (below 7.0) and HRTs of 6 h or lower, for instance in the presence of higher biomass concentrations possibly entailing higher REs, and to reduce energy consumption associated with the process. Future research should also focus on the combination of the biological nitrogen removal via SND to P removal in the UAGSB reactor. Furthermore, although the morphological changes of the granules were not specifically evaluated in this study, the granule structure was clearly distinguishable throughout the experiment. However, applications of this technology on the pilot- and full-scale would allow to better assess the effect of the feed wastewater composition on C and N removal, granule stability, as well as to evaluate the associated operating costs.

One drawback of the process that emerged in this study is that the effluent NO_2^- concentration often exceeded the Italian standard (D. Lgs. 152/2006, Annex V, Part III) for industrial wastewater discharge into sewers (0.6 mg $N\text{-}NO_2^-$ L^{-1}) even under the best operating conditions. Therefore, a post-treatment aiming to reduce NO_2^- levels should be considered. An interesting approach to reduce the residual $N\text{-}NO_3^-$ and $N\text{-}NO_2^-$

concentrations could be the study of a symbiotic process between aerobic granules and microalgae to remove the residual fraction of nitrogen and further reduce the operational costs of the whole process, by using part of the oxygen needed from the microalgal metabolism.

3.5. Conclusions

The continuous-flow UAGSB system investigated in this study was able to obtain COD, $N\text{-}NH_4^+$ and TIN REs up to 86, 99 and 84%, respectively, at a C/N ratio of 13.6, an HRT of 24 h and DO concentrations as low as 0.01 - 0.30 mg $O_2 \cdot L^{-1}$, indicating that bacterial communities playing different roles are properly retained in a single-stage system. Under the best performing conditions, the preliminary cost evaluation showed that the UAGSB reactor could result in a capital and energy cost savings of around 14 and 7 %, respectively, compared to a MLE system. Higher effluent COD and $N\text{-}NH_4^+$ concentrations un the UAGSB reactor were observed when decreasing the C/N ratio to 4.7-8.0 and the HRT to 6 h. These results suggest that the use of the UAGSB technology can be highly recommended, both from engineering and economic perspective, for the treatment of urban wastewater, but further research efforts are needed for its validation on a larger scale.

CHAPTER 4

Continuous bioelectrochemical treatment of nitrate-containing wastewater in a double-chamber bioelectrochemical system

Article under preparation

4.1. Introduction

Nitrate (NO_3^-) is one of the most common water pollutants in the world, leading to eutrophication of surface waters, increased risk of intoxication, and disruption of aquatic ecosystems threatening biodiversity [51,300–302]. Anthropogenic activities such as the intensive use of agricultural fertilizers and nitrogen-based chemicals in pharmaceutical, food processing, chemical, and petroleum refining industries [303] are the major sources of NO_3^- pollution in aquatic environments [302]. The most widespread and harmful effects of the excessive use of nitrogen fertilizers in agriculture are the deterioration of groundwater quality and the contamination of drinking water supplies, which can pose a direct risk to human health [304]. High NO_3^- consumption could cause preterm births [305], birth defects [306], congenital anomalies, methemoglobinemia in infants up to 6 months [307,308], and elevated cancer risk for adults [309,310]. Currently, to reduce the impact of NO_3^- contamination on drinking water quality and human health, the EU regulation (Directive 2020/2184) and the World Health Organization (WHO) have set the acceptable threshold of nitrate concentration in groundwater at 50 $mg \cdot L^{-1}$ as NO_3^- and 10 mg $N\text{-}NO_3^- \cdot L^{-1}$ as nitrate-nitrogen ($N\text{-}NO_3^-$) [311,312].

NO_3^- removal from water primarily relies on biological denitrification with physicochemical (e.g., ion exchange, adsorption, membrane separation and reverse osmosis) [313,314] and electrochemical [315,316] methods as potential alternatives. Biological denitrification is performed by denitrifying microorganisms using NO_3^- as a terminal electron acceptor and organic, inorganic, or both substances as electron donors in heterotrophic, autotrophic, and mixotrophic denitrification, respectively, and as energy source to maintain microbial growth [48,317,318]. Physicochemical treatments for NO_3^-

removal have been largely investigated, but they are associated with high operating costs, low selectivity, and the formation of by-products such as sludge [319].

Recently, NO_3^- treatment has also been applied in bioelectrochemical systems (BESs) [320–323]. In BES, microorganisms are used to catalyze the electrochemical reactions by interacting with the electrodes [206]. Typically, a BES consists of anode and cathode electrodes where oxidation and reduction reactions occur, respectively. To enhance ion separation, the chambers containing the electrodes can be separated with an ion-exchange membrane [324]. At the anode, degradation of the organic substrate generates electrons and protons, which are transferred to the cathode via an external circuit or ion exchange membrane [206]. Reduction reactions at the cathode may include H_2 evolution [207] or direct electron transfer by microorganisms capable of transferring electrons from the electrode through transport chains to extracellular electron acceptors [325].

In BESs, NO_3^- removal can occur through autotrophic or heterotrophic denitrification or simultaneously with both of them [326–329]. H_2 can be used as an electron donor in the autotrophic denitrification process to convert NO_3^- into nitrogen gas (N_2) or denitrifiers can uptake electrons directly from the electrode [330]. In addition, heterotrophic bacteria can utilize organic substrates for further NO_3^- removal, thereby increasing the NO_3^- removal efficiency [326,331].

Recent research has focused on the study of denitrifying BES. Different bioelectrochemical configurations have been investigated, as well as the effect of key parameters such as pH, hydraulic retention time (HRT), cathode potential and conductivity on the bacterial community involved in the process [332–336]. Recent studies have also focused on the development of BESs as an alternative to conventional wastewater treatment [337–339] or their integration into wastewater and sludge treatment

[340,341]. Furthermore, several promising integrated bioelectrochemical technologies have been developed alongside traditional wastewater treatment methods in response to the need for sustainable technological solutions for wastewater management at various scales. Combining BES with existing technologies could not only reduce overall costs but also improve the efficiency of wastewater treatment and the reliability of the combined system [342]. This highlights the importance of enriching the existing literature in this field.

For this purpose, this study aimed to investigate the NO_3^- removal potential of denitrifying BES as a post-treatment of an aerobic granular sludge system used to combined carbon and nitrogen removal. In a previous study, Lanzetta et al. [91] operated a continuous-upflow (micro)aerobic granular sludge blanket reactor (UAGSB) to concomitantly remove C and N under different DO ranges (0.01–6.00 $mg \cdot L^{-1}$), feed C/N ratios (4.7–13.6), and HRTs (6–24 h). However, reducing the C/N ratio to 4.7 resulted in the lowest total inorganic nitrogen (TIN) removal efficiency of 28%, with an effluent $N\text{-}NO_3^-$ concentration of 31.1 ± 4.1 mg $N \cdot L^{-1}$, being above the regulatory limit for wastewater discharge into sewers [91]. Therefore, to improve TIN removal even at low feed C/N ratio, the donwstream use of a BES was investigated in this study. Specifically, the main goal of this study was to understand whether the bioelectrochemical system could successfully complement the aerobic granular sludge process for N removal at low feed C/N ratios, by eliminating the need for external organic carbon addition through the establishment of an autotrophic denitrification process in the BES. The NO_3^- removal efficiency of a continuous double-chamber BES was evaluated for 63 days at different feeding conditions and HRTs. In addition, 16S rRNA high-throughput sequencing was

used to determine the microbial community structure and gain insight into the key functional microorganisms responsible for N removal.

4.2. Materials and methods

4.2.1. Experimental set-up

The experiments were carried out in duplicate in two double-chamber flow-through BES reactors, reactor 1 (R1) and reactor 2 (R2). Each reactor consisted of anode and cathode chambers (33 mL each with an effective projected surface area of each electrode of 33 cm^2) separated by a cation-exchange membrane (CEM) (CMI-7000, Membranes International, USA) (**Figure 4.1**). Before operation, the CEM was soaked overnight in 5% (w/w) NaCl solution and washed with MilliQ water. The reactor parts were made of polycarbonate and hydraulically connected to each other. To make the system liquid- and air-tight, rubber seals (1.5 mm thick) were used between the chamber plates and membranes. Both the anode and cathode chambers were filled with graphite granules (EC-100, Graphite Sales, USA) that acted as electrodes and biofilm carriers. Prior to being added to the chambers, the graphite granules were acid- and alkaline-washed according to Jermakka et al. [343]. Graphite rods (l=75 mm, d=6 mm, 99.995% trace metals basis, Sigma-Aldrich) were inserted into each anodic and cathodic chamber as current collectors. Anode and cathode potentials were measured against Ag/AgCl reference electrodes placed in both chambers (+0.197 V vs SHE, RE-5B, BASi, United Kingdom). Two different potentiostats (Bank Elektronik, Germany and BioLogic VMP3, France) were used to maintain the anodic and cathodic potentials at +0.2 V and -0.65 V vs. SHE, respectively, during the enrichment periods and to maintain the cathodic potential at -0.65 V vs. SHE during the experimental phases. A peristaltic pump

(Masterflex™ 77912-10, Pennsylvania) was used to feed the influent solution to the BESs. The influent solution was purged with N_2 gas to ensure anaerobic conditions.

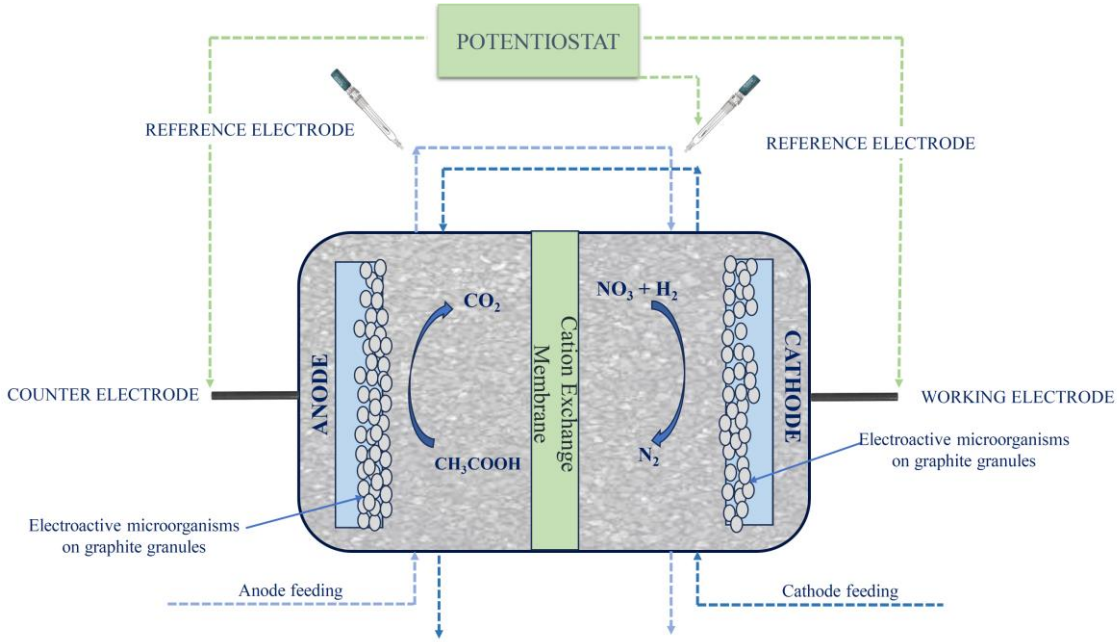

Figure 4.1. Schematic diagram of the BES reactor configuration, consisting of anodic and cathodic chambers containing graphite granules (EC-100, Graphite Sales, USA), which acted as electrodes and supports for the biofilm. Anode loading (i.e., feeding from anode to cathode, in light blue) and cathode loading (i.e., feeding from cathode to anode, in dark blue) were implemented separately.

4.2.2. Biomass enrichment at the electrodes

The anode and cathode electrodes were separately enriched for electroactive microorganisms responsible for acetate oxidation and autotrophic denitrification, respectively (**Table 4.1**). A synthetic wastewater containing ($mg \cdot L^{-1}$) NH_4Cl (6), KH_2PO_4 (25), $NaHCO_3$ (95.4), CH_3COONa (150), and trace element solution (TES) [344] was used as feed during the anode enrichment. In contrast, a synthetic wastewater containing (in $mg \cdot L^{-1}$) KNO_3 (217), NH_4Cl (6), KH_2PO_4 (25), $NaHCO_3$ (95.4), $NaNO_2$ (5), and TES

[344] was used as feed for the cathode enrichment. In addition, during both anode and cathode enrichments, 1 g/L of 2-bromoethanesulphonic acid (BESA) was added to the influent to inhibit the growth of methanogens [345].

The anodic enrichment period (days 0-61) was conducted in fed-batch mode under anaerobic conditions at an anode potential of +200 mV vs. an Ag/AgCl reference electrode. A digested sewage sludge from a local municipal wastewater treatment plant (Viinikanlahti, Tampere, Finland) was used as inoculum. The enrichment medium used was recirculated through the anode at a constant rate of 105 $mL \cdot min^{-1}$ (Cole-Parmer Masterflex Peristaltic Pump 7553-20, Pennsylvania, U.S.A). Gas bags were connected to the recirculation bottles to collect gaseous compounds produced in the reactor. Subsequently (days 62-83), the anode chambers were operated in continuous mode at an HRT of 10 h using the same enrichment medium.

After the enrichment of electroactive biomass on the anode (0-61 days), the enrichment of denitrifying biomass took place at the cathode side (62-83 days). The denitrifying inoculum was taken from the effluent of a previously operated 2-chamber bioelectrochemical cell optimized for efficient denitrification. The enrichment of denitrifying biomass was conducted under anaerobic conditions at a cathode potential of -650 mV vs. an Ag/AgCl reference electrode. The enrichment medium used was recirculated through the cathode at a constant rate of 105 $mL \cdot min^{-1}$ (Cole-Parmer Masterflex Peristaltic Pump 7553-20, Pennsylvania). Gas bags were connected to the effluent bottles to collect gaseous compounds produced in the reactor.

4.2.3 Reactor operation

After the anode and cathode enrichment phases, the two BESs (R1 and R2) were operated in continuous mode for 63 days divided into seven experimental periods, as reported in

Table 4.1, at a cathode potential of -650 mV vs. an Ag/AgCl reference electrode. The start of this experimental period was considered as day 0.

A synthetic wastewater containing ($mg \cdot L^{-1}$) KNO_3 (217), NH_4Cl (6), KH_2PO_4 (25), $NaHCO_3$ (95.4), $NaNO_2$ (5), CH_3COONa (150), and TES [344] was used as feed to mimic the UAGSB reactor effluent characterized by a $N\text{-}NO_3^-$ concentration of 31.1 ± 4.1 mg $N \cdot L^{-1}$ [91]. In addition, 1 $g \cdot L^{-1}$ of BESA was added to the influent solution to inhibit the growth of methanogens [345]. The stock solutions of NH_4Cl and $NaNO_2$ were sterilized by filtration (0.2 µm polyethersulfone membrane syringe filter, VWR International, North America), whereas the rest of the stock solutions were sterilized by autoclaving at 121°C for 20 min.

During the first two periods (days 0-15), the influent was fed to the anode from where it flowed to the cathode, and the HRT was reduced from 10 to 7 h to increase the organic and N loads. From period III (days 16-22) to period VII (days 59-63), the influent was fed to the cathode from where it flowed to the anode, while the HRT was progressively decreased from 7 to 2 h. During period VI, an acetate-free influent was fed to the cathode at an HRT of 2 h to evaluate the denitrification performance using cathodic H_2 as the only electron donor. In the last period, the two reactors (R1 and R2) were used to test two different conditions and evaluate the extent of autotrophic and heterotrophic denitrification in the bioreactors. In particular, R1 was operated with an HRT of 4 h and an acetate-free influent. In contrast, R2 was operated with acetate as the sole electron donor, thus removing the potential applied to the cathode. During the study, the shift from an experimental period to the following was carried out when the NO_3^- removal performance of both reactors was considered stable, i.e., when three consecutive samples gave similar results with differences between sampling points of less than 10 %. To

investigate the feasibility of the method, the results in terms of $N\text{-}NO_3^-$ and $N\text{-}NO_2^-$ concentrations were then compared with the Italian standards (D. Lgs. 152/2006, Annex V, Part III) for industrial wastewater discharge into sewers (30 mg $N\text{-}NO_3^- \cdot L^{-1}$ and 0.6 mg $N\text{-}NO_2^- \cdot L^{-1}$).

Table 4.1. Operating conditions and duration of each experimental period during the anodic and cathodic enrichment and continuous operation of the two-chamber flow-through bioelectrochemical system (Reactor 1 (R1) and Reactor 2 (R2)). NLR= nitrogen loading rate.

Period	Duration (days)	Operational mode	Reactor	Feeding	Potential (mV)	Stock solution added	HRT (h)	NLR (g $N\text{-}NO_3^-$ $\cdot m^{-3} \cdot d^{-1}$)
Enrichment period								
Anode enrichment	0-61	Fed-batch	R1-R2	Anode	+200 at the anode	NH_4Cl, KH_2PO_4, $NaHCO_3$, CH_3COONa and TES*	/	
	62-83	Continuous	R1-R2	Anode	-650 at the cathode	NH_4Cl, KH_2PO_4, $NaHCO_3$, CH_3COONa and TES	10	
Cathode enrichment	62-83	Fed-batch	R1-R2	Cathode	-650 at the cathode	KNO_3, NH_4Cl, KH_2PO_4, $NaHCO_3$, $NaNO_2$ and TES	/	
Long-term reactor operation								
I	0-9	Continuous	R1-R2	Anode	-650 at the cathode	KNO_3, NH_4Cl, KH_2PO_4, $NaHCO_3$, $NaNO_2$, CH_3COONa and TES	10	10.6
II	10-15	Continuous	R1-R2	Anode	-650 at the cathode	KNO_3, NH_4Cl, KH_2PO_4, $NaHCO_3$, $NaNO_2$, CH_3COONa and TES	7	9.6

Period	Duration (days)	Operational mode	Reactor	Feeding	Potential (mV)	Stock solution added	HRT (h)	NLR (g $N\text{-}NO_3^-$ $\cdot m^{-3} \cdot d^{-1}$)
III	16-22	Continuous	R1-R2	Cathode	-650 at the cathode	KNO_3, NH_4Cl, KH_2PO_4, $NaHCO_3$, $NaNO_2$, CH_3COONa and TES	7	10.1
IV	23-36	Continuous	R1-R2	Cathode	-650 at the cathode	KNO_3, NH_4Cl, KH_2PO_4, $NaHCO_3$, $NaNO_2$, CH_3COONa and TES	4	4.6
V	37-46	Continuous	R1-R2	Cathode	-650 at the cathode	KNO_3, NH_4Cl, KH_2PO_4, $NaHCO_3$, $NaNO_2$, CH_3COONa and TES	2	2.1
VI	47-63	Continuous	R1	Cathode	-650 at the cathode	KNO_3, NH_4Cl, KH_2PO_4, $NaHCO_3$, $NaNO_2$ and TES	2	2.5
	47-58	Continuous	R2	Cathode	-650 at the cathode	KNO_3, NH_4Cl, KH_2PO_4, $NaHCO_3$, $NaNO_2$ and TES	2	2.5
VII	64-75	Continuous	R1	Cathode	-650 at the cathode	KNO_3, NH_4Cl, KH_2PO_4, $NaHCO_3$, $NaNO_2$ and TES	4	5.6
	59-63	Continuous	R2	Cathode	No applied potential	KNO_3, NH_4Cl, KH_2PO_4, $NaHCO_3$, $NaNO_2$, CH_3COONa and TES	2	2.5

*TES: trace element solution

4.2.4 Analytical methods

Liquid samples were collected daily from both the anode and cathode chambers. pH and conductivity were measured from unfiltered liquid samples shortly after sampling. The pH was monitored with a pH-meter 3110 (WTW GmbH, Germany) and a Slim Trode electrode (Hamilton®), whereas the conductivity was measured with a FiveEasy F30 conductivity meter with Mettler Toledo Conductivity Probe Sensors (Mettler Toledo, Milano, Italy). The potentials at the electrodes (counter electrode (CE), working electrode (WE), and reference electrode) were manually monitored with a CEM DT-922 voltmeter. The samples for detection of NO_3^-, NO_2^-, and volatile fatty acids (VFAs) concentrations, were filtered with 0.45 µm and 0.2 µm sterile filters (CHROMAFIL® Xtra polyester membrane filter, Macherey-Nagel, Germany), respectively. The concentrations of NO_3^- and NO_2^- were measured by using a Dionex ICS-1600 (Thermo Scientific, Waltham, Massachusetts, USA) ion chromatography (IC) as described by Sun et al. [346], whereas the VFA content, focusing on acetate, was measured with Shimadzu GC-2010 Plus gas chromatograph equipped with a Zebran ZB-WAX Plus column and a flame ionization (FID) detector [347]. The filtered liquid samples were stored at -20ºC when the ion-chromatography and VFA analysis were not available at the sampling occasions. The content of gas formed during the experiments was measured by a Shimadzu GC-2014 gas chromatograph equipped with a Porapak N 80-100 column and a thermal conductivity detector [348].

4.2.5 Calculations

Removal efficiencies in terms of N-NO_3^-, NO_x (NO_3^- + NO_2^-), and acetate were calculated by comparing the concentrations in the influent and effluent, as described by the equations

Eqs. 1-3. For each experimental step, the HRT was calculated based on the total reactor volume, i.e., the sum of the volume of the anode and cathode chambers.

The concentration values reported for the influent and the effluent are the average values at three sampling points for each reactor (R1 and R2) with standard deviations (±) unless otherwise indicated. The NO_x concentration removed via heterotrophic denitrification ($NO_{xREM,het.}$) is evaluated considering the stoichiometry of the denitrification reaction using acetate as an electron donor [51] (**Eq. 4**). The NO_x removed by the autotrophic pathway ($NO_{xREM,aut.}$) is represented by the remaining NO_x concentration (**Eq. 5**).

$$\text{N-NO}_3^-{}_{\text{Removal efficiency}} = \frac{([\text{N-NO}_3^-{}_{\text{INF}}] - [\text{N-NO}_3^-{}_{\text{EFF}}])}{([\text{N-NO}_3^-{}_{\text{INF}}])} \times 100 \quad (1)$$

$$Acetate_{\text{Removal efficiency}} = \frac{([acetate_{\text{IN}}] - [acetate_{\text{EFF}}])}{([acetate_{\text{INF}}])} \times 100 \quad (2)$$

$$NOx_{\text{Removal efficiency}} = \frac{([\text{N-NO}_3^-{}_{\text{INF}}] + [\text{N-NO}_2^-{}_{INF}]) - ([\text{N-NO}_3^-{}_{EFF}] + [\text{N-NO}_2^-{}_{EFF}])}{([\text{N-NO}_3^-{}_{\text{INF}}] + [\text{N-NO}_2^-{}_{INF}])}, \quad (3)$$

$$NOx_{\text{Rem, het.}} = \frac{([acetate_{\text{IN}}] - [acetate_{\text{EFF}}])}{3.63} \quad (4)$$

$$NOx_{\text{Rem, aut.}} = ([NOx_{\text{IN}}] - [NOx_{\text{EFF}}]) - NOx_{\text{RE, het.}} \quad (5)$$

where $[\text{N-NO}_3^-{}_{\text{INF}}]$, $[\text{N-NO}_3^-{}_{\text{EFF}}]$ and $[\text{N-NO}_2^-{}_{\text{INF}}]$, $[\text{N-NO}_2^-{}_{\text{EFF}}]$ are the influent and effluent N-NO_3^- and N-NO_2^- concentrations, respectively; $[acetate_{\text{INF}}]$ and $[acetate_{\text{EFF}}]$ are the influent and effluent acetate concentrations, respectively.

The current density was calculated against the effective surface area of each electrode (33 cm^2) (**Eq. 6**). The energy consumption by the potentiostat was calculated from the hourly

average of current and voltage data (**Eq. 7**) and as specific energy consumption (SEC) based on the mass of N removed from the double-chamber systems (**Eq. 8**).

$$Current\ density\ (mA \cdot cm^{-2}) = \frac{I\ (mA)}{Effective\ surface\ area\ of\ each\ electrode\ (cm^2)} \quad (6)$$

$$Energy\ required\ (kWh) = E_{WE} - E_{CE}(V) \cdot I\ (A) \cdot h \quad (7)$$

$$SEC = \frac{Energy\ required\ (kWh)}{\left(\left[N - NO_3^-{}_{INF}\right] + \left[N - NO_2^-{}_{INF}\right] - \left[N - NO_3^-{}_{EFF}\right] + \left[N - NO_2^-{}_{EFF}\right]\right)} \quad (8)$$

where E_{WE} and E_{CE} are the working and the counter electrode potential, respectively; I is the current intensity measured by the potentiostat.

4.2.6 Statistical data analysis

The Data Analysis Tool of Excel 2016 (Microsoft Corporation, USA) was used to perform a one-way analysis of variance (ANOVA) to determine the statistical differences in the performance parameters in terms of CH_3COOH and $N\text{-}NO_3^-$ removal. The significant difference was set at 95% (p<0.05).

4.3 Results and discussion

4.3.1 Biomass enrichment in the anodic and cathodic chambers

The values of pH and acetate concentration in the anode and cathode chambers were as shown in **Figure 4.2**. For the cathodic enrichment period, in addition to pH, the trend of $N\text{-}NO_3^-$ concentration over time was evaluated, as shown in **Figure 4.3**.

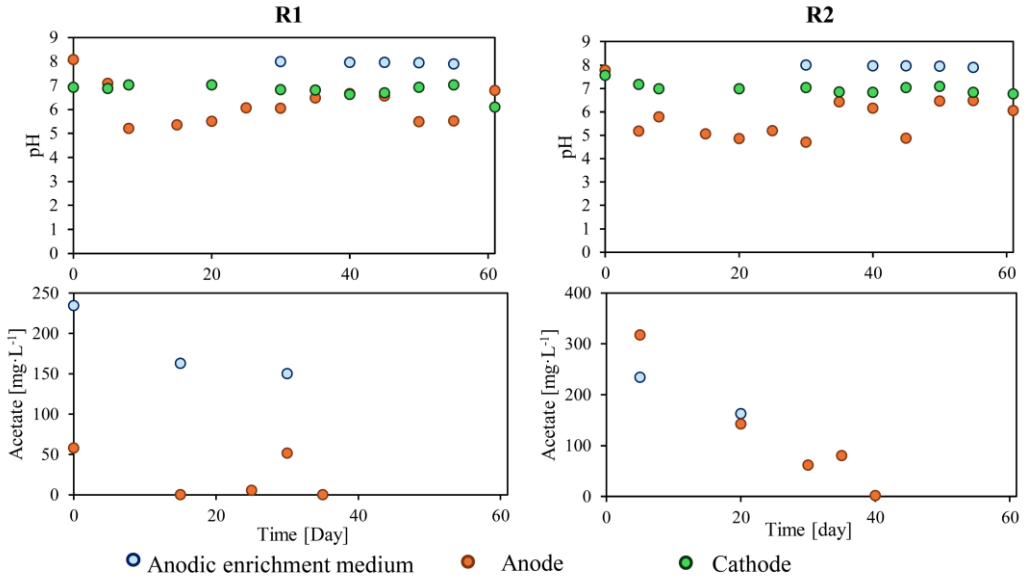

Figure. 4.2. Daily evolution of pH in the anodic enrichment medium as well as at the anode and cathode and of acetate concentration ($mg \cdot L^{-1}$) in the anodic enrichment medium and at the anode during the anode enrichment.

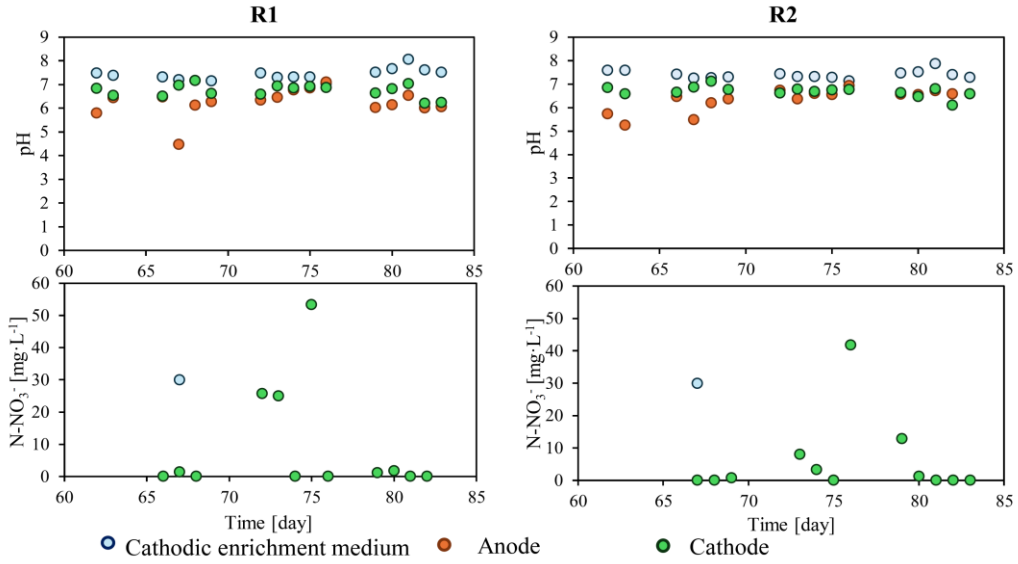

Figure. 4.3. Daily evolution of pH in the cathodic enrichment medium as well as at the anode and cathode and of $N\text{-}NO_3^-$ concentration ($mg \cdot L^{-1}$) in the cathodic enrichment and at the cathode during the cathode enrichment.

In BES, the biodegradation of organic compounds results in the production of protons, which lower the pH of the electrolyte. Therefore, the decrease in pH at the anode (**Figure 4.2**) likely indicated the presence of microbial activity during the anodic enrichment period. In contrast, during the cathode enrichment period, the proton consumption during the reduction reactions did not allow an increase in pH, probably due to the low current present (**Figure 4.3**). In addition, the effects of the anodic and cathodic enrichment periods were evident from the decreasing trends in acetate and $N\text{-}NO_3^-$ concentrations. During the enrichment periods, continuous monitoring of current density was not possible due to limitations in the availability of the potentiostat. After the successful enrichment of anodic and cathodic communities, the simultaneous removal of acetate and NO_3^- was studied.

4.3.2 Effect of anodic and cathodic feeding and different HRTs on $N\text{-}NO_3^-$ removal

The temporal profiles of $N\text{-}NO_3^-$, $N\text{-}NO_2^-$ and acetate concentrations in the influent and effluent of anode and cathode during the continuous operation of R1 and R2 are shown in **Figure 4.4**.

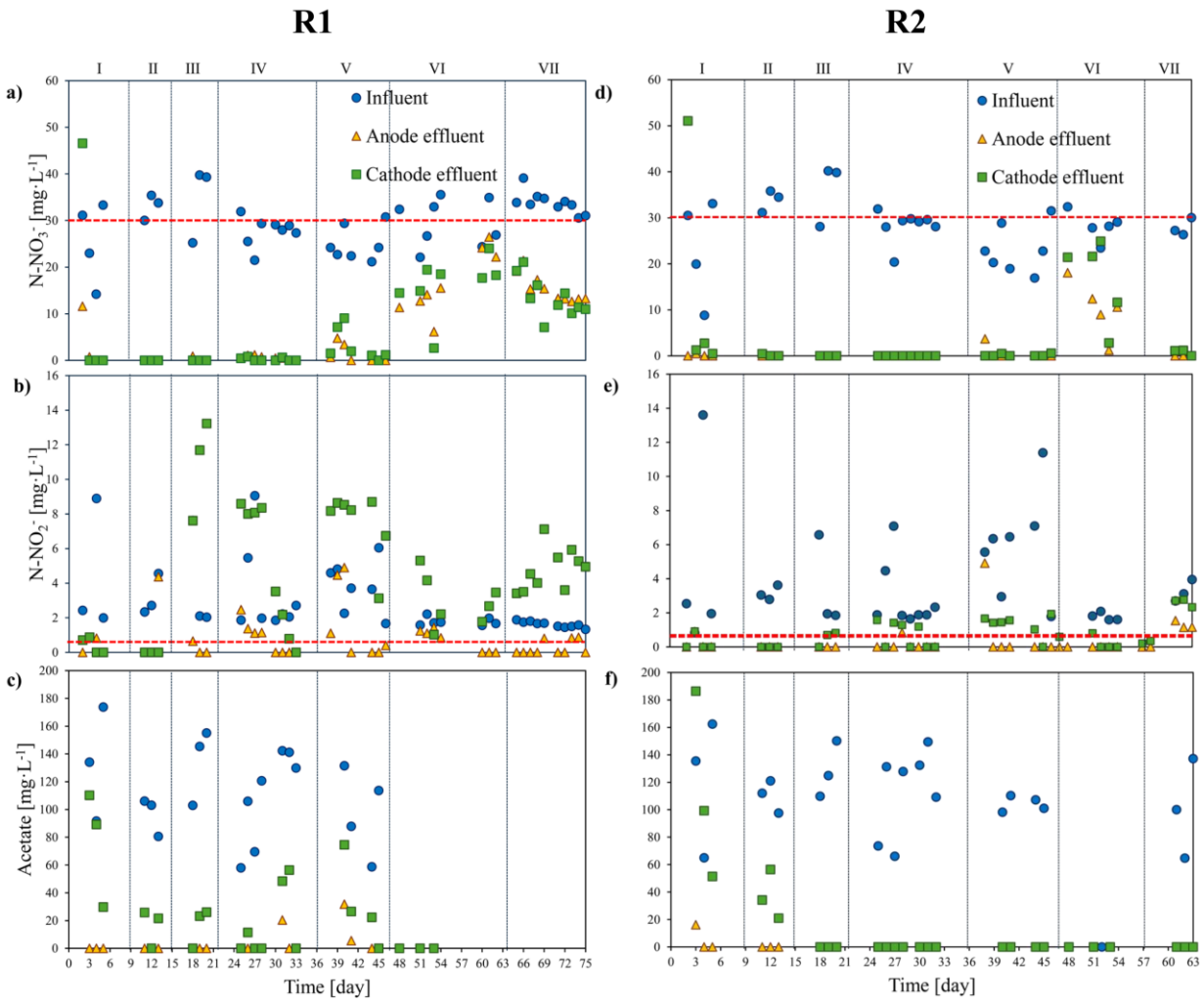

Figure 4.4. Temporal trends of $N\text{-}NO_3^-$(a,d), $N\text{-}NO_2^-$(b,e), and acetate concentrations (c,f) ($mg \cdot L^{-1}$) in the influent and effluent of the anode and cathode during the 7 experimental periods of R1 and R2 operation (**Table 4.1**). The red line indicates the Italian standard for industrial effluent discharge to sewers.

The first two periods (days 0-15) were characterized by a decreasing HRT from 10 to 7 h and the influent wastewater was fed to the anode and then flowed towards the cathode. As shown in **Figure 4.4**, the anodic feeding during periods I and II resulted in almost complete NOx removal with an average NOx and acetate removal efficiencies at the anode of 96 ± 4 and 100 ± 0 % in R1, respectively, while these reached 99 ± 2 and 98 ± 4 % in R2. The results indicate that heterotrophic denitrification with acetate as the

electron donor occurred. The feed acetate concentration in these two periods was equal to 133 ± 33 and 97 ± 11 mg·L^{-1} in R1 and 121 ± 41 and 110 ± 10 mg·L^{-1} in R2, respectively. Considering the stoichiometry of the denitrification reaction using acetate as an electron donor [51], the estimated effluent NOx removed by heterotrophic denitrification ($NOx_{Rem,het}$) at the anode accounted for 100% (R1) and 100% (R2) in period I and for 73% (R1) and 83% (R2) in period II (**Table 4.2**).

Table 4.2. The percentage of NOx removed in the reactors ($NOx_{Removal\ efficiency}$) and the specific percentage of NOx removed by heterotrophic ($NOx_{Rem,het.}$) and autotrophic denitrification ($NOx_{Rem,aut.}$) in R1 and R2 during the study evaluated by considering the stoichiometry of the denitrification reaction using acetate as an electron donor (Eq. 4 and 5).

Period	Reactor	$NOx_{Removal\ efficiency}$ (%)	$NOx_{Rem,het.}$ (%)	$NOx_{Rem,aut.}$ (%)
I	R1	99 ± 2	100	0
	R2	94 ± 5	100	0
II	R1	100 ± 0	73	27
	R2	100 ± 1	83	17
III	R1	98 ± 2	97	3
	R2	100 ± 0	90	10
IV	R1	96 ± 3	99	1
	R2	100 ± 1	100	0
V	R1	90 ± 13	94	6
	R2	96 ± 11	100	0
VI	R1	43 ± 22	0	100
	R2	65 ± 16	0	100
VII	R1	56 ± 5	0	100
	R2	96 ± 1	100	0

When the anode effluent flowed to the cathode chamber, a significant cathodic production of acetate occurred during periods I and II (p<0.05), being 46 ± 39 and 75 ± 55 mg·L^{-1} in R1 and R2, respectively (**Figure. 4.4**c and **4.4**f), which indicates the presence of homoacetogenic bacteria in the cathode biofilm. Under the anaerobic conditions present in both reactors, H_2 was potentially produced by electrolysis of water on the surface of the cathode [349]. Subsequently, homoacetogenic bacteria could have produced acetate using HCO_3^- and H_2 as substrates, as reported by Zabranska et al. [350]. Although below the Italian standard (D. Lgs. 152/2006, Annex V, Part III), in view of the variability of the organic matter content in real wastewater, this production could compromise the reliability of the process with respect to the treatment objectives.

From the beginning of period III (day 16), the influent was fed first to the cathode and then to the anode using an HRT of 7 h to evaluate the NOx and acetate removal efficiencies as well as acetate production in both chambers. The reversal of influent feed resulted in a stable (p>0.05) NOx removal efficiency of 98 ± 2 and 100 ± 0 % in both R1 and R2 (**Table 4.1**). In R1 and R2, a cathodic N-NO_2^- accumulation of 10.8 ± 2.4 and 0.5 ± 0.4 mg N·L^{-1}, respectively, was observed, which was then followed by complete denitrification at the anode. Additionally, an acetate removal efficiency of 89 ± 8 and 100 ± 0 % was achieved at the cathode of R1 and R2, respectively, showing that most of the removal mechanisms occurred at the cathode. No acetate production occurred at the anode. Considering the average feed acetate concentration of 134 ± 23 and 128 ± 17 mg·L^{-1} in R1 and R2, respectively, the estimated $NOx_{Rem,het}$ accounted for 97 and 90 % in R1 and R2, respectively.

In period IV, the HRT was further reduced to 4 h, with a nitrogen loading rate (NLR) of 4.6 g N-NO_3^-·m^{-3}·d^{-1}. This resulted in overall NOx and acetate removal efficiencies of 96

± 3 and 94 ± 15 % in R1 and of 100 ± 1 and 100 ± 0 % in R2, respectively. Additionally, the percentage of $NOx_{Rem,het}$ reached 99 and 100 % in R1 and R2, respectively. An HRT reduction to 2 h (period V) had little impact on the effluent NOx and acetate removal efficiencies, which were 90 ± 13 and 92 ± 10 % in R1 and 96 ± 11 % and 100 ± 0 % in R2, respectively. Also, an average $N\text{-}NO_2^-$ accumulation of 7.4 ± 1.9 and 1.3 ± 0.6 mg $N \cdot L^{-1}$ occurred at the cathodes of R1 and R2, respectively. However, after biomass acclimation (day 37-43) at an HRT of 2 h, the average effluent $N\text{-}NO_2^-$ concentration was below 0.6 mg $N\text{-}NO_2^- \cdot L^{-1}$, in compliance with the Italian standard (D. Lgs. 152/2006, Annex V, Part III) for industrial wastewater discharge into sewers.

4.3.3 Contribution of autotrophic and heterotrophic denitrification to $N\text{-}NO_3^-$ removal

In periods I-V, the synergistic relationship between autotrophic and heterotrophic denitrification for $N\text{-}NO_3^-$ removal was assessed. During these five periods, heterotrophic denitrification was predominant in both reactors, with a predominance in R2 (**Table 4.2**). In a study by Zhao et al. [351], an intensive biofilm-electrode reactor (IBER) was developed to treat nitrate-contaminated groundwater through a combination of heterotrophic and hydrogenotrophic denitrification, at different HRTs (8-24 h) and C/N (0.75-3). Bacteria used fiber threads as independent carrier to form a biofilm, carbon rods were used as the anode, with stainless steel wire embedded in fiber threads acting as the cathode to provide H_2 for autotrophic bacteria. Their results showed a complete removal of $N\text{-}NO_3^-$ and $N\text{-}NO_2^-$ by the IBER at an HRT of 8 h (NLR of 16.7 g $N\text{-}NO_3^- \cdot m^{-3}\, d^{-1}$) after 20 days of biomass acclimatization [351]. Specifically, heterotrophic denitrifiers predominated when the organic carbon source was supplemented with a C/N ratio higher than 1. On the other hand, when the C/N ratio was 0.75, the activity of the autotrophic

denitrifying bacteria became more significant, supporting heterotrophic denitrification in enhancing the NO_3^- removal efficiency. In contrast to Zhao et al. [351], the denitrification process in this study was complete at an HRT of 2 h with a NLR of 2.5 g $N\text{-}NO_3^-\cdot m^{-3}\, d^{-1}$ and after 6 days of biomass acclimatization from the previous condition tested (HRT of 4 h, period IV). In Period VI, the potential contribution of autotrophic denitrification to NO_3^- removal was evaluated in R1 and R2 by eliminating acetate in the influent (**Table 4.1**). Only relying on the electron donors provided by the electrode at an HRT of 2 h resulted in NOx removal efficiencies of 43 ± 22 and 65 ± 16 % in R1 and R2, respectively. The higher NOx removal efficiency in R2 compared to R1 could be attributed to the higher current density achieved in R2, which may have led to a higher availability of reducing electrons [352]. Nevertheless, in both R1 and R2, after biomass acclimation (day 48-54), the effluent $N\text{-}NO_3^-$ and $N\text{-}NO_2^-$ concentrations never exceeded the Italian standard (D. Lgs. 152/2006, Annex V, Part III) for the release of industrial wastewater into the sewage system (30 mg $N\text{-}NO_3^-\cdot L^{-1}$ and 0.6 mg $N\text{-}NO_2^-\cdot L^{-1}$, respectively). (**Figure. 4.4**). To improve the NOx removal efficiency in R1, the HRT was increased from 2 to 4 h (period VII), resulting in a NOx removal efficiency of 56 ± 5% and an average effluent $N\text{-}NO_3^-$ concentration of 13.1 ± 0.2 mg $N^-\cdot L^{-1}$ in the final five experimental days (days 71-75), demonstrating the good applicability of the system even in the absence of acetate.

Period VII of R2, on the other hand, was designed to study the effect of heterotrophic denitrification alone at open circuit conditions by feeding acetate with the influent medium and providing no cathodic potential. Although a high effluent NOx removal efficiency of 96 ± 1 % was achieved, a slight increase in the effluent $N\text{-}NO_2^-$ concentration (i.e., 1.3 ± 0.2 mg $N\cdot L^{-1}$) was observed, exceeding the Italian standard for wastewater

discharge into sewers. These results indicate that in the previous operational phases autotrophic denitrification contributed to NOx removal at the cathode, allowing to comply with regulatory limits for NO_2^- concentration. Generally, within the BES, an excess supply of organic compounds may encourage heterotrophic denitrification, thereby impeding bioelectrochemical denitrification [353]. Real wastewaters, however, show significant variability in the concentrations of organic matter [354]. Hence, the integration of autotrophic and heterotrophic denitrification within the same system ensures the attainment of consistently high removal efficiencies in the presence of variable levels of organic content or in its absence in incoming wastewater.

4.3.4 Economic and energetic considerations

The average current and final specific energy consumption calculated for each experimental period are shown in **Table 4.3.** Some fluctuations in current density mainly occurred in R2.

Table 4.3. Performances of R1 and R2 in terms of current density and specific energy consumption (SEC). The value is not present in period 7, as this period was characterized by the absence of an applied potential.

	Current density ($mA \cdot cm^{-2}$)		**SEC ($kWh \cdot g\ NO_{x,removed}^{-1}$)**	
Period	**R1**	**R2**	**R1**	**R2**
I	-0.3	3.8	$1.4 \cdot 10^{-4}$	$1.5 \cdot 10^{-4}$
II	-2.3	-0.6	$2.0 \cdot 10^{-3}$	$1.1 \cdot 10^{-3}$
III	-5.3	-0.2	$7.4 \cdot 10^{-4}$	$1.9 \cdot 10^{-4}$
IV	-155.1	-0.06	$6.5 \cdot 10^{-2}$	$8.5 \cdot 10^{-5}$

	Current density ($mA \cdot cm^{-2}$)		SEC ($kWh \cdot g\ NO_{x,removed}^{-1}$)	
Period	**R1**	**R2**	**R1**	**R2**
V	-83.1	0.04	$2.3 \cdot 10^{-2}$	$9.6 \cdot 10^{-5}$
VI	-211.0	-0.5	$7.4 \cdot 10^{-1}$	$8.2 \cdot 10^{-3}$
VII	-168.4		$1.3 \cdot 10^{-1}$	-

The final SEC calculated in period V in R1 and R2 was estimated to be $2.3 \cdot 10^{-2}$ and $9.6 \cdot 10^{-5}$ $kWh \cdot g\ NOx_{removed}^{-1}$, respectively (**Table 4.3**). Additionally, by comparing the SEC values for R1 and R2 in period VI (without the addition of acetate) with that of the previous period, the presence of heterotrophic denitrification was found to be advantageous from an energy point of view, as it significantly reduced the SEC value ($p<0.05$) for each experimental period (**Table 4.3**).

Molognoni et al. [322] investigated the nitrate removal capacity of a BES denitrification reactor for groundwater autotrophic denitrification consisting of a biological cathode and abiotic anode separated by a CEM. The study showed a $N\text{-}NO_3^-$ removal efficiency over 90%, with a specific energy consumption of $2.22 \cdot 10^{-3}$ $kWh \cdot g\ N\text{-}NO_3^-{}_{removed}^{-1}$. In addition, Pous et al. [335] evaluated the operation of a denitrifying BES for the treatment of nitrate-polluted groundwater, with energy consumption ranging from 0.7 to 1.3 $kWh \cdot g\ N\text{-}NO_3^-{}_{removed}^{-1}$. Compared to these values, the SEC reported in this study in period V for R1 and R2 was lower, demonstrating the effectiveness of the process here implemented.

4.4 Conclusions

In this study, a double-chamber BES was used to treat wastewater with a low C/N ratio. After 6 days of biomass acclimatization from the previous condition tested and at an HRT of 2 h, complete removal of $N\text{-}NO_3^-$ and $N\text{-}NO_2^-$ was achieved mainly by heterotrophic denitrification due to the presence of acetate. Nevertheless, the use of only electrode as the electron source could also achieve $N\text{-}NO_3^-$ and $N\text{-}NO_2^-$ concentrations consistently below the Italian standard for industrial effluent discharge into sewers (30 mg $N\text{-}NO_3^-\cdot L^{-1}$ and 0.6 mg $N\text{-}NO_2^-\cdot L^{-1}$). Given the considerable variability in organic matter concentration in municipal wastewater, integrating autotrophic and heterotrophic denitrification within the same treatment unit is a more reliable approach to obtain high nitrogen removal efficiencies and effluent quality standards. Additionally, the techno-economic feasibility of the process here investigated was also demonstrated by the low specific energy consumption required, which ranged from $2.3\cdot10^{-2}$ to $9.6\cdot10^{-5}$ kWh·g $NOx_{removed}^{-1}$ at an HRT of 2 h.

CHAPTER 5

Conclusions and Future Perspectives

5.1. Chapters overview

Over the past few decades, the expansion of urban populations has led to increased wastewater production characterized by elevated levels of nitrogen (N) and phosphorus (P) compounds, which contribute to oxygen depletion and eutrophication of surface waters [254]. In wastewater treatment plants (WWTPs), conventional activated systems (CAS) systems and the modified-Ludzack–Ettinger (MLE) process are commonly used for the removal of organic matter and N through separate stages of nitrification and denitrification, while P is removed through chemicals addition or biologically with complex process configurations [124]. Hence, traditional approaches to N and P removal from wastewater typically require separate operating units, proper sludge disposal, and high management and operating costs [31,126]. The simultaneous nitrification and denitrification (SND) process, achieved by simultaneously performing nitrification and denitrification processes in a single reactor, offers several advantages, including lower capital and operating costs [233], reduced carbon requirements, and lower sludge production [122]. In particular, the successful removal of nutrients from wastewater has been observed in biofilm systems, overcoming the limitations associated with suspended culture systems due to higher organic and hydraulic loads [355], and also allowing the elimination of sludge recirculation by introducing more active biomass in the biofilm reactors [66].

Starting from a comprehensive review of the state of the art in complete and shortcut SND, also coupled to P removal (SNDPR) (*Chapter 1*), the aim of this thesis was, firstly, to improve the understanding of these biological processes in moving bed biofilm reactors (MBBRs) through a modeling approach (*Chapter 2*) and, secondly, to propose a compact and cost-effective treatment solution for SND in a continuous (micro) aerobic granular

sludge (AGS) reactor (*Chapter 3*) coupled with a bioelectrochemical system (BES) as a post-treatment solution for wastewaters characterized by a low carbon to nitrogen (C/N) ratio (4.7) (*Chapter 4*).

5.2. Operational and management strategies for improvement and scale-up of the SND process in MBBR

The MBBR technology harnesses the presence of biofilm attached to mobile carriers to enable SND processes, providing an innovative and efficient solution for municipal and industrial wastewater treatment [356]. Additionally, recent studies have demonstrated the feasibility of implementing operational strategies to enhance the growth of ammonia oxidizing bacteria (AOB) while inhibiting nitrite oxidizing bacteria (NOB), thus facilitating the adoption of the short-cut SND process. These strategies include maintaining high pH and temperature, regulating SRT, establishing optimal dissolved oxygen (DO) levels, and ensuring that free ammonia (FA) and free nitrous acid (FNA) concentrations are within ranges that suppress NOB activity. The development of SND processes in biofilm reactors has been accompanied by an increase in the focus on numerical analysis and biofilm modeling studies. Mathematical modeling can be a critical tool to support the experimental phase by predicting the performance of a process, aiding problem-solving, and improving plant design by providing different operating scenarios [226].

From this perspective, *Chapter 2* proposed the modeling with the BioWin software 6.0 of complete and shortcut SNDPR in lab-scale MBBRs based on data collected during two previous experimental campaigns. The calibrated and validated models presented in this

study satisfactorily reproduced the experimental data for all experimental campaigns and within the acceptance criteria, resulting in a suitable tool for predicting process efficiency. Moreover, the calibrated and validated data were used to test different DO ranges (0.6–0.8 mg $O_2 \cdot L^{-1}$), pH (6.5–9.0), and hydraulic retention times (HRTs) (0.5–1.0 d) to improve the short-cut SND efficiencies. Based on the different simulated scenarios, a DO concentration of 0.6 mg $O_2 \cdot L^{-1}$ negatively affected AOBs activity, impacting on N-NH_4^+ removal. Additionally, a DO value of 0.8 mg $O_2 \cdot L^{-1}$ led to an overgrowth of NOBs, causing an increase in NO_3^- and NO_2^- concentrations. On the other hand, intermittent aeration (IA) (DO = 0.2-2.0 and 0.2-3.0 mg $O_2 \cdot L^{-1}$) facilitated the implementation of the short-cut SNDPR process, resulting in maximum effluent N-NH_4^+, N-NO_3^- and N-NO_2^- values below 5.5, 0.4, and 1.7 mg $N \cdot L^{-1}$, respectively, in agreement with the literature [83,153,167]. Typically, a pH range of 7.5 to 8.5 is conducive to NO_2^- accumulation [120]. As described in *Chapter 2*, selecting a pH value of 8.4 can be considered the most suitable option for achieving effective NOB inhibition and efficient N removal, resulting in average effluent concentrations of N-NH_4^+, N-NO_3^-, and N-NO_2^- at 2.6, 0.04, and 0.5 mg $N \cdot L^{-1}$, respectively. In addition, changes in HRT can significantly affect the inhibition of NOBs [357]. Also, the mathematical modeling discussed in *Chapter 2* allowed a detailed examination of biomass trends within the biofilm under different HRTs. Specifically, the maximum reduction in the AOB biomass occurred when the HRT was set at 0.5 d, reaching a value of 0.01 g by the end of the simulation period. Moreover, compared to the results obtained with an HRT of 1 d, a reduction to 0.9 d resulted in an increased inhibition of NOB, with average concentrations of N-NH_4^+, N-NO_3^- and N-NO_2^- of 4.0, 0.02, and 0.07 mg $\cdot L^{-1}$, respectively, suggesting favorable conditions for the SND process.

Both full-scale and pilot-scale studies are required to gain a thorough understanding of the operating costs associated with microaerobic conditions and to gain insight into the effects of scaling and the use of real wastewater on carbon and nutrient removal. At present, pilot- and real-scale studies of the SND process in MBBR have not been yet undertaken but experiments by our research group in this direction are ongoing. To fill this gap, it would be advisable to explore the use of mathematical modeling to simulate the process on a real scale, carefully examining the different removal efficiencies under different operating conditions that have already been studied at the laboratory scale. In addition, the mathematical modeling using the BioWin software makes possible to analyze in detail the energy consumption of each phase, quantifying the time trends of the total power consumed and of each energy-intensive system, such as blowers, mixers, pumps, and mechanical equipment, which are essential for the proper functioning of the plant.

5.3. Operational and management strategies for improvement and the scale-up of the SND process with AGS

The mechanisms of the SND process are those being mainly associated with N removal in AGS systems [92], although an analysis of literature data has shown that the reported total nitrogen (TN) efficiencies for these systems at the laboratory scale are highly variable [193,358,359]. *Chapter 3* explores the (micro)aerobic removal of C and N from synthetic municipal wastewater. This investigation involved a continuous double-column UAGSB system, with variations in reactor operating conditions, including different DO ranges (0.01-6.00 $mg \cdot L^{-1}$), feed C/N ratios (4.7-13.6), and HRTs (6-24 h).

Specifically, the decrease of the C/N ratio from 7.0 up to 4.7 led to insufficient organic C to support denitrification, resulting in an effluent $N\text{-}NO_3^-$ concentration of 31.1 ± 4.1 mg $N \cdot L^{-1}$, which represents the main limiting factor in the denitrification process [360]. Reducing the HRT from 12 to 6 h resulted in a decrease in reactor performance and significant accumulation of $N\text{-}NH_4^+$ in the effluent due to insufficient contact time between pollutants and microorganisms [67]. At a DO range of 0.01–0.30 $mg \cdot L^{-1}$, feed C/N ratio of 13.6, and HRT of 24 h, the UAGSB achieved the highest chemical oxygen demand (COD), $N\text{-}NH_4^+$, and total inorganic nitrogen (TIN) REs of 86, 99, and 84 %, respectively, which makes the UAGSB system a highly promising and effective alternative for the removal of C and N from wastewater.

A notable drawback identified in the process was the exceeding the Italian standard (D. Lgs. 152/2006, Annex V, Part III) for industrial wastewater discharge into sewers, specifically in terms of NO_3^- and NO_2^- effluent concentrations, under certain operating conditions. Consequently, to improve the efficiency of the process, implementing post-treatment measures is essential to bring these residual concentrations below regulatory standards. For instance, future studies could include the development of algae-bacteria symbiotic granules to reduce residual $N\text{-}NO_3^-$ and $N\text{-}NO_2^-$concentrations and exploit the benefits of photo-oxygenation to minimize aeration costs of wastewater treatment plants [191,361]. In particular, the aeration column associated with the UAGSB reactor (**Figure 3.1**, *Chapter 3*) could be replaced by an algal biomass reactor (**Figure 5.1**). This reactor could receive the effluent from the bioreactor and serve the dual purpose of oxygenating the effluent while reducing excess residual $N\text{-}NO_3^-$ and $N\text{-}NO_2^-$ concentrations.

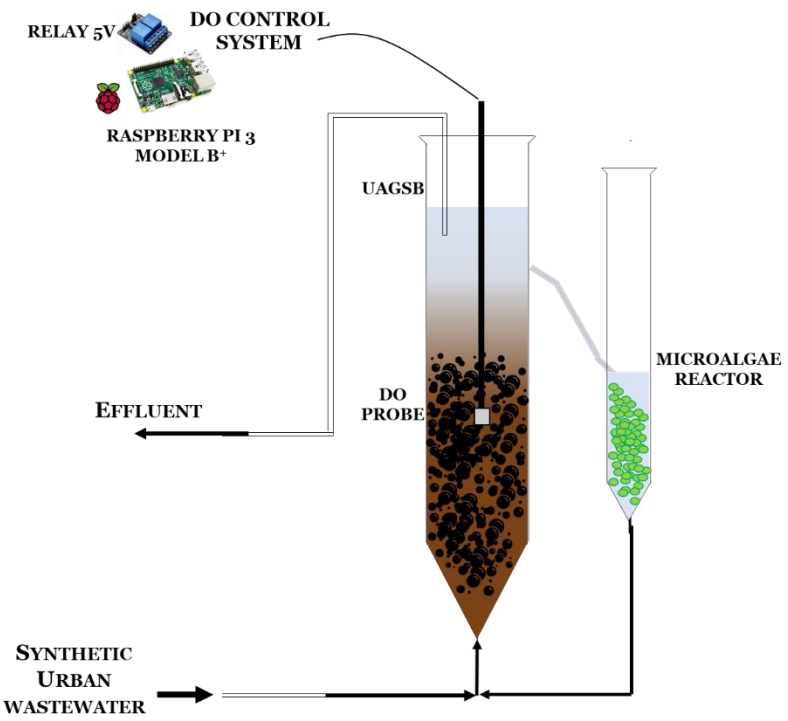

Figure 5.1. Hypothetic schematics of the symbiotic microalgae reactor-UAGSB process.

In addition, the implementation of this technology at pilot- and full-scale would allow a more accurate assessment of the influence of the composition of the feed effluent on the removal of C and N, the stability of the granules, and the associated operating costs. Although the full-scale AGS process in sequencing batch reactors (SBR) has been patented with the Nereda® process [189], there is a strong need for research on continuously-fed AGS reactors to test different strategies to facilitate granulation, such as substrate composition, organic loading rate, hydrodynamic shear force, feast-famine regime, feeding strategy, DO concentration, reactor configuration [192], which have only been studied on a laboratory scale using synthetic wastewater [362]. Specifically, it would be interesting to assess the applicability of continuous AGS systems in existing full-scale plants, monitoring the evolution of the granulation process over time by calculating the main chemical (i.e., protein/carbohydrate ratio of extracellular polymeric substances (EPS)), kinetic and stoichiometric (i.e., biomass growth rate of heterotrophic (μ_H) and

autotrophic biomass ($\mu_{aut.}$) and heterotrophic biomass yield (Y_H)) parameters characterizing the biomass present.

5.4. Strategies to improve the applicability of BES for C, N, and P removal from wastewater

Based on the results of *Chapter 3*, it seemed interesting to investigate the feasibility of a double two-chamber bioelectrochemical system (BES) consisting of anode and cathode chambers separated by a cation-exchange membrane, as a possible integrated reactor to be coupled to the UAGSB to remove the residual fraction of NO_3^- from the UAGSB effluent. A synthetic wastewater with a low C/N ratio of 4.7 was used (*Chapter 4*). The obtained results showed complete removal of N-NO_3^- and N-NO_2^- by the BES at an HRT of 2 h after 6 days of biomass acclimatization. Furthermore, the research showed that while heterotrophic denitrification was dominant, the use of H_2 as the sole electron donor resulted in N-NO_3^- and N-NO_2^-concentrations consistently below the Italian standard (D. Lgs. 152/2006, Annex V, Part III) for industrial wastewater discharge into sewers. Therefore, given the considerable variability in the feed organic concentrations, integrating autotrophic and heterotrophic denitrification within the same system could ensure consistently high removal efficiencies.

Regarding the energy needed, a specific energy consumption of $2.3 \cdot 10^{-2}$ and $9.6 \cdot 10^{-5}$ kWh·g $NOx_{removed}^{-1}$ was reported for reactor 1 (R1) and 2 (R2), respectively, demonstrating the effectiveness of the method. However, although BES is an emerging treatment technology that allows the simultaneous treatment of wastewater and recovery of resources such as energy, nutrients, and value-added organic matter, the technical and

economic feasibility of this technology for wastewater treatment requires extensive research and demonstration through the implementation of pilot scale systems, taking into account the type of wastewater, the operating environment and the stability of performance during long-term operation [363]. At present, there are several barriers that limit the use of electrochemical technologies, including the short life of electrode materials, high operating costs, electrode stability and low current efficiency. However, coupling wastewater treatment plants with electrochemical technologies could increase energy recovery to the point where energy self-sufficiency is achieved and greenhouse gas emissions are reduced [364].

References

[1] M. Qadir, P. Drechsel, B. Jiménez Cisneros, Y. Kim, A. Pramanik, P. Mehta, O. Olaniyan, Global and regional potential of wastewater as a water, nutrient and energy source, Nat. Resour. Forum 44 (2020) 40–51. https://doi.org/10.1111/1477-8947.12187.

[2] M. Preisner, E. Neverova-Dziopak, Z. Kowalewski, Analysis of eutrophication potential of municipal wastewater, Water Sci. Technol. 81 (2020) 1994–2003. https://doi.org/10.2166/wst.2020.254.

[3] C. Wang, Z. Wang, P. Wang, S. Zhang, Multiple Effects of Environmental Factors on Algal Growth and Nutrient Thresholds for Harmful Algal Blooms: Application of Response Surface Methodology, Environ. Model. Assess. 21 (2016) 247–259. https://doi.org/10.1007/s10666-015-9481-3.

[4] W.M. Ni, J.Y. Zhang, T. Da Ding, R.J. Stevenson, Y.M. Zhu, Environmental factors regulating cyanobacteria dominance and microcystin production in a subtropical lake within the Taihu watershed, China, J. Zhejiang Univ. Sci. A 13 (2012) 311–322. https://doi.org/10.1631/jzus.A1100197.

[5] M. Le Moal, C. Gascuel-Odoux, A. Ménesguen, Y. Souchon, C. Étrillard, A. Levain, F. Moatar, A. Pannard, P. Souchu, A. Lefebvre, G. Pinay, Eutrophication: A new wine in an old bottle?, Sci. Total Environ. 651 (2019) 1–11. https://doi.org/10.1016/j.scitotenv.2018.09.139.

[6] A.A.; Ansari, Eutrophication: causes, consequences and control, n.d. https://www.ptonline.com/articles/how-to-get-better-mfi-results.

[7] X. Ren, F.J. Yue, J. Tang, C. Li, S.L. Li, Nitrate transformation and source tracking of rivers draining into the Bohai Sea using a multi-tracer approach combined with

an optimized Bayesian stable isotope mixing model, J. Hazard. Mater. 463 (2024) 132901. https://doi.org/10.1016/j.jhazmat.2023.132901.

[8] J.N. Galloway, E.B. Cowling, Reflections on 200 years of Nitrogen, 20 years later: This article belongs to Ambio's 50th Anniversary Collection. Theme: Eutrophication, Ambio 50 (2021) 745–749. https://doi.org/10.1007/s13280-020-01464-z.

[9] A.L. Morée, A.H.W. Beusen, A.F. Bouwman, W.J. Willems, Exploring global nitrogen and phosphorus flows in urban wastes during the twentieth century, Global Biogeochem. Cycles 27 (2013) 836–846. https://doi.org/10.1002/gbc.20072.

[10] Z. Zhang, M. Xu, Y. Fan, L. Zhang, H. Wang, Using microalgae to reduce the use of conventional fertilizers in hydroponics and soil-based cultivation, Sci. Total Environ. 912 (2024) 169424. https://doi.org/10.1016/j.scitotenv.2023.169424.

[11] S. Rahimi, O. Modin, I. Mijakovic, Technologies for biological removal and recovery of nitrogen from wastewater, Biotechnol. Adv. 43 (2020) 107570. https://doi.org/10.1016/j.biotechadv.2020.107570.

[12] M.N. Hasan, M.M. Altaf, N.A. Khan, A.H. Khan, A.A. Khan, S. Ahmed, P.S. Kumar, M. Naushad, A.U. Rajapaksha, J. Iqbal, V. Tirth, S. Islam, Recent technologies for nutrient removal and recovery from wastewaters: A review, Chemosphere 277 (2021) 130328. https://doi.org/10.1016/j.chemosphere.2021.130328.

[13] M.K. Manu, D. Li, L. Liwen, Z. Jun, S. Varjani, J.W.C. Wong, A review on nitrogen dynamics and mitigation strategies of food waste digestate composting, Bioresour. Technol. 334 (2021) 125032.

https://doi.org/10.1016/j.biortech.2021.125032.

[14] H. Lu, K. Chandran, D. Stensel, Microbial ecology of denitrification in biological wastewater treatment, Water Res. 64 (2014) 237–254. https://doi.org/10.1016/j.watres.2014.06.042.

[15] M.K. Winkler, L. Straka, New directions in biological nitrogen removal and recovery from wastewater, Curr. Opin. Biotechnol. 57 (2019) 50–55. https://doi.org/10.1016/j.copbio.2018.12.007.

[16] L. Yan, S. Liu, Q. Liu, M. Zhang, Y. Liu, Y. Wen, Z. Chen, Y. Zhang, Q. Yang, Improved performance of simultaneous nitrification and denitrification via nitrite in an oxygen-limited SBR by alternating the DO, Bioresour. Technol. 275 (2019) 153–162. https://doi.org/10.1016/j.biortech.2018.12.054.

[17] X. Li, H. Nan, H. Jiang, H. Wang, C. Wang, Research trends on phosphorus removal from wastewater: A review and bibliometric analysis from 2000 to 2022, J. Water Process Eng. 55 (2023) 104201. https://doi.org/10.1016/j.jwpe.2023.104201.

[18] F. Di Capua, S. de Sario, A. Ferraro, A. Petrella, M. Race, F. Pirozzi, U. Fratino, D. Spasiano, Phosphorous removal and recovery from urban wastewater: Current practices and new directions, Sci. Total Environ. 823 (2022) 153750. https://doi.org/10.1016/j.scitotenv.2022.153750.

[19] X. Li, H. Nan, H. Jiang, H. Wang, C. Wang, Research trends on phosphorus removal from wastewater: A review and bibliometric analysis from 2000 to 2022, J. Water Process Eng. 55 (2023) 104201. https://doi.org/10.1016/j.jwpe.2023.104201.

[20] J.T. Bunce, E. Ndam, I.D. Ofiteru, A. Moore, D.W. Graham, A review of

phosphorus removal technologies and their applicability to small-scale domestic wastewater treatment systems, Front. Environ. Sci. 6 (2018) 1–15. https://doi.org/10.3389/fenvs.2018.00008.

[21] F. Iannacone, F. Di Capua, F. Granata, R. Gargano, G. Esposito, Simultaneous nitrification, denitrification and phosphorus removal in a continuous-flow moving bed biofilm reactor alternating microaerobic and aerobic conditions, Bioresour. Technol. 310 (2020) 123453. https://doi.org/10.1016/j.biortech.2020.123453.

[22] G.K. Morse, S.W. Brett, J.A. Guy, J.N. Lester, Review: Phosphorus removal and recovery technologies, Sci. Total Environ. 212 (1998) 69–81. https://doi.org/10.1016/S0048-9697(97)00332-X.

[23] D.W. De Haas, M.C. Wentzel, G.A. Ekama, The use of simultaneous chemical precipitation in modified activated sludge systems exhibiting biological excess phosphate removal. Part 7: Application of the IAWQ model, Water SA 27 (2001) 151–165. https://doi.org/10.4314/wsa.v27i2.4989.

[24] R. Liu, X. Hao, Q. Chen, J. Li, Research advances of Tetrasphaera in enhanced biological phosphorus removal: A review, Water Res. 166 (2019). https://doi.org/10.1016/j.watres.2019.115003.

[25] A.J. Schuler, D. Jenkins, Enhanced Biological Phosphorus Removal from Wastewater by Biomass with Different Phosphorus Contents, Part II: Anaerobic Adenosine Triphosphate Utilization and Acetate Uptake Rates, Water Environ. Res. 75 (2003) 499–511. https://doi.org/10.2175/106143003x141295.

[26] W. Zhao, X. Bi, Y. Peng, M. Bai, Research advances of the phosphorus-accumulating organisms of Candidatus Accumulibacter, Dechloromonas and Tetrasphaera: Metabolic mechanisms, applications and influencing factors,

Chemosphere 307 (2022) 135675. https://doi.org/10.1016/j.chemosphere.2022.135675.

[27] M. Ni, Y. Pan, X. Zhang, L. Wen, W. Yang, Y. Chen, Y. Huang, Z. Song, Effects of P/C ratios on the growth, phosphorus removal and phosphorus recovery of a novel strain of highly efficient PAO, Process Biochem. 111 (2021) 109–117. https://doi.org/10.1016/j.procbio.2021.08.010.

[28] M. Kube, B. Jefferson, L. Fan, F. Roddick, The impact of wastewater characteristics, algal species selection and immobilisation on simultaneous nitrogen and phosphorus removal, Algal Res. 31 (2018) 478–488. https://doi.org/10.1016/j.algal.2018.01.009.

[29] A. Ding, R. Zhang, H.H. Ngo, X. He, J. Ma, J. Nan, G. Li, Life cycle assessment of sewage sludge treatment and disposal based on nutrient and energy recovery: A review, Sci. Total Environ. 769 (2021). https://doi.org/10.1016/j.scitotenv.2020.144451.

[30] D. Panepinto, S. Fiore, M. Zappone, G. Genon, L. Meucci, Evaluation of the energy efficiency of a large wastewater treatment plant in Italy, Appl. Energy 161 (2016) 404–411. https://doi.org/10.1016/j.apenergy.2015.10.027.

[31] P. Foladori, M. Vaccari, F. Vitali, Energy audit in small wastewater treatment plants: Methodology, energy consumption indicators, and lessons learned, Water Sci. Technol. 72 (2015) 1007–1015. https://doi.org/10.2166/wst.2015.306.

[32] Z. Zhang, W. Xing, J. Lu, X. Gao, F. Jia, H. Yao, Nitrogen removal and nitrous oxide emission in the partial nitritation/anammox process at different reflux ratios, Sci. Total Environ. 906 (2024) 167520. https://doi.org/10.1016/j.scitotenv.2023.167520.

[33] M. Yang, J. Li, Z. Li, Y. Peng, L. Zhang, Enhancing anammox bacteria enrichment in integrated fixed-film activated sludge partial nitritation/anammox process via floc retention control, Bioresour. Technol. 391 (2024) 129938. https://doi.org/10.1016/j.biortech.2023.129938.

[34] X. Hou, X. Li, X. Zhu, W. Li, C. Kao, Y. Peng, Advanced nitrogen removal from municipal wastewater through partial nitrification-denitrification coupled with anammox in step-feed continuous system, Bioresour. Technol. 391 (2024) 129967. https://doi.org/10.1016/j.biortech.2023.129967.

[35] F. Chen, H. Cheng, Y. Qian, J. Shen, W. Zhao, Y. Qin, Y.-Y. Li, Improved performance of single-stage partial nitritation-anammox membrane bioreactor (PN/A MBR) by adding biofilm carriers: start-up, membrane operation and microbial structure, Chem. Eng. J. 480 (2024) 148112. https://doi.org/10.1016/j.cej.2023.148112.

[36] N. Tran Dinh, L. Phuong Thu, N. Thanh Dat, N. Khanh Toan, P. Le Anh, The roles of microalgae and bacteria in wastewater treatment, Vietnam J. Biotechnol. 20 (2022) 573–588. https://doi.org/10.15625/1811-4989/16645.

[37] Q. Jiang, H. Chen, Z. Fu, X. Fu, J. Wang, Y. Liang, H. Yin, J. Yang, J. Jiang, X. Yang, H. Wang, Z. Liu, R. Su, Current Progress, Challenges and Perspectives in the Microalgal-Bacterial Aerobic Granular Sludge Process: A Review, Int. J. Environ. Res. Public Health 19 (2022). https://doi.org/10.3390/ijerph192113950.

[38] J.A. Oviedo, R. Muñoz, A. Donoso-bravo, O. Bernard, F. Casagli, D. Jeison, J.A. Oviedo, R. Muñoz, A. Donoso-bravo, O. Bernard, F. Casagli, A half-century of research on microalgae-bacteria for wastewater treatment To cite this version : HAL Id : hal-03935846, (2023).

[39] C. Zhang, X. Chen, M. Han, X. Li, H. Chang, N. Ren, S.H. Ho, Revealing the role of microalgae-bacteria niche for boosting wastewater treatment and energy reclamation in response to temperature, Environ. Sci. Ecotechnology 14 (2023) 100230. https://doi.org/10.1016/j.ese.2022.100230.

[40] M. Qv, D. Dai, D. Liu, Q. Wu, C. Tang, S. Li, L. Zhu, Towards advanced nutrient removal by microalgae-bacteria symbiosis system for wastewater treatment, Bioresour. Technol. 370 (2023) 128574. https://doi.org/10.1016/j.biortech.2022.128574.

[41] T. Liu, X. He, G. Jia, J. Xu, X. Quan, S. You, Simultaneous nitrification and denitrification process using novel surface-modified suspended carriers for the treatment of real domestic wastewater, Chemosphere 247 (2020) 125831. https://doi.org/10.1016/j.chemosphere.2020.125831.

[42] L. Yan, S. Zhang, G. Hao, X. Zhang, Y. Ren, Y. Wen, Y. Guo, Y. Zhang, Simultaneous nitrification and denitrification by EPSs in aerobic granular sludge enhanced nitrogen removal of ammonium-nitrogen-rich wastewater, Bioresour. Technol. 202 (2016) 101–106. https://doi.org/10.1016/j.biortech.2015.11.088.

[43] L. WU, C. PENG, S. ZHANG, Y. PENG, Nitrogen removal via nitrite from municipal landfill leachate, J. Environ. Sci. 21 (2009) 1480–1485. https://doi.org/10.1016/S1001-0742(08)62443-2.

[44] P. Roots, F. Sabba, A.F. Rosenthal, Y. Wang, Q. Yuan, L. Rieger, F. Yang, J.A. Kozak, H. Zhang, G.F. Wells, Integrated shortcut nitrogen and biological phosphorus removal from mainstream wastewater: Process operation and modeling, Environ. Sci. Water Res. Technol. 6 (2020) 566–580. https://doi.org/10.1039/c9ew00550a.

[45] D.J. Arp, Nitrification, (2009) 1–6. https://doi.org/10.1002/9780470015902.a0021154.

[46] B. Zhao, X.C. Ran, Q. An, Y.S. Huang, Q.H. Lv, Q. Dan, N2O production from hydroxylamine oxidation and corresponding hydroxylamine oxidoreductase involved in a heterotrophic nitrifier A. faecalis strain NR, Bioprocess Biosyst. Eng. 42 (2019) 1983–1992. https://doi.org/10.1007/s00449-019-02191-w.

[47] S. Rahimi, O. Modin, I. Mijakovic, Technologies for biological removal and recovery of nitrogen from wastewater, Biotechnol. Adv. 43 (2020) 107570. https://doi.org/10.1016/j.biotechadv.2020.107570.

[48] T. Tian, H.Q. Yu, Denitrification with non-organic electron donor for treating low C/N ratio wastewaters, Bioresour. Technol. 299 (2020) 122686. https://doi.org/10.1016/j.biortech.2019.122686.

[49] N. Adouani, L. Limousy, T. Lendormi, O. Sire, N2O and NO emissions during wastewater denitrification step: Influence of temperature on the biological process, Comptes Rendus Chim. 18 (2015) 15–22. https://doi.org/10.1016/j.crci.2014.11.005.

[50] F. Rezvani, M.H. Sarrafzadeh, S. Ebrahimi, H.M. Oh, Nitrate removal from drinking water with a focus on biological methods: a review, Environ. Sci. Pollut. Res. 26 (2019) 1124–1141. https://doi.org/10.1007/s11356-017-9185-0.

[51] F. Di Capua, F. Pirozzi, P.N.L. Lens, G. Esposito, Electron donors for autotrophic denitrification, Chem. Eng. J. 362 (2019) 922–937. https://doi.org/10.1016/j.cej.2019.01.069.

[52] L. Miao, Z. Liu, Microbiome analysis and -omics studies of microbial denitrification processes in wastewater treatment: recent advances, Sci. China Life

Sci. 61 (2018) 753–761. https://doi.org/10.1007/s11427-017-9228-2.

[53] N. Wrage, G.L. Velthof, M.L. Van Beusichem, O. Oenema, Role of nitrifier denitrification in the production of nitrous oxide, Soil Biol. Biochem. 33 (2001) 1723–1732. https://doi.org/10.1016/S0038-0717(01)00096-7.

[54] F. Azam, C. Müller, A. Weiske, G. Benckiser, J.C.G. Ottow, Nitrification and denitrification as sources of atmospheric nitrous oxide - Role of oxidizable carbon and applied nitrogen, Biol. Fertil. Soils 35 (2002) 54–61. https://doi.org/10.1007/s00374-001-0441-5.

[55] B. Han, Y. Yao, B. Liu, Y. Wang, X. Su, L. Ma, D. Liu, S. Niu, X. Chen, Z. Li, Relative importance between nitrification and denitrification to N 2 O from a global perspective , Glob. Chang. Biol. 30 (2024) 1–14. https://doi.org/10.1111/gcb.17082.

[56] T.M. Massara, S. Malamis, A. Guisasola, J.A. Baeza, C. Noutsopoulos, E. Katsou, A review on nitrous oxide (N2O) emissions during biological nutrient removal from municipal wastewater and sludge reject water, Sci. Total Environ. 596–597 (2017) 106–123. https://doi.org/10.1016/j.scitotenv.2017.03.191.

[57] T. Wu, S.S. Yang, L. Zhong, J.W. Pang, L. Zhang, X.F. Xia, F. Yang, G.J. Xie, B.F. Liu, N.Q. Ren, J. Ding, Simultaneous nitrification, denitrification and phosphorus removal: What have we done so far and how do we need to do in the future?, Sci. Total Environ. 856 (2023). https://doi.org/10.1016/j.scitotenv.2022.158977.

[58] F. Di Capua, F. Iannacone, F. Sabba, G. Esposito, Simultaneous nitrification–denitrification in biofilm systems for wastewater treatment: Key factors, potential routes, and engineered applications, Bioresour. Technol. 361 (2022) 127702.

https://doi.org/10.1016/j.biortech.2022.127702.

[59] M.K. Winkler, L. Straka, New directions in biological nitrogen removal and recovery from wastewater, Curr. Opin. Biotechnol. 57 (2019) 50–55. https://doi.org/10.1016/j.copbio.2018.12.007.

[60] A. Lanzetta, D. Mattioli, F. Di Capua, G. Sabia, L. Petta, G. Esposito, G. Andreottola, G. Gatti, W. Merz, M. Langone, Anammox-based processes for mature leachate treatment in sbr: A modelling study, Processes 9 (2021). https://doi.org/10.3390/pr9081443.

[61] B. Kartal, J.G. Kuenen, M.C.M. Van Loosdrecht, Sewage treatment with anammox, Science (80-.). 328 (2010) 702–703. https://doi.org/10.1126/science.1185941.

[62] X. Ji, M. Jiang, J. Zhang, X. Jiang, Z. Zheng, The interactions of algae-bacteria symbiotic system and its effects on nutrients removal from synthetic wastewater, Bioresour. Technol. 247 (2018) 44–50. https://doi.org/10.1016/j.biortech.2017.09.074.

[63] M. Kesaano, R.C. Sims, Algal biofilm based technology for wastewater treatment, Algal Res. 5 (2014) 231–240. https://doi.org/10.1016/j.algal.2014.02.003.

[64] J. Liu, Y. Wu, C. Wu, K. Muylaert, W. Vyverman, H.Q. Yu, R. Muñoz, B. Rittmann, Advanced nutrient removal from surface water by a consortium of attached microalgae and bacteria: A review, Bioresour. Technol. 241 (2017) 1127–1137. https://doi.org/10.1016/j.biortech.2017.06.054.

[65] J. Su, D. Kang, W. Xiang, C. Wu, Periphyton biofilm development and its role in nutrient cycling in paddy microcosms, J. Soils Sediments 17 (2017) 810–819. https://doi.org/10.1007/s11368-016-1575-2.

[66] R. Bhattacharya, D. Mazumder, Simultaneous nitrification and denitrification in moving bed bioreactor and other biological systems, Bioprocess Biosyst. Eng. 44 (2021) 635–652. https://doi.org/10.1007/s00449-020-02475-6.

[67] S.N. James, A. Vijayanandan, Recent advances in simultaneous nitrification and denitrification for nitrogen and micropollutant removal: a review, Biodegradation (2023). https://doi.org/10.1007/s10532-023-10015-8.

[68] M. Zaman, M. Kim, G. Nakhla, Simultaneous nitrification-denitrifying phosphorus removal (SNDPR) at low DO for treating carbon-limited municipal wastewater, Sci. Total Environ. 760 (2021) 143387. https://doi.org/10.1016/j.scitotenv.2020.143387.

[69] Z.Z. Loh, N.S. Zaidi, E.L. Yong, M.B. Bahrodin, A. Aris, Simultaneous nitrification and denitrification of real domestic wastewater using novel biodegradable Cocos Nucifera fibre as biofilter media and carbon source: Performances and microbial community composition, J. Water Process Eng. 57 (2024) 104592. https://doi.org/10.1016/j.jwpe.2023.104592.

[70] N.A. Khan, S. Singh, P.C. Ramamurthy, I.H. Aljundi, Exploring nutrient removal mechanisms in column-type SBR with simultaneous nitrification and denitrification, J. Environ. Manage. 349 (2024) 119485. https://doi.org/10.1016/j.jenvman.2023.119485.

[71] S. Shi, X. He, L. He, X. Fan, B. Shu, J. Zhou, Q. He, Overlooked pathways of endogenous simultaneous nitrification and denitrification in anaerobic/aerobic/anoxic sequencing batch reactors with organic supplementation, Water Res. 230 (2023) 119493. https://doi.org/10.1016/j.watres.2022.119493.

[72] X. Bai, M.M. McKnight, J.D. Neufeld, W. J. Parker, Simultaneous nitrification,

denitrification, and phosphorus removal from municipal wastewater at low temperature, Bioresour. Technol. 368 (2023) 128261. https://doi.org/10.1016/j.biortech.2022.128261.

[73] M. Seyedsalehi, J. Jaafari, C. Hélix-Nielsen, G. Hodaifa, M. Manshouri, S. Ghadimi, H. Hafizi, H. Barzanouni, Evaluation of moving-bed biofilm sequencing batch reactor (MBSBR) in operating A2O process with emphasis on biological removal of nutrients existing in wastewater, Int. J. Environ. Sci. Technol. 15 (2018) 199–206. https://doi.org/10.1007/s13762-017-1360-9.

[74] J. Wang, H. Rong, Y. Cao, C. Zhang, Factors affecting simultaneous nitrification and denitrification (SND) in a moving bed sequencing batch reactor (MBSBR) system as revealed by microbial community structures, Bioprocess Biosyst. Eng. 43 (2020) 1833–1846. https://doi.org/10.1007/s00449-020-02374-w.

[75] Y. Jin, W. Zhan, R. Wu, Y. Han, S. Yang, J. Ding, N. Ren, Insight into the roles of microalgae on simultaneous nitrification and denitrification in microalgal-bacterial sequencing batch reactors: Nitrogen removal, extracellular polymeric substances, and microbial communities, Bioresour. Technol. 379 (2023) 129038. https://doi.org/10.1016/j.biortech.2023.129038.

[76] J. Liu, Q. Zhang, G. Xu, F. Gao, Simultaneous nitritation, denitritation and phosphorus removal in an algal-bacterial consortium system treating low-strength mariculture wastewater, J. Water Process Eng. 49 (2022) 103056. https://doi.org/10.1016/j.jwpe.2022.103056.

[77] L. Zhang, C. Wei, K. Zhang, C. Zhang, Q. Fang, S. Li, Effects of temperature on simultaneous nitrification and denitrification via nitrite in a sequencing batch biofilm reactor, Bioprocess Biosyst. Eng. 32 (2009) 175–182.

https://doi.org/10.1007/s00449-008-0235-3.

[78] Y. Lu, L. Feng, G. Yang, Q. Yang, X. Zhang, J. Mu, Intensification and microbial pathways of simultaneous nitrification–denitrification in a sequencing batch biofilm reactor for seawater-based saline wastewater treatment, J. Chem. Technol. Biotechnol. 93 (2018) 2766–2773. https://doi.org/10.1002/jctb.5652.

[79] A. Gieseke, P. Arnz, R. Amann, A. Schramm, Simultaneous P and N removal in a sequencing batch biofilm reactor: Insights from reactor- and microscale investigations, Water Res. 36 (2002) 501–509. https://doi.org/10.1016/S0043-1354(01)00232-9.

[80] Z. She, L. Wu, Q. Wang, M. Gao, C. Jin, Y. Zhao, L. Zhao, L. Guo, Salinity effect on simultaneous nitrification and denitrification, microbial characteristics in a hybrid sequencing batch biofilm reactor, Bioprocess Biosyst. Eng. 41 (2018) 65–75. https://doi.org/10.1007/s00449-017-1844-5.

[81] Z. Yang, S. Shi, X. He, M. Cao, H. Lin, J. Fu, J. Zhou, High-efficient nutrient removal in a single-stage electrolysis-integrated sequencing batch biofilm reactor (E-SBBR) for low C/N sanitary sewage treatment, J. Environ. Manage. 351 (2024) 119848. https://doi.org/10.1016/j.jenvman.2023.119848.

[82] F. Iannacone, F. Di Capua, F. Granata, R. Gargano, F. Pirozzi, G. Esposito, Effect of carbon-to-nitrogen ratio on simultaneous nitrification denitrification and phosphorus removal in a microaerobic moving bed biofilm reactor, J. Environ. Manage. 250 (2019) 109518. https://doi.org/10.1016/j.jenvman.2019.109518.

[83] F. Iannacone, F. Di Capua, F. Granata, R. Gargano, G. Esposito, Shortcut nitrification-denitrification and biological phosphorus removal in acetate- and ethanol-fed moving bed biofilm reactors under microaerobic/aerobic conditions,

Bioresour. Technol. 330 (2021). https://doi.org/10.1016/j.biortech.2021.124958.

[84] Y. nan Luan, Y. Yin, Z. Guo, J. Yang, G. Wang, F. Zhang, Y. Xiao, C. Liu, Achieving simultaneous nitrification and endogenous denitrifying phosphorus removal in anaerobic/intermittently-aerated moving bed biofilm reactor for low carbon-to-nitrogen ratio wastewater treatment, Bioresour. Technol. 394 (2024) 130178. https://doi.org/10.1016/j.biortech.2023.130178.

[85] W. Shi, Z. Tian, Y. Wang, B. Yu, Y. Tian, M. Yang, Effects of biocarrier type and size on the performance of nitrification and simultaneous nitrification and denitrification, J. Environ. Chem. Eng. 11 (2023). https://doi.org/10.1016/j.jece.2023.110000.

[86] Y. Song, D. Zheng, S. Fan, S. Li, L. Zhang, H. Wang, D. Li, Simultaneous nitrification/denitrification in a single-chamber stainless steel bioelectrochemical reactor, J. Power Sources 591 (2024) 233810. https://doi.org/10.1016/j.jpowsour.2023.233810.

[87] H.D. Nguyen, S. Babel, Bioelectricity recovery through isolation and removal of nitrogen from wastewater by shortcut nitrification-denitrification in a coupled microbial fuel cell system, Fuel 359 (2024) 130497. https://doi.org/10.1016/j.fuel.2023.130497.

[88] X.A. Walter, A. Kostrytsia, H. Watson, J. Winfield, A. Baran, S. Gillman, Novel self-stratifying bioelectrochemical system for municipal wastewater treatment halves nitrous oxide emissions, Bioresour. Technol. 392 (2024) 129969. https://doi.org/10.1016/j.biortech.2023.129969.

[89] H. Li, W. Zuo, Y. Tian, J. Zhang, S. Di, L. Li, X. Su, Simultaneous nitrification and denitrification in a novel membrane bioelectrochemical reactor with low

membrane fouling tendency, Environ. Sci. Pollut. Res. 24 (2017) 5106–5117. https://doi.org/10.1007/s11356-016-6084-8.

[90] G. Zhu, S. Huang, Y. Lu, X. Gu, Simultaneous nitrification and denitrification in the bio-cathode of a multi-anode microbial fuel cell, Environ. Technol. (United Kingdom) 42 (2021) 1260–1270. https://doi.org/10.1080/09593330.2019.1663938.

[91] A. Lanzetta, F. Di Capua, B. Panneerselvam, D. Mattioli, G. Esposito, S. Papirio, Impact of Influent Composition and Operating Conditions on Carbon and Nitrogen Removal from Urban Wastewater in a Blanket Reactor, (2023).

[92] M. Layer, M.G. Villodres, A. Hernandez, E. Reynaert, E. Morgenroth, N. Derlon, Limited simultaneous nitrification-denitrification (SND) in aerobic granular sludge systems treating municipal wastewater: Mechanisms and practical implications, Water Res. X 7 (2020) 100048. https://doi.org/10.1016/j.wroa.2020.100048.

[93] B. Peng, H. Liang, S. Wang, D. Gao, Effects of DO on N2O emission during biological nitrogen removal using aerobic granular sludge via shortcut simultaneous nitrification and denitrification, Environ. Technol. (United Kingdom) 41 (2020) 251–259. https://doi.org/10.1080/09593330.2018.1494757.

[94] Y. Zhao, D. Liu, W. Huang, Y. Yang, M. Ji, L.D. Nghiem, Q.T. Trinh, N.H. Tran, Insights into biofilm carriers for biological wastewater treatment processes: Current state-of-the-art, challenges, and opportunities, Bioresour. Technol. 288 (2019) 121619. https://doi.org/10.1016/j.biortech.2019.121619.

[95] R.J. Zeng, R. Lemaire, Z. Yuan, J. Keller, Simultaneous nitrification, denitrification, and phosphorus removal in a lab-scale sequencing batch reactor,

Biotechnol. Bioeng. 84 (2003) 170–178. https://doi.org/10.1002/bit.10744.

[96] S. Xie, J. Zhao, Q. Zhang, J. Zhao, S. Lei, X. Ma, C. Yan, Improvement of the performance of simultaneous nitrification denitrification and phosphorus removal (SNDPR) system by nitrite stress, Sci. Total Environ. 788 (2021) 147825. https://doi.org/10.1016/j.scitotenv.2021.147825.

[97] J. Ma, Y. Ji, Z. Fu, X. Yan, P. Xu, J. Li, L. Liu, P. Bi, L. Zhu, B. Xu, Q. He, Performance of anaerobic/oxic/anoxic simultaneous nitrification, denitrification and phosphorus removal system overwhelmingly dominated by Candidatus_Competibacter: Effect of aeration time, Bioresour. Technol. 384 (2023). https://doi.org/10.1016/j.biortech.2023.129312.

[98] H. Chen, X. Hu, W. Song, Z. Wang, M. Li, H. Liu, J. Li, Effect of pistachio shell as a carbon source to regulate C/N on simultaneous removal of nitrogen and phosphorus from wastewater, Bioresour. Technol. 367 (2023) 128234. https://doi.org/10.1016/j.biortech.2022.128234.

[99] J. Huang, L. Xu, Y. Guo, D. Liu, S. Chen, Q. Tang, H. Zheng, J. Tan, F. Peng, Intermittent aeration improving activated granular sludge granulation for nitrogen and phosphorus removal from domestic wastewater, Bioresour. Technol. Reports 15 (2021) 100739. https://doi.org/10.1016/j.biteb.2021.100739.

[100] L. Su, Y. Li, L. Chao, Q. Li, Z. Hu, Enhanced Simultaneous Nitrogen and Phosphorus Removal Performance of the AGS-SBR Reactor Based on the Effects of the C/N Ratio and Microbial Community Change, Sustain. 15 (2023). https://doi.org/10.3390/su15097691.

[101] J. Zhou, Q. Sun, Performance and microbial characterization of aerobic granular sludge in a sequencing batch reactor performing simultaneous nitrification,

denitrification and phosphorus removal with varying C/N ratios, Bioprocess Biosyst. Eng. 43 (2020) 663–672. https://doi.org/10.1007/s00449-019-02264-w.

[102] J. Wang, H. Rong, Y. Cao, C. Zhang, Factors affecting simultaneous nitrification and denitrification (SND) in a moving bed sequencing batch reactor (MBSBR) system as revealed by microbial community structures, Bioprocess Biosyst. Eng. 43 (2020) 1833–1846. https://doi.org/10.1007/s00449-020-02374-w.

[103] R. Huang, T. Meng, G. Liu, S. Gao, J. Tian, Simultaneous nitrification and denitrification in membrane bioreactor: Effect of dissolved oxygen, J. Environ. Manage. 323 (2022). https://doi.org/10.1016/j.jenvman.2022.116183.

[104] Z. Xia, Q. Wang, Z. She, M. Gao, Y. Zhao, L. Guo, C. Jin, Nitrogen removal pathway and dynamics of microbial community with the increase of salinity in simultaneous nitrification and denitrification process, Sci. Total Environ. 697 (2019) 134047. https://doi.org/10.1016/j.scitotenv.2019.134047.

[105] T. Liu, G. Jia, J. Xu, X. He, X. Quan, Simultaneous nitrification and denitrification in continuous flow MBBR with novel surface-modified carriers, Environ. Technol. (United Kingdom) 3330 (2020). https://doi.org/10.1080/09593330.2020.1735526.

[106] Z. Song, X. Zhang, H.H. Ngo, W. Guo, P. Song, Y. Zhang, H. Wen, J. Guo, Zeolite powder based polyurethane sponges as biocarriers in moving bed biofilm reactor for improving nitrogen removal of municipal wastewater, Sci. Total Environ. 651 (2019) 1078–1086. https://doi.org/10.1016/j.scitotenv.2018.09.173.

[107] D. Pan, S. Shao, J. Zhong, M. Wang, X. Wu, Performance and mechanism of simultaneous nitrification–denitrification and denitrifying phosphorus removal in long-term moving bed biofilm reactor (MBBR), Bioresour. Technol. 348 (2022) 126726. https://doi.org/10.1016/j.biortech.2022.126726.

[108] Y. Wu, A. Wan, B. Zhao, S. Xue, A. Xu, Single-stage MBBR using novel carriers to remove nitrogen in rural domestic sewage: The effect of carrier structure on biofilm morphology and SND, J. Environ. Chem. Eng. 10 (2022). https://doi.org/10.1016/j.jece.2022.108267.

[109] Y. Jin, J. Ding, W. Zhan, J. Du, G. Wang, J. Pang, N. Ren, S. Yang, Effect of dissolved oxygen concentration on performance and mechanism of simultaneous nitrification and denitrification in integrated fixed-film activated sludge sequencing batch reactors, Bioresour. Technol. 387 (2023) 129616. https://doi.org/10.1016/j.biortech.2023.129616.

[110] Y. Song, D. Zheng, S. Fan, S. Li, L. Zhang, H. Wang, D. Li, Simultaneous nitrification/denitrification in a single-chamber stainless steel bioelectrochemical reactor, J. Power Sources 591 (2024) 233810. https://doi.org/10.1016/j.jpowsour.2023.233810.

[111] T. Zhu, Y. Zhang, X. Quan, H. Li, Effects of an electric field and iron electrode on anaerobic denitrification at low C / N ratios, Chem. Eng. J. 266 (2015) 241–248. https://doi.org/10.1016/j.cej.2014.12.082.

[112] M. Chang, Y. Wang, Y. Pan, K. Zhang, L. Lyu, M. Wang, T. Zhu, Nitrogen removal from wastewater via simultaneous nitrification and denitrification using a biological folded non-aerated filter, Bioresour. Technol. 289 (2019). https://doi.org/10.1016/j.biortech.2019.121696.

[113] S.N. James, A. Vijayanandan, Recent advances in simultaneous nitrification and denitrification for nitrogen and micropollutant removal: a review, Biodegradation 34 (2023) 103–123. https://doi.org/10.1007/s10532-023-10015-8.

[114] J. Guo, Y. Peng, H. Huang, S. Wang, S. Ge, J. Zhang, Z. Wang, Short- and long-

term effects of temperature on partial nitrification in a sequencing batch reactor treating domestic wastewater, J. Hazard. Mater. 179 (2010) 471–479. https://doi.org/10.1016/j.jhazmat.2010.03.027.

[115] Q. Yao, D.C. Peng, Nitrite oxidizing bacteria (NOB) dominating in nitrifying community in full-scale biological nutrient removal wastewater treatment plants, AMB Express 7 (2017). https://doi.org/10.1186/s13568-017-0328-y.

[116] Y.H. Ong, A.S.M. Chua, T. Fukushima, G.C. Ngoh, T. Shoji, A. Michinaka, High-temperature EBPR process: The performance, analysis of PAOs and GAOs and the fine-scale population study of Candidatus "Accumulibacter phosphatis," Water Res. 64 (2014) 102–112. https://doi.org/10.1016/j.watres.2014.06.038.

[117] W. Jianlong, Y. Ning, Partial nitrification under limited dissolved oxygen conditions, Process Biochem. 39 (2004) 1223–1229. https://doi.org/10.1016/S0032-9592(03)00249-8.

[118] W. Qu, L. Suo, R. Liu, M. Liu, Y. Zhao, L. Xia, Y. Fan, Q. Zhang, Z. Gao, Influence of Temperature on Denitrification and Microbial Community Structure and Diversity: A Laboratory Study on Nitrate Removal from Groundwater, Water (Switzerland) 14 (2022) 1–15. https://doi.org/10.3390/w14030436.

[119] C. Li, S. Liu, T. Ma, M. Zheng, J. Ni, Simultaneous nitrification, denitrification and phosphorus removal in a sequencing batch reactor (SBR)under low temperature, Chemosphere 229 (2019) 132–141. https://doi.org/10.1016/j.chemosphere.2019.04.185.

[120] S. Ge, S. Wang, X. Yang, S. Qiu, B. Li, Y. Peng, Detection of nitrifiers and evaluation of partial nitrification for wastewater treatment: A review, Chemosphere 140 (2015) 85–98.

https://doi.org/10.1016/j.chemosphere.2015.02.004.

[121] L. Yan, S. Liu, Q. Liu, M. Zhang, Y. Liu, Y. Wen, Z. Chen, Y. Zhang, Q. Yang, Improved performance of simultaneous nitrification and denitrification via nitrite in an oxygen-limited SBR by alternating the DO, Bioresour. Technol. 275 (2019) 153–162. https://doi.org/10.1016/j.biortech.2018.12.054.

[122] W. Ma, Y. Han, W. Ma, H. Han, H. Zhu, C. Xu, K. Li, D. Wang, Enhanced nitrogen removal from coal gasification wastewater by simultaneous nitrification and denitrification (SND) in an oxygen-limited aeration sequencing batch biofilm reactor, Bioresour. Technol. 244 (2017) 84–91. https://doi.org/10.1016/j.biortech.2017.07.083.

[123] M. Ghasemi, S. Chang, S. Sivaloganathan, Modeling and simulation study of simultaneous nitrification–denitrification in membrane aerated bioreactor, J. Memb. Sci. 668 (2023) 121210. https://doi.org/10.1016/j.memsci.2022.121210.

[124] V. Van Huynh, M.T.T. Ngo, T. Itayama, M.B. Nguyen, T.D.H. Vo, T.K.Q. Vo, V.G. Le, S. jie You, P.T. Nguyen, X.T. Bui, Dynamic of microbial community in simultaneous nitrification and denitrification process: A review, Bioresour. Technol. Reports 22 (2023) 101415. https://doi.org/10.1016/j.biteb.2023.101415.

[125] Y. Zhang, X. Wang, M. Liu, C. Liu, Z. Yin, Simultaneous nitrogen and phosphorus removal from black water: Effects of dissolved oxygen level and sludge concentration on full-scale performance and bacterial community dynamics, J. Water Process Eng. 57 (2024) 104735. https://doi.org/10.1016/j.jwpe.2023.104735.

[126] L. Yan, S. Liu, Q. Liu, M. Zhang, Y. Liu, Y. Wen, Z. Chen, Y. Zhang, Q. Yang, Improved performance of simultaneous nitrification and denitrification via nitrite

in an oxygen-limited SBR by alternating the DO, Bioresour. Technol. 275 (2019) 153–162. https://doi.org/10.1016/j.biortech.2018.12.054.

[127] M. Deng, X. Zhao, Y. Senbati, K. Song, X. He, Nitrogen removal by heterotrophic nitrifying and aerobic denitrifying bacterium Pseudomonas sp. DM02: Removal performance, mechanism and immobilized application for real aquaculture wastewater treatment, Bioresour. Technol. 322 (2021) 124555. https://doi.org/10.1016/j.biortech.2020.124555.

[128] D. Wang, G. Wang, F. Yang, C. Liu, Treatment of municipal sewage with low carbon-to-nitrogen ratio via a novel integrated process, Chem. Eng. J. 341 (2018) 58–64. https://doi.org/10.1016/j.cej.2018.02.011.

[129] D. Wang, G. Wang, X. Xu, F. Yang, Multiple factors influencing anaerobic acidogenic pretreatment in an up-flow non-woven biofilm reactor, Chem. Eng. J. 221 (2013) 37–43. https://doi.org/10.1016/j.cej.2013.01.104.

[130] H. Chai, Y. Xiang, R. Chen, Z. Shao, L. Gu, L. Li, Q. He, Bioresource Technology Enhanced simultaneous nitrification and denitrification in treating low carbon-to-nitrogen ratio wastewater : Treatment performance and nitrogen removal pathway, 280 (2019) 51–58. https://doi.org/10.1016/j.biortech.2019.02.022.

[131] G. Mannina, G.A. Ekama, M. Capodici, A. Cosenza, D. Di Trapani, H. Ødegaard, M.M.C. van Loosdrecht, Influence of carbon to nitrogen ratio on nitrous oxide emission in an Integrated Fixed Film Activated Sludge Membrane BioReactor plant, J. Clean. Prod. 176 (2018) 1078–1090. https://doi.org/10.1016/j.jclepro.2017.11.222.

[132] G.C. Zhu, Y.Z. Lu, L.R. Xu, Effects of the carbon/nitrogen (C/N) ratio on a system coupling simultaneous nitrification and denitrification (SND) and denitrifying

phosphorus removal (DPR), Environ. Technol. (United Kingdom) 42 (2021) 3048–3054. https://doi.org/10.1080/09593330.2020.1720310.

[133] M. Hagman, J.L. Nielsen, P.H. Nielsen, J. la C. Jansen, Mixed carbon sources for nitrate reduction in activated sludge-identification of bacteria and process activity studies, Water Res. 42 (2008) 1539–1546. https://doi.org/10.1016/j.watres.2007.10.034.

[134] Q. He, Q. Song, S. Zhang, W. Zhang, H. Wang, Simultaneous nitrification, denitrification and phosphorus removal in an aerobic granular sequencing batch reactor with mixed carbon sources: reactor performance, extracellular polymeric substances and microbial successions, Chem. Eng. J. 331 (2018) 841–849. https://doi.org/10.1016/j.cej.2017.09.060.

[135] N. Shen, Y. Chen, Y. Zhou, Multi-cycle operation of enhanced biological phosphorus removal (EBPR) with different carbon sources under high temperature, Water Res. 114 (2017) 308–315. https://doi.org/10.1016/j.watres.2017.02.051.

[136] Q. He, J. Song, W. Zhang, S. Gao, H. Wang, J. Yu, Enhanced simultaneous nitrification, denitrification and phosphorus removal through mixed carbon source by aerobic granular sludge, J. Hazard. Mater. 382 (2020) 121043. https://doi.org/10.1016/j.jhazmat.2019.121043.

[137] X. Wang, W. Wang, Y. Zhang, Z. Sun, J. Zhang, G. Chen, J. Li, Simultaneous nitrification and denitrification by a novel isolated Pseudomonas sp. JQ-H3 using polycaprolactone as carbon source, Bioresour. Technol. 288 (2019). https://doi.org/10.1016/j.biortech.2019.121506.

[138] X. Fu, R. Hou, P. Yang, S. Qian, Z. Feng, Z. Chen, F. Wang, R. Yuan, H. Chen, B. Zhou, Application of external carbon source in heterotrophic denitrification of

domestic sewage: A review, Sci. Total Environ. 817 (2022) 153061. https://doi.org/10.1016/j.scitotenv.2022.153061.

[139] H. Sun, T. Wang, Z. Yang, C. Yu, W. Wu, Simultaneous removal of nitrogen and pharmaceutical and personal care products from the effluent of waste water treatment plants using aerated solid-phase denitrification system, Bioresour. Technol. 287 (2019) 121389. https://doi.org/10.1016/j.biortech.2019.121389.

[140] Z.L. She, X.L. Zhang, M. Gao, Y.C. Guo, L.T. Zhao, Y.G. Zhao, Effect of salinity on nitrogen removal by simultaneous nitrification and denitrification in a sequencing batch biofilm reactor, Desalin. Water Treat. 57 (2016) 7378–7386. https://doi.org/10.1080/19443994.2015.1016459.

[141] L. Luo, W. Zhou, Y. Yuan, H. Zhong, C. Zhong, Effects of salinity shock on simultaneous nitrification and denitrification by a membrane bioreactor: Performance, sludge activity, and functional microflora, Sci. Total Environ. 801 (2021). https://doi.org/10.1016/j.scitotenv.2021.149748.

[142] Q. He, H. Wang, L. Chen, S. Gao, W. Zhang, J. Song, J. Yu, Elevated salinity deteriorated enhanced biological phosphorus removal in an aerobic granular sludge sequencing batch reactor performing simultaneous nitrification, denitrification and phosphorus removal, J. Hazard. Mater. 390 (2020) 121782. https://doi.org/10.1016/j.jhazmat.2019.121782.

[143] Y. Yang, Z. Chen, X. Wang, L. Zheng, X. Gu, Partial nitrification performance and mechanism of zeolite biological aerated filter for ammonium wastewater treatment, Bioresour. Technol. 241 (2017) 473–481. https://doi.org/10.1016/j.biortech.2017.05.151.

[144] S. jun ZHANG, Y. zhen PENG, S. ying WANG, S. wen ZHENG, J. GUO, Organic

matter and concentrated nitrogen removal by shortcut nitrification and denitrification from mature municipal landfill leachate, J. Environ. Sci. 19 (2007) 647–651. https://doi.org/10.1016/S1001-0742(07)60108-9.

[145] S. Ge, S. Wang, X. Yang, S. Qiu, B. Li, Y. Peng, Detection of nitrifiers and evaluation of partial nitrification for wastewater treatment: A review, Chemosphere 140 (2015) 85–98. https://doi.org/10.1016/j.chemosphere.2015.02.004.

[146] L. Miao, G. Yang, T. Tao, Y. Peng, Recent advances in nitrogen removal from landfill leachate using biological treatments – A review, J. Environ. Manage. 235 (2019) 178–185. https://doi.org/10.1016/j.jenvman.2019.01.057.

[147] S. Yang, F. Yang, Nitrogen removal via short-cut simultaneous nitrification and denitrification in an intermittently aerated moving bed membrane bioreactor, J. Hazard. Mater. 195 (2011) 318–323. https://doi.org/10.1016/j.jhazmat.2011.08.045.

[148] X. Liu, M. Kim, G. Nakhla, M. Andalib, Y. Fang, Partial nitrification-reactor configurations, and operational conditions: Performance analysis, J. Environ. Chem. Eng. 8 (2020) 103984. https://doi.org/10.1016/j.jece.2020.103984.

[149] H. Sun, Y. Peng, X. Shi, Advanced treatment of landfill leachate using anaerobic-aerobic process: Organic removal by simultaneous denitritation and methanogenesis and nitrogen removal via nitrite, Bioresour. Technol. 177 (2015) 337–345. https://doi.org/10.1016/j.biortech.2014.10.152.

[150] M. Han, S.E. Vlaeminck, A. Al-Omari, B. Wett, C. Bott, S. Murthy, H. De Clippeleir, Uncoupling the solids retention times of flocs and granules in mainstream deammonification: A screen as effective out-selection tool for nitrite

oxidizing bacteria, Bioresour. Technol. 221 (2016) 195–204. https://doi.org/10.1016/j.biortech.2016.08.115.

[151] A. di Biase, M.S. Kowalski, T.R. Devlin, J.A. Oleszkiewicz, Moving bed biofilm reactor technology in municipal wastewater treatment: A review, J. Environ. Manage. 247 (2019) 849–866. https://doi.org/10.1016/j.jenvman.2019.06.053.

[152] J. Wu, C. He, M.C.M. van Loosdrecht, J. Pérez, Selection of ammonium oxidizing bacteria (AOB) over nitrite oxidizing bacteria (NOB) based on conversion rates, Chem. Eng. J. 304 (2016) 953–961. https://doi.org/10.1016/j.cej.2016.07.019.

[153] K. Fu, Y. Bian, F. Yang, J. Xu, F. Qiu, Achieving partial nitrification: A strategy for washing NOB out under high DO condition, J. Environ. Manage. 347 (2023) 119186. https://doi.org/10.1016/j.jenvman.2023.119186.

[154] B. Nowka, H. Daims, E. Spieck, Comparison of oxidation kinetics of nitrite-oxidizing bacteria: Nitrite availability as a key factor in niche differentiation, Appl. Environ. Microbiol. 81 (2015) 745–753. https://doi.org/10.1128/AEM.02734-14.

[155] A. Val del Rio, J.L. Campos, C. Da Silva, A. Pedrouso, A. Mosquera-Corral, Determination of the intrinsic kinetic parameters of ammonia-oxidizing and nitrite-oxidizing bacteria in granular and flocculent sludge, Sep. Purif. Technol. 213 (2019) 571–577. https://doi.org/10.1016/j.seppur.2018.12.048.

[156] C. Duan, Q. Zhang, J. Li, W. Feng, L. Zhang, Y. Peng, Partial nitrification response to dissolved oxygen variation and aerobic starvation: Kinetics and microbial community analyses, Chem. Eng. J. 481 (2024) 148621. https://doi.org/10.1016/j.cej.2024.148621.

[157] R. Ganigué, H. López, M.D. Balaguer, J. Colprim, Partial ammonium oxidation to nitrite of high ammonium content urban landfill leachates, Water Res. 41 (2007)

3317–3326. https://doi.org/10.1016/j.watres.2007.04.027.

[158] M. Zhou, Y. Han, Y. Zhuo, F. Yu, G. Hu, D. Peng, Effect of initial ammonium concentration on a one-stage partial nitrification/anammox biofilm system: Nitrogen removal performance and the microbial community, J. Environ. Sci. 143 (2023) 176–188. https://doi.org/10.1016/j.jes.2023.07.026.

[159] Q. Wang, H. Duan, W. Wei, B.J. Ni, A. Laloo, Z. Yuan, Achieving Stable Mainstream Nitrogen Removal via the Nitrite Pathway by Sludge Treatment Using Free Ammonia, Environ. Sci. Technol. 51 (2017) 9800–9807. https://doi.org/10.1021/acs.est.7b02776.

[160] W. Bae, S. Baek, J. Chung, Y. Lee, Optimal operational factors for nitrite accumulation in batch reactors, Biodegradation 12 (2001) 359–366. https://doi.org/10.1023/A:1014308229656.

[161] Y. Zhou, A. Oehmen, M. Lim, V. Vadivelu, W.J. Ng, The role of nitrite and free nitrous acid (FNA) in wastewater treatment plants, Water Res. 45 (2011) 4672–4682. https://doi.org/10.1016/j.watres.2011.06.025.

[162] R. Chen, S. Cao, L. Zhang, Y. Zhou, NOB suppression strategies in a mainstream membrane aerated biofilm reactor under exceptionally low lumen pressure, Chemosphere 290 (2022) 133386. https://doi.org/10.1016/j.chemosphere.2021.133386.

[163] W. Qian, Y. Peng, X. Li, Q. Zhang, B. Ma, The inhibitory effects of free ammonia on ammonia oxidizing bacteria and nitrite oxidizing bacteria under anaerobic condition, Bioresour. Technol. 243 (2017) 1247–1250. https://doi.org/10.1016/j.biortech.2017.07.119.

[164] Y. Zhou, C. Wang, X. Xu, L. Liu, G. Zhang, F. Yang, Advance nitrogen removal

from anaerobic sludge digestion liquor using partial nitrification and denitrification coupled with simultaneous partial nitrification, anammox, and denitrification process, Bioresour. Technol. 393 (2024) 130117. https://doi.org/10.1016/j.biortech.2023.130117.

[165] E.M. Gilbert, S. Agrawal, F. Brunner, T. Schwartz, H. Horn, S. Lackner, Response of different Nitrospira Species to anoxic periods depends on operational DO, Environ. Sci. Technol. 48 (2014) 2934–2941. https://doi.org/10.1021/es404992g.

[166] Z. Zhou, M. Qi, H. Wang, Achieving partial nitrification via intermittent aeration in sbr and short-term effects of different c/n ratios on reactor performance and microbial community structure, Water (Switzerland) 12 (2020) 1–16. https://doi.org/10.3390/w12123485.

[167] M.O. Hassan, K.M. Gani, S. Kumari, O. Awolusi, L. Gumede, M. Seyam, F. Bux, Start-up of partial nitrification by intermittent aeration, pH shocks and sulfide addition in a sequential batch reactor, J. Chem. Technol. Biotechnol. 97 (2022) 2186–2195. https://doi.org/10.1002/jctb.7097.

[168] Z. Xu, L. Zhang, X. Gao, Y. Peng, Optimization of the intermittent aeration to improve the stability and flexibility of a mainstream hybrid partial nitrification-anammox system, Chemosphere 261 (2020) 127670. https://doi.org/10.1016/j.chemosphere.2020.127670.

[169] Y. Luan, Y. Yin, Z. Guo, Q. Wang, Y. Xu, F. Zhang, Y. Xiao, C. Liu, Partial nitrification-denitrification and enrichment of paracoccus induced by iron-chitosan beads addition in an intermittently-aerated activated sludge system, J. Environ. Manage. 353 (2024) 120189. https://doi.org/10.1016/j.jenvman.2024.120189.

[170] M. Chang, B. Liang, K. Zhang, Y. Wang, D. Jin, Q. Zhang, L. Hao, T. Zhu,

Simultaneous shortcut nitrification and denitrification in a hybrid membrane aerated biofilms reactor (H-MBfR) for nitrogen removal from low COD/N wastewater, Water Res. 211 (2022). https://doi.org/10.1016/j.watres.2021.118027.

[171] Y. Zhao, D. Liu, W. Huang, Y. Yang, M. Ji, L.D. Nghiem, Q.T. Trinh, N.H. Tran, Insights into biofilm carriers for biological wastewater treatment processes: Current state-of-the-art, challenges, and opportunities, Bioresour. Technol. 288 (2019) 121619. https://doi.org/10.1016/j.biortech.2019.121619.

[172] C. Bumbac, I.A. Ionescu, O. Tiron, V.R. Badescu, Continuous flow aerobic granular sludge reactor for dairy wastewater treatment, Water Sci. Technol. 71 (2015) 440–445. https://doi.org/10.2166/wst.2015.007.

[173] R. Campo, C. Lubello, T. Lotti, G. Di Bella, Aerobic granular sludge–membrane bioreactor (Ags–mbr) as a novel configuration for wastewater treatment and fouling mitigation: A mini-review, Membranes (Basel). 11 (2021). https://doi.org/10.3390/membranes11040261.

[174] V. Pratap, R. Kumar, S. Kumar, B.R. Yadav, Optimization of moving bed biofilm reactors for the treatment of municipal wastewater, Environ. Res. 241 (2024) 117560. https://doi.org/10.1016/j.envres.2023.117560.

[175] K.A. Garcia, P. McLee, A.J. Schuler, Effects of media length on biofilms and nitrification in moving bed biofilm reactors, Biofilm 4 (2022) 100091. https://doi.org/10.1016/j.bioflm.2022.100091.

[176] M. Zheng, Y. Han, H. Han, C. Xu, Z. Zhang, W. Ma, Synergistic degradation on phenolic compounds of coal pyrolysis wastewater (CPW) by lignite activated coke-active sludge (LAC-AS) process: Insights into succession of microbial community under selective pressure, Bioresour. Technol. 281 (2019) 126–134.

https://doi.org/10.1016/j.biortech.2019.02.074.

[177] S. Goswami, D. Mazumder, Comparative study between activated sludge process (ASP) and moving bed bioreactor (MBBR) for treating composite chrome tannery wastewater, Mater. Today Proc. 3 (2016) 3337–3342. https://doi.org/10.1016/j.matpr.2016.10.015.

[178] R.K. Sonwani, G. Swain, R.P. Jaiswal, R.S. Singh, B.N. Rai, Moving bed biofilm reactor with immobilized low-density polyethylene–polypropylene for Congo red dye removal, Environ. Technol. Innov. 23 (2021) 101558. https://doi.org/10.1016/j.eti.2021.101558.

[179] L. Chu, J. Wang, F. Quan, X.H. Xing, L. Tang, C. Zhang, Modification of polyurethane foam carriers and application in a moving bed biofilm reactor, Process Biochem. 49 (2014) 1979–1982. https://doi.org/10.1016/j.procbio.2014.07.018.

[180] Y. Luo, W. Guo, H.H. Ngo, L.D. Nghiem, F.I. Hai, J. Kang, S. Xia, Z. Zhang, W.E. Price, Removal and fate of micropollutants in a sponge-based moving bed bioreactor, Bioresour. Technol. 159 (2014) 311–319. https://doi.org/10.1016/j.biortech.2014.02.107.

[181] X. Zhang, X. Chen, C. Zhang, H. Wen, W. Guo, H.H. Ngo, Effect of filling fraction on the performance of sponge-based moving bed biofilm reactor, Bioresour. Technol. 219 (2016) 762–767. https://doi.org/10.1016/j.biortech.2016.08.031.

[182] M. Lu, F. Zhao, F. Qin, F. Zhang, Q. Feng, Novel flocking materials as biocarriers in moving bed biofilm reactor for improving simultaneous nitrification and denitrification performance, Bioresour. Technol. 396 (2024) 130430. https://doi.org/10.1016/j.biortech.2024.130430.

[183] X.L. Yang, Q. Jiang, H.L. Song, T.T. Gu, M.Q. Xia, Selection and application of agricultural wastes as solid carbon sources and biofilm carriers in MBR, J. Hazard. Mater. 283 (2015) 186–192. https://doi.org/10.1016/j.jhazmat.2014.09.036.

[184] S. Madan, R. Madan, A. Hussain, Advancement in biological wastewater treatment using hybrid moving bed biofilm reactor (MBBR): a review, Appl. Water Sci. 12 (2022) 1–13. https://doi.org/10.1007/s13201-022-01662-y.

[185] Q. Feng, Y. Wang, T. Wang, H. Zheng, L. Chu, C. Zhang, H. Chen, X. Kong, X.H. Xing, Effects of packing rates of cubic-shaped polyurethane foam carriers on the microbial community and the removal of organics and nitrogen in moving bed biofilm reactors, Bioresour. Technol. 117 (2012) 201–207. https://doi.org/10.1016/j.biortech.2012.04.076.

[186] X. Zhang, Z. Song, W. Guo, Y. Lu, L. Qi, H. Wen, H.H. Ngo, Behavior of nitrogen removal in an aerobic sponge based moving bed biofilm reactor, Bioresour. Technol. 245 (2017) 1282–1285. https://doi.org/10.1016/j.biortech.2017.08.106.

[187] S. Shao, J. Zhong, C. Wang, D. Pan, X. Wu, Performance of simultaneous nitrification–denitrification and denitrifying phosphorus and manganese removal by driving a single-stage moving bed biofilm reactor based on manganese redox cycling, Bioresour. Technol. 362 (2022) 127846. https://doi.org/10.1016/j.biortech.2022.127846.

[188] M.K. De Kreuk, N. Kishida, M.C.M. Van Loosdrecht, Aerobic granular sludge – state of the art, (2007) 3–4. https://doi.org/10.2166/wst.2007.244.

[189] M. Pronk, M.K. de Kreuk, B. de Bruin, P. Kamminga, R. Kleerebezem, M.C.M. van Loosdrecht, Full scale performance of the aerobic granular sludge process for sewage treatment, Water Res. 84 (2015) 207–217.

https://doi.org/10.1016/j.watres.2015.07.011.

[190] C. Yu, K. Wang, K. Zhang, R. Liu, P. Zheng, Full-scale upgrade activated sludge to continuous-flow aerobic granular sludge: Implementing microaerobic-aerobic configuration with internal separators, Water Res. 248 (2024) 120870. https://doi.org/10.1016/j.watres.2023.120870.

[191] L.D.A. Purba, H.T. Ibiyeye, A. Yuzir, S.E. Mohamad, K. Iwamoto, A. Zamyadi, N. Abdullah, Various applications of aerobic granular sludge: A review, Environ. Technol. Innov. 20 (2020) 101045. https://doi.org/10.1016/j.eti.2020.101045.

[192] S.L. de Sousa Rollemberg, A.R. Mendes Barros, P.I. Milen Firmino, A. Bezerra dos Santos, Aerobic granular sludge: Cultivation parameters and removal mechanisms, Bioresour. Technol. 270 (2018) 678–688. https://doi.org/10.1016/j.biortech.2018.08.130.

[193] Q. He, L. Chen, S. Zhang, R. Chen, H. Wang, Hydrodynamic shear force shaped the microbial community and function in the aerobic granular sequencing batch reactors for low carbon to nitrogen (C / N) municipal wastewater treatment, Bioresour. Technol. 271 (2019) 48–58. https://doi.org/10.1016/j.biortech.2018.09.102.

[194] M. Coma, M. Verawaty, M. Pijuan, Z. Yuan, P.L. Bond, Enhancing aerobic granulation for biological nutrient removal from domestic wastewater, Bioresour. Technol. 103 (2012) 101–108. https://doi.org/10.1016/j.biortech.2011.10.014.

[195] B. Nguyen Quoc, S. Wei, M. Armenta, R. Bucher, P. Sukapanpotharam, D.A. Stahl, H.D. Stensel, M.K.H. Winkler, Aerobic granular sludge: Impact of size distribution on nitrification capacity, Water Res. 188 (2021) 116445. https://doi.org/10.1016/j.watres.2020.116445.

[196] B. Nguyen Quoc, M. Armenta, J.A. Carter, R. Bucher, P. Sukapanpotharam, S.J. Bryson, D.A. Stahl, H.D. Stensel, M.K.H. Winkler, An investigation into the optimal granular sludge size for simultaneous nitrogen and phosphate removal, Water Res. 198 (2021) 117119. https://doi.org/10.1016/j.watres.2021.117119.

[197] F.A. Dahalan, N. Abdullah, A. Yuzir, G. Olsson, Salmiati, M. Hamdzah, M.F.M. Din, S.A. Ahmad, K.A. Khalil, A.N. Anuar, Z.Z. Noor, Z. Ujang, A proposed aerobic granules size development scheme for aerobic granulation process, Bioresour. Technol. 181 (2015) 291–296. https://doi.org/10.1016/j.biortech.2015.01.062.

[198] C. Yuan, Y. Peng, B. Wang, X. Li, Q. Zhang, Facilitating sludge granulation and favoring glycogen accumulating organisms by increased salinity in an anaerobic/micro-aerobic simultaneous partial nitrification, denitrification and phosphorus removal (SPNDPR) process, Bioresour. Technol. 313 (2020) 123698. https://doi.org/10.1016/j.biortech.2020.123698.

[199] D. Chen, H. Li, X. Xue, L. Zhang, Y. Hou, H. Chen, Y. Zhang, Y. Song, S. Zhao, J. Guo, Enhanced simultaneous partial nitrification and denitrification performance of aerobic granular sludge via tapered aeration in sequencing batch reactor for treating low strength and low COD/TN ratio municipal wastewater, Environ. Res. 209 (2022) 112743. https://doi.org/10.1016/j.envres.2022.112743.

[200] A. ElMekawy, S. Srikanth, S. Bajracharya, H.M. Hegab, P.S. Nigam, A. Singh, S.V. Mohan, D. Pant, Food and agricultural wastes as substrates for bioelectrochemical system (BES): The synchronized recovery of sustainable energy and waste treatment, Food Res. Int. 73 (2015) 213–225. https://doi.org/10.1016/j.foodres.2014.11.045.

[201] D. Su, Y. Chen, Advanced bioelectrochemical system for nitrogen removal in wastewater, Chemosphere 292 (2022) 133206. https://doi.org/10.1016/j.chemosphere.2021.133206.

[202] Y. V. Nancharaiah, S. Venkata Mohan, P.N.L. Lens, Recent advances in nutrient removal and recovery in biological and bioelectrochemical systems, Bioresour. Technol. 215 (2016) 173–185. https://doi.org/10.1016/j.biortech.2016.03.129.

[203] M. Al-Sahari, A. Al-Gheethi, R.M.S. Radin Mohamed, E. Noman, M. Naushad, M.B. Rizuan, D.V.N. Vo, N. Ismail, Green approach and strategies for wastewater treatment using bioelectrochemical systems: A critical review of fundamental concepts, applications, mechanism, and future trends, Chemosphere 285 (2021). https://doi.org/10.1016/j.chemosphere.2021.131373.

[204] B. Virdis, K. Rabaey, R.A. Rozendal, Z. Yuan, J. Keller, Simultaneous nitrification, denitrification and carbon removal in microbial fuel cells, Water Res. 44 (2010) 2970–2980. https://doi.org/10.1016/j.watres.2010.02.022.

[205] A.S. Ali, K. Tahir, B. Kim, Y. Lim, D.S. Lee, Microbially catalyzed anode and cathode microbial electrosynthesis system for efficient metformin removal and volatile fatty acid production, Fuel 358 (2024) 130237. https://doi.org/10.1016/j.fuel.2023.130237.

[206] W.T. Mook, M.K.T. Aroua, M.H. Chakrabarti, I.M. Noor, M.F. Irfan, C.T.J. Low, A review on the effect of bio-electrodes on denitrification and organic matter removal processes in bio-electrochemical systems, J. Ind. Eng. Chem. 19 (2013) 1–13. https://doi.org/10.1016/j.jiec.2012.07.004.

[207] A.W. Jeremiasse, H.V.M. Hamelers, C.J.N. Buisman, Microbial electrolysis cell with a microbial biocathode, Bioelectrochemistry 78 (2010) 39–43.

https://doi.org/10.1016/j.bioelechem.2009.05.005.

[208] T. Watanabe, S. Hashimoto, M. Kuroda, Simultaneous nitrification and denitrification in a single reactor using bio-electrochemical process, Water Sci. Technol. 46 (2002) 163–169. https://doi.org/10.2166/wst.2002.0577.

[209] D. Zheng, W. Gu, Q. Zhou, L. Zhang, C. Wei, Q. Yang, D. Li, Ammonia oxidation and denitrification in a bio-anode single-chambered microbial electrolysis cell, Bioresour. Technol. 310 (2020) 123466. https://doi.org/10.1016/j.biortech.2020.123466.

[210] S. Huang, G. Zhu, X. Gu, The relationship between energy production and simultaneous nitrification and denitrification via bioelectric derivation of microbial fuel cells at different anode numbers, Environ. Res. 184 (2020) 109247. https://doi.org/10.1016/j.envres.2020.109247.

[211] M. Isabel San-Martín, R. Mateos, B. Carracedo, A. Escapa, A. Morán, Pilot-scale bioelectrochemical system for simultaneous nitrogen and carbon removal in urban wastewater treatment plants, J. Biosci. Bioeng. 126 (2018) 758–763. https://doi.org/10.1016/j.jbiosc.2018.06.008.

[212] J.P. Boltz, E. Morgenroth, D. Sen, Mathematical modelling of biofilms and biofilm reactors for engineering design, Water Sci. Technol. 62 (2010) 1821–1836. https://doi.org/10.2166/wst.2010.076.

[213] A. Eldyasti, G. Nakhla, J. Zhu, Development of a calibration protocol and identification of the most sensitive parameters for the particulate biofilm models used in biological wastewater treatment, Bioresour. Technol. 111 (2012) 111–121. https://doi.org/10.1016/j.biortech.2012.02.021.

[214] M. Dolatshah, A. Asadi, F. Gholami, S. Nazari, Development and modeling of an

integrated fixed-film activated sludge (IFAS) system for simultaneous nitrogen and carbon removal from an industrial estate wastewater, Biotechnol. Reports 41 (2024) e00831. https://doi.org/10.1016/j.btre.2024.e00831.

[215] S.H. Baek, H.J. Kim, Mathematical model for simultaneous nitrification and denitrification (SND) in membrane bioreactor (MBR) under Low Dissolved Oxygen (DO) concentrations, Biotechnol. Bioprocess Eng. 18 (2013) 104–110. https://doi.org/10.1007/s12257-011-0419-6.

[216] G. Insel, S. Erol, S. Övez, Effect of simultaneous nitrification and denitrification on nitrogen removal performance and filamentous microorganism diversity of a full-scale MBR plant, Bioprocess Biosyst. Eng. 37 (2014) 2163–2173. https://doi.org/10.1007/s00449-014-1193-6.

[217] L. Chu, J. Wang, Nitrogen removal using biodegradable polymers as carbon source and biofilm carriers in a moving bed biofilm reactor, Chem. Eng. J. 170 (2011) 220–225. https://doi.org/10.1016/j.cej.2011.03.058.

[218] L.W. Ngatia, Y.P. Hsieh, D. Nemours, R. Fu, R.W. Taylor, Potential phosphorus eutrophication mitigation strategy: Biochar carbon composition, thermal stability and pH influence phosphorus sorption, Chemosphere 180 (2017) 201–211. https://doi.org/10.1016/j.chemosphere.2017.04.012.

[219] G. Zou, S. Papirio, E.D. van Hullebusch, J.A. Puhakka, Fluidized-bed denitrification of mining water tolerates high nickel concentrations, Bioresour. Technol. 179 (2015) 284–290. https://doi.org/10.1016/j.biortech.2014.12.044.

[220] S. Papirio, G. Esposito, F. Pirozzi, Biological inverse fluidized-bed reactors for the treatment of low pH- and sulphate-containing wastewaters under different COD/SO2-4 conditions, Environ. Technol. (United Kingdom) 34 (2013) 1141–

1149. https://doi.org/10.1080/09593330.2012.737864.

[221] P.L. Rittman, B.E., McCarty, Environmental Biotechnology:Principles and Applications, (2001).

[222] Metcalf & Eddy, Wastewater engineering: treatment, disposal, and reuse, 1991.

[223] N. Di Costanzo, A. Cesaro, F. Di Capua, G. Esposito, Exploiting the nutrient potential of anaerobically digested sewage sludge: A review, Energies 14 (2021) 1–25. https://doi.org/10.3390/en14238149.

[224] E. V. Münch, P. Lant, J. Keller, Simultaneous nitrification and denitrification in bench-scale sequencing batch reactors, Water Res. 30 (1996) 277–284. https://doi.org/10.1016/0043-1354(95)00174-3.

[225] A. Maurya, R. Kumar, A. Raj, Biofilm-based technology for industrial wastewater treatment: current technology, applications and future perspectives, World J. Microbiol. Biotechnol. 39 (2023). https://doi.org/10.1007/s11274-023-03567-7.

[226] M. Revilla, B. Galán, J.R. Viguri, An integrated mathematical model for chemical oxygen demand (COD) removal in moving bed biofilm reactors (MBBR) including predation and hydrolysis, Water Res. 98 (2016) 84–97. https://doi.org/10.1016/j.watres.2016.04.003.

[227] A.M. Faris, H.M. Zwain, M. Hosseinzadeh, H.S. Majdi, S.M. Siadatmousavi, Start-up and operation of novel EN-MBBR system for sidestreams treatment and sensitivity analysis modeling using GPS-X simulation, Alexandria Eng. J. 61 (2022) 10805–10818. https://doi.org/10.1016/j.aej.2022.04.026.

[228] O. Wanner, P. Reichert, Mathematical modeling of mixed-culture biofilms, Biotechnol. Bioeng. 49 (1996) 172–184. https://doi.org/10.1002/(SICI)1097-0290(19960120)49:2<172::AID-BIT6>3.0.CO;2-N.

[229] M.R. Mattei, L. Frunzo, B. D'Acunto, Y. Pechaud, F. Pirozzi, G. Esposito, Continuum and discrete approach in modeling biofilm development and structure: a review, J. Math. Biol. 76 (2018) 945–1003. https://doi.org/10.1007/s00285-017-1165-y.

[230] EnviroSim Associates Ltd, Biowin 6 Help Manual, 2019.

[231] O. Wanner, W. Gujer, A Multispecies Biofilm Model, Biotechnol. Bioeng. 28 (1986) 314–328.

[232] R. Ferrentino, A. Ferraro, M.R. Mattei, G. Esposito, G. Andreottola, Process performance optimization and mathematical modelling of a SBR-MBBR treatment at low oxygen concentration, Process Biochem. 75 (2018) 230–239. https://doi.org/10.1016/j.procbio.2018.08.023.

[233] A.A.L. Zinatizadeh, E. Ghaytooli, Simultaneous nitrogen and carbon removal from wastewater at different operating conditions in a moving bed biofilm reactor (MBBR): Process modeling and optimization, J. Taiwan Inst. Chem. Eng. 53 (2015) 98–111. https://doi.org/10.1016/j.jtice.2015.02.034.

[234] L. Rieger, Guidelines for Using Activated Sludge Models, 2012. https://doi.org/10.2166/9781780401164.

[235] Sabine Julien, Modélisation et estimation pour le contrôle d'un procédé boues activées éliminant l'azote des eaux résiduaires urbaines, 1997.

[236] N. Hvala, S. Strmčnik, D. Šel, S. Milanič, B. Banko, Influence of model validation on proper selection of process models - An industrial case study, Comput. Chem. Eng. 29 (2005) 1507–1522. https://doi.org/10.1016/j.compchemeng.2004.11.013.

[237] M. Zeng, A. Soric, N. Roche, Modeling partial nitrification and denitrification in a hybrid biofilm reactor: calibration by retention time distribution and

respirometric tests, Environ. Sci. Pollut. Res. 22 (2015) 12849–12860. https://doi.org/10.1007/s11356-014-3667-0.

[238] A. Rajta, R. Bhatia, H. Setia, P. Pathania, Role of heterotrophic aerobic denitrifying bacteria in nitrate removal from wastewater, J. Appl. Microbiol. 128 (2020) 1261–1278. https://doi.org/10.1111/jam.14476.

[239] J. Guerrero, A. Guisasola, J.A. Baeza, The nature of the carbon source rules the competition between PAO and denitrifiers in systems for simultaneous biological nitrogen and phosphorus removal, Water Res. 45 (2011) 4793–4802. https://doi.org/10.1016/j.watres.2011.06.019.

[240] E. Casey, B. Glennon, G. Hamer, Biofilm development in a membrane-aerated biofilm reactor: Effect of flow velocity on performance, Biotechnol. Bioeng. 67 (2000) 476–486. https://doi.org/10.1002/(SICI)1097-0290(20000220)67:4<476::AID-BIT11>3.0.CO;2-2.

[241] M.C.M. Van Loosdrecht, J.J. Heijnen, H. Eberl, J. Kreft, & C. Picioreanu, Mathematical modelling of biofilm structures, 2002.

[242] W. Trojanowicz, W. Styka, T. Baczynski, Experimental determination of kinetic parameters for heterotrophic microorganisms in bioflim under petrochemical wastewater conditions, Polish J. Environ. Stud. 18 (2009) 913–921.

[243] K.F. Liau, T. Shoji, Y.H. Ong, A.S.M. Chua, H.K. Yeoh, P.Y. Ho, Kinetic and stoichiometric characterization for efficient enhanced biological phosphorus removal (EBPR) process at high temperatures, Bioprocess Biosyst. Eng. 38 (2015) 729–737. https://doi.org/10.1007/s00449-014-1313-3.

[244] D. Orhon, D. Okutman, Respirometric assessment of residual organic matter for domestic sewage, Enzyme Microb. Technol. 32 (2003) 560–566.

https://doi.org/10.1016/S0141-0229(03)00023-1.

[245] V. Van Huynh, M.T.T. Ngo, T. Itayama, M.B. Nguyen, T.D.H. Vo, T.K.Q. Vo, V.G. Le, S. jie You, P.T. Nguyen, X.T. Bui, Dynamic of microbial community in simultaneous nitrification and denitrification process: A review, Bioresour. Technol. Reports 22 (2023). https://doi.org/10.1016/j.biteb.2023.101415.

[246] M.C.M. van L. Mogens Henze, W. Gujer, T. Mino, Activated sludge models ASM1, ASM2, ASM2d and ASM3, reprint, IWA Publishing, London, 2000.

[247] C. Lopez, M.N. Pons, E. Morgenroth, Endogenous processes during long-term starvation in activated sludge performing enhanced biological phosphorus removal, Water Res. 40 (2006) 1519–1530. https://doi.org/10.1016/j.watres.2006.01.040.

[248] K. Masmoudi Jabri, T. Fiedler, A. Saidi, E. Nolde, M. Ogurek, S.U. Geissen, L. Bousselmi, Steady-state modeling of the biodegradation performance of a multistage moving bed biofilm reactor (MBBR) used for on-site greywater treatment, Environ. Sci. Pollut. Res. 26 (2019) 19047–19062. https://doi.org/10.1007/s11356-018-3984-9.

[249] J.P. Boltz, E. Morgenroth, D. Brockmann, C. Bott, W.J. Gellner, P.A. Vanrelleghem, Critical components of biofilm models for engineering practice To cite this version : HAL Id : hal-01190424 Critical Components of Biofilm Models for Engineering, WWTmod2010 - 2nd IWA/WEF Wastewater Treat. Model. Semin. (2015).

[250] Z.R. Hu, M.C. Wentzel, G.A. Ekama, Modelling biological nutrient removal activated sludge systems - A review, Water Res. 37 (2003) 3430–3444. https://doi.org/10.1016/S0043-1354(03)00168-4.

[251] C.M. López-Vázquez, C.M. Hooijmans, D. Brdjanovic, H.J. Gijzen, M.C.M. van Loosdrecht, Factors affecting the microbial populations at full-scale enhanced biological phosphorus removal (EBPR) wastewater treatment plants in The Netherlands, Water Res. 42 (2008) 2349–2360. https://doi.org/10.1016/j.watres.2008.01.001.

[252] E. Jiménez, J.B. Giménez, A. Seco, J. Ferrer, J. Serralta, Effect of pH, substrate and free nitrous acid concentrations on ammonium oxidation rate, Bioresour. Technol. 124 (2012) 478–484. https://doi.org/10.1016/j.biortech.2012.07.079.

[253] E. Jiménez, J.B. Giménez, M. V. Ruano, J. Ferrer, J. Serralta, Effect of pH and nitrite concentration on nitrite oxidation rate, Bioresour. Technol. 102 (2011) 8741–8747. https://doi.org/10.1016/j.biortech.2011.07.092.

[254] W.K. Dodds, V.H. Smith, Nitrogen, phosphorus, and eutrophication in streams, Inl. Waters 6 (2016) 155–164. https://doi.org/10.5268/IW-6.2.909.

[255] M. Seifi, M.H. Fazaelipoor, Modeling simultaneous nitrification and denitrification (SND) in a fluidized bed biofilm reactor, Appl. Math. Model. 36 (2012) 5603–5613. https://doi.org/10.1016/j.apm.2012.01.004.

[256] Y. Yan, H. Lu, J. Zhang, S. Zhu, Y. Wang, Y. Lei, R. Zhang, L. Song, Simultaneous heterotrophic nitrification and aerobic denitrification (SND) for nitrogen removal: A review and future perspectives, Environ. Adv. 9 (2022) 100254. https://doi.org/10.1016/j.envadv.2022.100254.

[257] H. Chai, Y. Xiang, R. Chen, Z. Shao, L. Gu, L. Li, Q. He, Enhanced simultaneous nitrification and denitrification in treating low carbon-to-nitrogen ratio wastewater: Treatment performance and nitrogen removal pathway, Bioresour. Technol. 280 (2019) 51–58. https://doi.org/10.1016/j.biortech.2019.02.022.

[258] F. Wang, S. Lu, Y. Wei, M. Ji, Characteristics of aerobic granule and nitrogen and phosphorus removal in a SBR, J. Hazard. Mater. 164 (2009) 1223–1227. https://doi.org/10.1016/j.jhazmat.2008.09.034.

[259] D. Gao, L. Liu, H. Liang, W.M. Wu, Aerobic granular sludge: Characterization, mechanism of granulation and application to wastewater treatment, Crit. Rev. Biotechnol. 31 (2011) 137–152. https://doi.org/10.3109/07388551.2010.497961.

[260] G. Lettinga, A.F.M. van Velsen, S.W. Hobma, W. de Zeeuw, A. Klapwijk, Use of the upflow sludge blanket (USB) reactor concept for biological wastewater treatment, especially for anaerobic treatment, Biotechnol. Bioeng. 22 (1980) 699–734. https://doi.org/10.1002/bit.260220402.

[261] K. Kumari, S. Suresh, S. Arisutha, K. Sudhakar, Anaerobic co-digestion of different wastes in a UASB reactor, Waste Manag. 77 (2018) 545–554. https://doi.org/10.1016/j.wasman.2018.05.007.

[262] L.C. Tan, S. Papirio, V. Luongo, Y. V. Nancharaiah, P. Cennamo, G. Esposito, E.D. van Hullebusch, P.N.L. Lens, Comparative performance of anaerobic attached biofilm and granular sludge reactors for the treatment of model mine drainage wastewater containing selenate, sulfate and nickel, Chem. Eng. J. 345 (2018) 545–555. https://doi.org/10.1016/j.cej.2018.03.177.

[263] H.S. Shin, K.H. Lim, H.S. Park, Effect of shear stress on granulation in oxygen aerobic upflow sludge bed reactors, Water Sci. Technol. 26 (1992) 601–605. https://doi.org/10.2166/wst.1992.0440.

[264] H.G. Yang, J. Li, J. Liu, L.B. Ding, T. Chen, G.X. Huang, J.Y. Shen, A case for aerobic sludge granulation : from pilot to full scale, (2016) 188–194. https://doi.org/10.2166/wrd.2015.188.

[265] J. Li, L. Ding, A. Cai, G. Huang, H. Horn, Aerobic Sludge Granulation in a Full-Scale Sequencing Batch Reactor, 2014 (2014).

[266] J.H. Tay, Q.S. Liu, Y. Liu, The effects of shear force on the formation, structure and metabolism of aerobic granules, Appl. Microbiol. Biotechnol. 57 (2001) 227–233. https://doi.org/10.1007/s002530100766.

[267] Y. Liu, X. Kang, X. Li, Y. Yuan, Performance of aerobic granular sludge in a sequencing batch bioreactor for slaughterhouse wastewater treatment, Bioresour. Technol. 190 (2015) 487–491. https://doi.org/10.1016/j.biortech.2015.03.008.

[268] N.S.A. Ali, K. Muda, M.F. Mohd Amin, M.Z.M. Najib, E.H. Ezechi, M.S.J. Darwish, Initialization, enhancement and mechanisms of aerobic granulation in wastewater treatment, Sep. Purif. Technol. 260 (2021) 118220. https://doi.org/10.1016/j.seppur.2020.118220.

[269] A. Rosa-masegosa, B. Muñoz-palazon, A. Gonzalez-martinez, M. Fenice, S. Gorrasi, J. Gonzalez-lopez, New Advances in Aerobic Granular Sludge Technology Using Continuous Flow Reactors : Engineering and Microbiological Aspects, (2021) 1–20.

[270] Z. Li, Q. Meng, C. Wan, C. Zhang, X. Tan, X. Liu, Aggregation performance and adhesion behavior of microbes in response to feast/famine condition: Rapid granulation of aerobic granular sludge, Environ. Res. 208 (2022) 112780. https://doi.org/10.1016/j.envres.2022.112780.

[271] L. Changqing, L. Shuai, Z. Feng, The oxygen transfer efficiency and economic cost analysis of aeration system in municipal wastewater treatment plant, Energy Procedia 5 (2011) 2437–2443. https://doi.org/10.1016/j.egypro.2011.03.419.

[272] M. Campanelli, P. Foladori, M. Vaccari, Consumi elettrici ed efficienza energetica

nel trattamento delle acque reflue, 2013. isbn: 8838783683.

[273] Y. Gu, Y. Li, F. Yuan, Q. Yang, Optimization and control strategies of aeration in WWTPs: A review, J. Clean. Prod. 418 (2023). https://doi.org/10.1016/j.jclepro.2023.138008.

[274] A. Zidan, M. Nasr, M. Fujii, M.G. Ibrahim, Environmental and Economic Evaluation of Downflow Hanging Sponge Reactors for Treating High-Strength Organic Wastewater, Sustain. 15 (2023). https://doi.org/10.3390/su15076038.

[275] D. Dadebo, M.G. Ibrahim, M. Fujii, M. Nasr, Sequential treatment of surfactant-laden wastewater using low-cost rice husk ash coagulant and activated carbon: Modeling, optimization, characterization, and techno-economic analysis, Bioresour. Technol. Reports 22 (2023) 101464. https://doi.org/10.1016/j.biteb.2023.101464.

[276] Q. He, W. Zhang, S. Zhang, H. Wang, Enhanced nitrogen removal in an aerobic granular sequencing batch reactor performing simultaneous nitrification , endogenous denitrification and phosphorus removal with low superficial gas velocity, Chem. Eng. J. 326 (2017) 1223–1231. https://doi.org/10.1016/j.cej.2017.06.071.

[277] C. Wan, X. Yang, D.J. Lee, S. Sun, X. Liu, P. Zhang, Influence of hydraulic retention time on partial nitrification of continuous-flow aerobic granular-sludge reactor, Environ. Technol. (United Kingdom) 35 (2014) 1760–1765. https://doi.org/10.1080/09593330.2014.881423.

[278] J. Li, A. Cai, M. Wang, L. Ding, Y. Ni, Aerobic granulation in a modified oxidation ditch with an adjustable volume intraclarifier, Bioresour. Technol. 157 (2014) 351–354. https://doi.org/10.1016/j.biortech.2014.01.130.

[279] T.R. Kent, C.B. Bott, Z. Wang, State of the art of aerobic granulation in continuous fl ow bioreactors, Biotechnol. Adv. 36 (2018) 1139–1166. https://doi.org/10.1016/j.biotechadv.2018.03.015.

[280] D. Xu, J. Li, J. Liu, X. Qu, H. Ma, Advances in continuous flow aerobic granular sludge: A review, Process Saf. Environ. Prot. 163 (2022) 27–35. https://doi.org/10.1016/j.psep.2022.05.018.

[281] Y.Z. Li, Y.L. He, D.G. Ohandja, J. Ji, J.F. Li, T. Zhou, Simultaneous nitrification-denitrification achieved by an innovative internal-loop airlift MBR: Comparative study, Bioresour. Technol. 99 (2008) 5867–5872. https://doi.org/10.1016/j.biortech.2007.10.001.

[282] Y.C. Juang, S.S. Adav, D.J. Lee, J.H. Tay, Stable aerobic granules for continuous-flow reactors: Precipitating calcium and iron salts in granular interiors, Bioresour. Technol. 101 (2010) 8051–8057. https://doi.org/10.1016/j.biortech.2010.05.078.

[283] Y.C. Chen, C.J. Lin, H.L. Chen, S.Y. Fu, H.Y. Zhan, Cultivation of Biogranules in a continuous flow reactor at low dissolved oxygen, Water, Air, Soil Pollut. Focus 9 (2009) 213–221. https://doi.org/10.1007/s11267-009-9216-z.

[284] C. Wan, S. Sun, D.J. Lee, X. Liu, L. Wang, X. Yang, X. Pan, Partial nitrification using aerobic granules in continuous-flow reactor: Rapid startup, Bioresour. Technol. 142 (2013) 517–522. https://doi.org/10.1016/j.biortech.2013.04.120.

[285] J.J. Beun, M.C.M. Van Loosdrecht, J.J. Heijnen, Aerobic granulation in a sequencing batch airlift reactor, Water Res. 36 (2002) 702–712. https://doi.org/10.1016/S0043-1354(01)00250-0.

[286] W. Vishniac, M. Santer, The Thiobacilli, (n.d.).

[287] S. Sguanci, C. Lubello, S. Caffaz, T. Lotti, Long-term stability of aerobic granular

sludge for the treatment of very low-strength real domestic wastewater, J. Clean. Prod. 222 (2019) 882–890. https://doi.org/10.1016/j.jclepro.2019.03.061.

[288] K. Kiskira, S. Papirio, E.D. van Hullebusch, G. Esposito, Influence of pH, EDTA/Fe(II) ratio, and microbial culture on Fe(II)-mediated autotrophic denitrification, Environ. Sci. Pollut. Res. 24 (2017) 21323–21333. https://doi.org/10.1007/s11356-017-9736-4.

[289] F. WE, Standard Methods for the Examination of Water and Wastewater Standard Methods for the Examination of Water and Wastewater., 1999. https://doi.org/10.2105/AJPH.51.6.940-a.

[290] A. ISRA-CNR, Analytical Methods for Water. Agenzia per la protezione dell'ambiente e per i servizi tecnici (APAT) Istituto di Ricerca sulle Acque - Consiglio Nazionale delle Ricerche (ISRA-CNR), 2003.

[291] F. Di Capua, M.C. Mascolo, F. Pirozzi, G. Esposito, Simultaneous denitrification, phosphorus recovery and low sulfate production in a recirculated pyrite-packed biofilter (RPPB), Chemosphere 255 (2020) 126977. https://doi.org/10.1016/j.chemosphere.2020.126977.

[292] L.Bonomo, Trattamenti delle acque reflue, McGraw-Hil, 2008.

[293] A.S. Qambar, M.M. Al Khalidy, Optimizing dissolved oxygen requirement and energy consumption in wastewater treatment plant aeration tanks using machine learning, J. Water Process Eng. 50 (2022) 103237. https://doi.org/10.1016/j.jwpe.2022.103237.

[294] E. idrico Campano, Piano d'Ambito Regionale, (n.d.).

[295] X. Liu, C. Dong, Simultaneous COD and nitrogen removal in a micro-aerobic granular sludge reactor for domestic wastewater treatment, Syst. Eng. Procedia 1

(2011) 99–105. https://doi.org/10.1016/j.sepro.2011.08.017.

[296] K.Y. Show, D.J. Lee, J.H. Tay, Aerobic granulation: Advances and challenges, Appl. Biochem. Biotechnol. 167 (2012) 1622–1640. https://doi.org/10.1007/s12010-012-9609-8.

[297] D. Zhou, S. Niu, Y. Xiong, Y. Yang, S. Dong, Microbial selection pressure is not a prerequisite for granulation: Dynamic granulation and microbial community study in a complete mixing bioreactor, Bioresour. Technol. 161 (2014) 102–108. https://doi.org/10.1016/j.biortech.2014.03.001.

[298] R. Campo, S. Sguanci, S. Caffaz, L. Mazzoli, M. Ramazzotti, C. Lubello, T. Lotti, Efficient carbon, nitrogen and phosphorus removal from low C/N real domestic wastewater with aerobic granular sludge, Bioresour. Technol. 305 (2020) 122961. https://doi.org/10.1016/j.biortech.2020.122961.

[299] X. Wang, S. Wang, T. Xue, B. Li, X. Dai, Y. Peng, Treating low carbon/nitrogen (C/N) wastewater in simultaneous nitrification-endogenous denitrification and phosphorous removal (SNDPR) systems by strengthening anaerobic intracellular carbon storage, Water Res. 77 (2015) 191–200. https://doi.org/10.1016/j.watres.2015.03.019.

[300] S.O. Akinnawo, Eutrophication: Causes, consequences, physical, chemical and biological techniques for mitigation strategies, Environ. Challenges 12 (2023). https://doi.org/10.1016/j.envc.2023.100733.

[301] X. Zou, J. Xie, C. Wang, G. Jiang, K. Tang, C. Chen, Electrochemical nitrate reduction to produce ammonia integrated into wastewater treatment: Investigations and challenges, Chinese Chem. Lett. 34 (2023) 107908. https://doi.org/10.1016/j.cclet.2022.107908.

[302] F. Ortmeyer, B. Hansen, A. Banning, Groundwater nitrate problem and countermeasures in strongly affected EU countries—a comparison between Germany, Denmark and Ireland, Grundwasser 28 (2023) 3–22. https://doi.org/10.1007/s00767-022-00530-5.

[303] P. Yanisko, S. Zheng, J. Dumoit, B. Carlson, Nitrogen:A Security Blanket System for Chemical Industry, Fluids Solid Handl. (2011) 7.

[304] K. Wick, C. Heumesser, E. Schmid, Groundwater nitrate contamination: Factors and indicators, J. Environ. Manage. 111 (2012) 178–186. https://doi.org/10.1016/j.jenvman.2012.06.030.

[305] A.R. Sherris, M. Baiocchi, S. Fendorf, S.P. Luby, W. Yang, G.M. Shaw, Nitrate in drinking water during pregnancy and spontaneous preterm birth: A retrospective within-mother analysis in california, Environ. Health Perspect. 129 (2021) 1–11. https://doi.org/10.1289/EHP8205.

[306] L.T. Stayner, A.S. Jensen, J. Schullehner, V.R. Coffman, B.B. Trabjerg, J. Olsen, B. Hansen, M. Pedersen, C.B. Pedersen, T. Sigsgaard, Nitrate in drinking water and risk of birth defects: Findings from a cohort study of over one million births in Denmark, Lancet Reg. Heal. - Eur. 14 (2022) 1–15. https://doi.org/10.1016/j.lanepe.2021.100286.

[307] M.H. Ward, R.R. Jones, J.D. Brender, T.M. de Kok, P.J. Weyer, B.T. Nolan, C.M. Villanueva, S.G. van Breda, Drinking water nitrate and human health: An updated review, Int. J. Environ. Res. Public Health 15 (2018) 1–31. https://doi.org/10.3390/ijerph15071557.

[308] J. Shaban, H. Al-Najar, K. Kocadal, K. Almghari, S. Saygi, The Effect of Nitrate-Contaminated Drinking Water and Vegetables on the Prevalence of Acquired

Methemoglobinemia in Beit Lahia City in Palestine, Water (Switzerland) 15 (2023). https://doi.org/10.3390/w15111989.

[309] M. Inoue-Choi, R.R. Jones, K.E. Anderson, K.P. Cantor, J.R. Cerhan, S. Krasner, K. Robien, P.J. Weyer, M.H. Ward, Nitrate and nitrite ingestion and risk of ovarian cancer among postmenopausal women in Iowa, Int. J. Cancer 137 (2015) 173–182. https://doi.org/10.1002/ijc.29365.

[310] R.R. Jones, P.J. Weyer, C.T. Dellavalle, K. Robien, K.P. Cantor, S. Krasner, L.E. Beane Freeman, M.H. Ward, Ingested Nitrate, Disinfection By-products, and Kidney Cancer Risk in Older Women, Epidemiology 28 (2017) 703–711. https://doi.org/10.1097/EDE.0000000000000647.

[311] B.H. Jacobsen, B. Hansen, J. Schullehner, Health-economic valuation of lowering nitrate standards in drinking water related to colorectal cancer in Denmark, Sci. Total Environ. 906 (2024). https://doi.org/10.1016/j.scitotenv.2023.167368.

[312] M. Dettori, A. Arghittu, G. Deiana, P. Castiglia, A. Azara, The revised European Directive 2020/2184 on the quality of water intended for human consumption. A step forward in risk assessment, consumer safety and informative communication, Environ. Res. 209 (2022) 112773. https://doi.org/10.1016/j.envres.2022.112773.

[313] R.R. Yaragal, S. Mutnuri, Nitrates removal using ion exchange resin: batch, continuous column and pilot-scale studies, Int. J. Environ. Sci. Technol. 20 (2023) 739–754. https://doi.org/10.1007/s13762-021-03836-8.

[314] Y. Liu, X. Zhang, J. Wang, A critical review of various adsorbents for selective removal of nitrate from water: Structure, performance and mechanism, Chemosphere 291 (2022) 132728. https://doi.org/10.1016/j.chemosphere.2021.132728.

[315] Q. Song, M. Li, L. Wang, X. Ma, F. Liu, X. Liu, Mechanism and optimization of electrochemical system for simultaneous removal of nitrate and ammonia, J. Hazard. Mater. 363 (2019) 119–126. https://doi.org/10.1016/j.jhazmat.2018.09.046.

[316] D. Xu, Y. Li, L. Yin, Y. Ji, J. Niu, Y. Yu, Electrochemical removal of nitrate in industrial wastewater, Front. Environ. Sci. Eng. 12 (2018) 1–14. https://doi.org/10.1007/s11783-018-1033-z.

[317] K. Kiskira, S. Papirio, C. Fourdrin, E.D. van Hullebusch, G. Esposito, Effect of Cu, Ni and Zn on Fe(II)-driven autotrophic denitrification, J. Environ. Manage. 218 (2018) 209–219. https://doi.org/10.1016/j.jenvman.2018.04.050.

[318] A. Lanzetta, D. Mattioli, F. Di Capua, V. Minieri, S. Papirio, G. Esposito, Modeling complete and shortcut simultaneous nitrification and denitrification coupled to phosphorus removal in moving bed biofilm reactors, J. Water Process Eng. 59 (2024) 105022. https://doi.org/10.1016/j.jwpe.2024.105022.

[319] E. Sahinkaya, N. Dursun, A. Kilic, S. Demirel, S. Uyanik, O. Cinar, Simultaneous heterotrophic and sulfur-oxidizing autotrophic denitrification process for drinking water treatment: Control of sulfate production, Water Res. 45 (2011) 6661–6667. https://doi.org/10.1016/j.watres.2011.09.056.

[320] S.S. Gadegaonkar, Ü. Mander, M. Espenberg, A state-of-the-art review and guidelines for enhancing nitrate removal in bio-electrochemical systems (BES), J. Water Process Eng. 53 (2023). https://doi.org/10.1016/j.jwpe.2023.103788.

[321] D. Cecconet, M. Devecseri, A. Callegari, A.G. Capodaglio, Effects of process operating conditions on the autotrophic denitrification of nitrate-contaminated groundwater using bioelectrochemical systems, Sci. Total Environ. 613–614

(2018) 663–671. https://doi.org/10.1016/j.scitotenv.2017.09.149.

[322] D. Molognoni, M. Devecseri, D. Cecconet, A.G. Capodaglio, Cathodic groundwater denitrification with a bioelectrochemical system, J. Water Process Eng. 19 (2017) 67–73. https://doi.org/10.1016/j.jwpe.2017.07.013.

[323] F. Di Capua, S. Papirio, P.N.L. Lens, G. Esposito, Chemolithotrophic denitrification in biofilm reactors, Chem. Eng. J. 280 (2015) 643–657. https://doi.org/10.1016/j.cej.2015.05.131.

[324] S. V. Ramanaiah, K. Chandrasekhar, C.M. Cordas, I. Potoroko, Bioelectrochemical systems (BESs) for agro-food waste and wastewater treatment, and sustainable bioenergy-A review, Environ. Pollut. 325 (2023). https://doi.org/10.1016/j.envpol.2023.121432.

[325] M. Rosenbaum, F. Aulenta, M. Villano, L.T. Angenent, Cathodes as electron donors for microbial metabolism: Which extracellular electron transfer mechanisms are involved?, Bioresour. Technol. 102 (2011) 324–333. https://doi.org/10.1016/j.biortech.2010.07.008.

[326] V.K. Nguyen, S. Hong, Y. Park, K. Jo, T. Lee, Autotrophic denitrification performance and bacterial community at biocathodes of bioelectrochemical systems with either abiotic or biotic anodes, J. Biosci. Bioeng. 119 (2015) 180–187. https://doi.org/10.1016/j.jbiosc.2014.06.016.

[327] D. Cecconet, M. Devecseri, A. Callegari, A.G. Capodaglio, Effects of process operating conditions on the autotrophic denitrification of nitrate-contaminated groundwater using bioelectrochemical systems, Sci. Total Environ. 613–614 (2018) 663–671. https://doi.org/10.1016/j.scitotenv.2017.09.149.

[328] H. Feng, B. Huang, Y. Zou, N. Li, M. Wang, J. Yin, Y. Cong, D. Shen, The effect

of carbon sources on nitrogen removal performance in bioelectrochemical systems, Bioresour. Technol. 128 (2013) 565–570. https://doi.org/10.1016/j.biortech.2012.11.004.

[329] P. Srivastava, A.K. Yadav, R. Abbassi, V. Garaniya, T. Lewis, Denitrification in a low carbon environment of a constructed wetland incorporating a microbial electrolysis cell, J. Environ. Chem. Eng. 6 (2018) 5602–5607. https://doi.org/10.1016/j.jece.2018.08.053.

[330] L. Yu, Y. Yuan, S. Chen, L. Zhuang, S. Zhou, Direct uptake of electrode electrons for autotrophic denitrification by Thiobacillus denitrificans, Electrochem. Commun. 60 (2015) 126–130. https://doi.org/10.1016/j.elecom.2015.08.025.

[331] W. Xing, D. Li, J. Li, Q. Hu, S. Deng, Nitrate removal and microbial analysis by combined micro-electrolysis and autotrophic denitrification, Bioresour. Technol. 211 (2016) 240–247. https://doi.org/10.1016/j.biortech.2016.03.044.

[332] N. Pous, C. Koch, A. Vilà-Rovira, M.D. Balaguer, J. Colprim, J. Mühlenberg, S. Müller, F. Harnisch, S. Puig, Monitoring and engineering reactor microbiomes of denitrifying bioelectrochemical systems, RSC Adv. 5 (2015) 68326–68333. https://doi.org/10.1039/c5ra12113b.

[333] D. Chen, L. Wei, Z. Zou, K. Yang, H. Wang, Bacterial communities in a novel three-dimensional bioelectrochemical denitrification system: the effects of pH, Appl. Microbiol. Biotechnol. 100 (2016) 6805–6813. https://doi.org/10.1007/s00253-016-7499-3.

[334] N. Pous, S. Puig, M.D. Balaguer, J. Colprim, Effect of hydraulic retention time and substrate availability in denitrifying bioelectrochemical systems, Environ. Sci. Water Res. Technol. 3 (2017) 922–929. https://doi.org/10.1039/c7ew00145b.

[335] N. Pous, S. Puig, M. Dolors Balaguer, J. Colprim, Cathode potential and anode electron donor evaluation for a suitable treatment of nitrate-contaminated groundwater in bioelectrochemical systems, Chem. Eng. J. 263 (2015) 151–159. https://doi.org/10.1016/j.cej.2014.11.002.

[336] A. Ceballos-Escalera, N. Pous, B. Korth, F. Harnisch, M.D. Balaguer, S. Puig, Ex-situ electrochemical characterisation of fixed-bed denitrification biocathodes: A promising strategy to improve bioelectrochemical denitrification, Chemosphere 347 (2024) 1–9. https://doi.org/10.1016/j.chemosphere.2023.140699.

[337] A. Escapa, R. Mateos, E.J. Martínez, J. Blanes, Microbial electrolysis cells: An emerging technology for wastewater treatment and energy recovery. from laboratory to pilot plant and beyond, Renew. Sustain. Energy Rev. 55 (2016) 942–956. https://doi.org/10.1016/j.rser.2015.11.029.

[338] L. Gil-Carrera, A. Escapa, P. Mehta, G. Santoyo, S.R. Guiot, A. Morán, B. Tartakovsky, Microbial electrolysis cell scale-up for combined wastewater treatment and hydrogen production, Bioresour. Technol. 130 (2013) 584–591. https://doi.org/10.1016/j.biortech.2012.12.062.

[339] M. Zhou, H. Wang, D.J. Hassett, T. Gu, Recent advances in microbial fuel cells (MFCs) and microbial electrolysis cells (MECs) for wastewater treatment, bioenergy and bioproducts, J. Chem. Technol. Biotechnol. 88 (2013) 508–518. https://doi.org/10.1002/jctb.4004.

[340] K.P. Katuri, M. Ali, P.E. Saikaly, The role of microbial electrolysis cell in urban wastewater treatment: integration options, challenges, and prospects, Curr. Opin. Biotechnol. 57 (2019) 101–110. https://doi.org/10.1016/j.copbio.2019.03.007.

[341] U. Schröder, Bioelectrochemical Systems, 2023.

https://doi.org/10.1039/bk9781849739757-00347.

[342] M.M. Ghangrekar, S. Das, B.R. Tiwari, Integration of bioelectrochemical systems with other existing wastewater treatment processes, INC, 2020. https://doi.org/10.1016/B978-0-12-817493-7.00011-4.

[343] J. Jermakka, E. Thompson Brewster, P. Ledezma, S. Freguia, Electro-concentration for chemical-free nitrogen capture as solid ammonium bicarbonate, Sep. Purif. Technol. 203 (2018) 48–55. https://doi.org/10.1016/j.seppur.2018.04.023.

[344] K. Rabaey, W. Ossieur, M. Verhaege, W. Verstraete, Continuous microbial fuel cells convert carbohydrates to electricity, Water Sci. Technol. 52 (2005) 515–523. https://doi.org/10.2166/wst.2005.0561.

[345] P. Chatterjee, P. Dessì, M. Kokko, A.M. Lakaniemi, P. Lens, Selective enrichment of biocatalysts for bioelectrochemical systems: A critical review, Renew. Sustain. Energy Rev. 109 (2019) 10–23. https://doi.org/10.1016/j.rser.2019.04.012.

[346] Y. Sun, M. Kokko, I. Vassilev, Anode-assisted electro-fermentation with Bacillus subtilis under oxygen-limited conditions, Biotechnol. Biofuels Bioprod. 16 (2023) 1–12. https://doi.org/10.1186/s13068-022-02253-4.

[347] M. Kokko, V. Koskue, J. Rintala, Anaerobic digestion of 30−100-year-old boreal lake sedimented fibre from the pulp industry: Extrapolating methane production potential to a practical scale, Water Res. 133 (2018) 218–226. https://doi.org/10.1016/j.watres.2018.01.041.

[348] S. Singh, J.M. Rinta-Kanto, R. Kettunen, H. Tolvanen, P. Lens, G. Collins, M. Kokko, J. Rintala, Anaerobic treatment of LCFA-containing synthetic dairy wastewater at 20 °C: Process performance and microbial community dynamics,

Sci. Total Environ. 691 (2019) 960–968. https://doi.org/10.1016/j.scitotenv.2019.07.136.

[349] T. Kuroda, Masao and Watanabe, CO2 reduction to methane and acetate using a bio-electro reactor with immobilized methanogens and homoacetogens on electrodes, 36 (1995) 787–790.

[350] J. Zabranska, D. Pokorna, Bioconversion of carbon dioxide to methane using hydrogen and hydrogenotrophic methanogens, Biotechnol. Adv. 36 (2018) 707–720. https://doi.org/10.1016/j.biotechadv.2017.12.003.

[351] Y. Zhao, C. Feng, Q. Wang, Y. Yang, Z. Zhang, N. Sugiura, Nitrate removal from groundwater by cooperating heterotrophic with autotrophic denitrification in a biofilm-electrode reactor, J. Hazard. Mater. 192 (2011) 1033–1039. https://doi.org/10.1016/j.jhazmat.2011.06.008.

[352] X. Li, R. Zhang, Y. Qian, I. Angelidaki, Y. Zhang, The impact of anode acclimation strategy on microbial electrolysis cell treating hydrogen fermentation effluent, Bioresour. Technol. 236 (2017) 37–43. https://doi.org/10.1016/j.biortech.2017.03.160.

[353] P.T. Kelly, Z. He, Nutrients removal and recovery in bioelectrochemical systems: A review, Bioresour. Technol. 153 (2014) 351–360. https://doi.org/10.1016/j.biortech.2013.12.046.

[354] T. Siwiec, L. Reczek, M.M. Michel, B. Gut, P. Hawer-Strojek, J. Czajkowska, K. Jóźwiakowski, M. Gajewska, P. Bugajski, Correlations between organic pollution indicators in municipal wastewater, Arch. Environ. Prot. 44 (2018) 50–57. https://doi.org/10.24425/aep.2018.122296.

[355] M. Kermani, B. Bina, H. Movahedian, M.M. Amin, M. Nikaeen, Biological

phosphorus and nitrogen removal from wastewater using moving bed biofilm process, Iran. J. Biotechnol. 7 (2009) 19–27.

[356] E. Zkeri, A. Iliopoulou, A. Katsara, A. Korda, M. Aloupi, G. Gatidou, M.S. Fountoulakis, A.S. Stasinakis, Comparing the use of a two-stage MBBR system with a methanogenic MBBR coupled with a microalgae reactor for medium-strength dairy wastewater treatment, Bioresour. Technol. 323 (2021) 124629. https://doi.org/10.1016/j.biortech.2020.124629.

[357] A. González-Martínez, C. Pesciaroli, M. V. Martínez-Toledo, E. Hontoria, J. González-López, F. Osorio, Study of nitrifying microbial communities in a partial-nitritation bioreactor, Ecol. Eng. 64 (2014) 443–450. https://doi.org/10.1016/j.ecoleng.2014.01.009.

[358] I. Kocaturk, T.H. Erguder, Influent COD/TAN ratio affects the carbon and nitrogen removal efficiency and stability of aerobic granules, Ecol. Eng. 90 (2016) 12–24. https://doi.org/10.1016/j.ecoleng.2016.01.077.

[359] N. Derlon, J. Wagner, R.H.R. da Costa, E. Morgenroth, Formation of aerobic granules for the treatment of real and low-strength municipal wastewater using a sequencing batch reactor operated at constant volume, Water Res. 105 (2016) 341–350. https://doi.org/10.1016/j.watres.2016.09.007.

[360] Y. Feng, L. Wang, Z. Yin, Z. Cui, K. Qu, D. Wang, Z. Wang, S. Zhu, H. Cui, Comparative investigation on heterotrophic denitrification driven by different biodegradable polymers for nitrate removal in mariculture wastewater: Organic carbon release, denitrification performance, and microbial community, Front. Microbiol. 14 (2023) 1–13. https://doi.org/10.3389/fmicb.2023.1141362.

[361] K. Rajitha, M. Sarvajith, V.P. Venugopalan, Y. V. Nancharaiah, Development and

performance of halophilic microalgae-colonized aerobic granular sludge for treating seawater-based wastewater, Bioresour. Technol. Reports 11 (2020). https://doi.org/10.1016/j.biteb.2020.100432.

[362] S. Berzio, J.M. Araújo, T. Gehring, L.C. Phan, B. Teichgräber, M. Lübken, M. Wichern, Compact pilot-scale aerobic granular sludge system treating real wastewater continuously for over 500 days, J. Water Process Eng. 53 (2023). https://doi.org/10.1016/j.jwpe.2023.103847.

[363] Z. Wang, Z. He, Demystifying terms for understanding bioelectrochemical systems towards sustainable wastewater treatment, Curr. Opin. Electrochem. 19 (2020) 14–19. https://doi.org/10.1016/j.coelec.2019.09.001.

[364] J. Tang, C. Zhang, X. Shi, J. Sun, J.A. Cunningham, Municipal wastewater treatment plants coupled with electrochemical, biological and bio-electrochemical technologies: Opportunities and challenge toward energy self-sufficiency, J. Environ. Manage. 234 (2019) 396–403. https://doi.org/10.1016/j.jenvman.2018.12.097.